

SYNTHESIS, CHARACTERISATION AND APPLICATION  
OF Ni/ZnO/Al<sub>2</sub>O<sub>3</sub> CATALYST IN  
PARTIAL HYDROGENATION OF SUNFLOWER OIL

WONG FARNG HUI

MASTER OF ENGINEERING SCIENCE

LEE KONG CHIAN  
FACULTY OF ENGINEERING AND SCIENCE  
UNIVERSITI TUNKU ABDUL RAHMAN  
DECEMBER 2018

**SYNTHESIS, CHARACTERISATION AND APPLICATION  
OF Ni/ZnO/Al<sub>2</sub>O<sub>3</sub> CATALYST IN  
PARTIAL HYDROGENATION OF SUNFLOWER OIL**

By

**WONG FARNG HUI**

A dissertation submitted to the Department of Chemical Engineering,  
Lee Kong Chian Faculty of Engineering and Science,  
Universiti Tunku Abdul Rahman,  
in partial fulfillment of the requirements for the degree of  
Master of Engineering Science  
December 2018

## ABSTRACT

### SYNTHESIS, CHARACTERISATION AND APPLICATION OF Ni/ZnO/Al<sub>2</sub>O<sub>3</sub> CATALYST IN PARTIAL HYDROGENATION OF SUNFLOWER OIL

Wong Farn Hui

This work introduced the novelty of incorporating ZnO into Ni/Al<sub>2</sub>O<sub>3</sub> catalyst for application in partial hydrogenation of sunflower oil to enhance activity, reduce *trans*-fats formation and lower the material cost. Ni/ZnO/Al<sub>2</sub>O<sub>3</sub> catalysts at varying Ni:Zn molar ratios were synthesised by co-precipitation method. They were subsequently characterised and employed in partial hydrogenation to study the effect of ZnO incorporation on the characteristics of Ni/Al<sub>2</sub>O<sub>3</sub> catalyst and its catalytic performance in terms of activity and selectivity. From the study, migration of ZnO to the catalyst surface was observed and the extent of migration decreased with higher ZnO content present in the catalyst. The enrichment of ZnO at the surface was found to alter pore characteristics and resulted in larger pores with diameter up to 27.95 nm. ZnO also functioned as a physical spacer as visualized in the TEM images, which significantly increased the Ni dispersion and Ni surface area but the effect diminished when ZnO became the major constituent. Higher ZnO content in the catalyst was found to suppress *trans*-fats formation and promote saturated fats formation. Combination of large pore size and high ZnO content in Ni/ZnO/Al<sub>2</sub>O<sub>3</sub> catalyst with Ni:Zn = 1.5:1.5 resulted in improvement of hydrogenation activity by 23 % and reduction of *trans*-fats formation by 26 % as compared to Ni/Al<sub>2</sub>O<sub>3</sub> catalyst.

## **ACKNOWLEDGEMENT**

My deepest gratitude to my research supervisor Dr. Yap Yeow Hong for his invaluable advice, guidance and enormous patience throughout my study. Dr Yap has always encouraged me and provided ample opportunities to broaden my skills.

I would also like thank to my loving parents, family and friends who had given me endless support to persevere and complete this journey. Not to forget the dedicated lab officers who had generously helped to facilitate the use of research labs and equipment.

## APPROVAL SHEET

This dissertation entitled “**SYNTHESIS, CHARACTERISATION AND APPLICATION OF Ni/ZnO/Al<sub>2</sub>O<sub>3</sub> CATALYST IN PARTIAL HYDROGENATION OF SUNFLOWER OIL**” was prepared by WONG FARNG HUI and submitted as partial fulfillment of the requirements for the degree of Master of Engineering Science at Universiti Tunku Abdul Rahman.

Approved by:

---

(Dr. YAP YEOW HONG)

Date:

Supervisor

Department of Chemical Engineering

Lee Kong Chian Faculty of Engineering and Science

Universiti Tunku Abdul Rahman

---

(Dr. LEONG LOONG KONG)

Date:

Co-supervisor

Department of Chemical Engineering

Lee Kong Chian Faculty of Engineering and Science

Universiti Tunku Abdul Rahman

**LEE KONG CHIAN FACULTY OF ENGINEERING AND SCIENCE**

**UNIVERSITI TUNKU ABDUL RAHMAN**

Date: 28<sup>th</sup> December 2018

**SUBMISSION OF FINAL YEAR PROJECT /DISSERTATION/THESIS**

It is hereby certified that Wong Farng Hui  
(ID No: 11UEM06191) has completed this dissertation entitled  
“Synthesis, Characterisation and Application of Ni/ZnO/Al<sub>2</sub>O<sub>3</sub>  
Catalyst in Partial Hydrogenation of Sunflower Oil” under the supervision of  
Dr. Yap Yeow Hong (Supervisor) from the Department of Chemical  
Engineering, Lee Kong Chian Faculty of Engineering and Science, and Dr. Leong  
Loong Kong (Co-Supervisor)\* from the Department of Chemical Engineering,  
Lee Kong Chian Faculty of Engineering and Science.

I understand that University will upload softcopy of my dissertation in pdf format into UTAR Institutional Repository, which may be made accessible to UTAR community and public.

Yours truly,

\_\_\_\_\_  
(*Wong Farng Hui*)

\*Delete whichever not applicable

## DECLARATION

I hereby declare that the dissertation is based on my original work except for quotations and citations which have been duly acknowledged. I also declare that it has not been previously or concurrently submitted for any other degree at UTAR or other institutions.

Name Wong Farnng Hui

Date 28<sup>th</sup> December 2018

## TABLE OF CONTENTS

	<b>Page</b>
<b>ABSTRACT</b>	<b>iii</b>
<b>ACKNOWLEDGEMENTS</b>	<b>iv</b>
<b>APPROVAL SHEET</b>	<b>v</b>
<b>SUBMISSION SHEET</b>	<b>vi</b>
<b>DECLARATION</b>	<b>vii</b>
<b>LIST OF TABLES</b>	<b>x</b>
<b>LIST OF FIGURES</b>	<b>xi</b>
<b>LIST OF ABBREVIATION AND NOMENCLATURE</b>	<b>xiii</b>
<b>CHAPTER</b>	
<b>1.0 INTRODUCTION</b>	<b>1</b>
1.1 Background	1
1.2 Aim and Objectives	4
1.3 Problem Statement	4
<b>2.0 LITERATURE REVIEW</b>	<b>6</b>
2.1 Hydrogenation of Oils	6
2.2 Reaction Mechanism	8
2.3 Reaction Conditions	10
2.4 Control of <i>Trans</i> -fats Formation	11
2.4.1 Change in Reaction Condition	11
2.4.2 Change in Catalyst Type	13
2.4.3 Incorporation of Zinc into Nickel Catalyst	18
2.4.4 Other Alternatives	21
2.5 Catalyst Synthesis	23
2.5.1 Co-Precipitation Method	24
2.5.2 Impregnation Method	26
2.5.3 Heat Treatment	28
<b>3.0 METHODOLOGY</b>	<b>31</b>
3.1 Materials	31
3.2 Synthesis of Catalyst	32
3.3 Characterisation of Catalyst	34
3.3.1 Inductively-Coupled Plasma Optical Emission Spectroscopy (ICP-OES) Analysis	34
3.3.2 X-ray Photoelectron Spectroscopy (XPS) Analysis	35
3.3.3 Scanning Electron Microscopy and Energy Dispersive X-ray Spectroscopy (SEM-EDX) Analysis	36
3.3.4 Nitrogen Adsorption-Desorption Analysis	36

3.3.5	Hydrogen Temperature-Programmed Reduction (H <sub>2</sub> -TPR) Analysis	37
3.3.6	Pulse Chemisorption Analysis	37
3.3.7	X-ray Diffraction (XRD) Analysis	38
3.3.8	Transmission Electron Microscopy (TEM) Analysis	38
3.4	Partial Hydrogenation	39
3.5	Partial Hydrogenation Product Analyses	40
3.5.1	Iodine Value (IV) Test	40
3.5.2	Gas Chromatography (GC) Analysis	42
3.5.3	Evaluation of Catalyst Activity and Selectivity	43
<b>4.0</b>	<b>RESULTS AND DISCUSSION</b>	<b>45</b>
4.1	Catalyst Characterisation	45
4.1.1	Catalyst Composition	45
4.1.2	Pore Structure	54
4.1.3	XRD and TEM Analyses	56
4.1.4	TPR Profiles	61
4.1.5	Hydrogen Pulse Chemisorption	65
4.2	Catalyst Test in Partial Hydrogenation	67
4.2.1	Hydrogenation Activity	67
4.2.2	Hydrogenation Selectivity	71
4.2.3	Comparison of Results with Literature	76
<b>5.0</b>	<b>CONCLUSION</b>	<b>78</b>
5.1	Conclusion	78
5.2	Recommendation	79
	<b>LIST OF REFERENCES</b>	<b>80</b>
	<b>APPENDICES</b>	<b>90</b>
A	ICP-OES Analysis	90
B1	XRD Analysis	93
B2	TEM Analysis	94
C	Iodine Value Test	95
D1	Gas Chromatography Analysis	97
D2	Activity and Selectivity of Catalyst	98
E	XPS Curve-Fitting	100
F	EDX Elemental Mapping	105
G	Pulse Chemisorption Analysis	108
H	Nitrogen Adsorption-Desorption Isotherm	111
	<b>LIST OF PUBLICATIONS</b>	<b>112</b>

## LIST OF TABLES

Table		Page
2.1	Common fatty acids with 18-carbons	6
2.2	Typical partial hydrogenation conditions	10
3.1	Fatty acids composition in Olife Sunflower Oil analysed by GC	31
3.2	Designated stoichiometric molar ratio of synthesised catalysts	32
3.3	In-situ conditioning stages prior to pulse chemisorption	38
4.1	Elemental composition for synthesised catalyst samples from XPS, EDXS and ICP-OES analyses	46
4.2	Specific surface area, $S_{BET}$ , specific pore volume, $V_p$ and average pore diameter, $d_p$ of the catalysts obtained from nitrogen adsorption-desorption analysis	54
4.3	Crystallite size of Ni(111) lattice based on XRD spectra of reduced catalysts as calculated by Scherrer's equation	60
4.4	Amount of hydrogen adsorbed, Ni dispersion, $D_{Ni}$ and Ni specific surface area, $SA_{Ni}$ of the catalysts obtained from hydrogen pulse chemisorption analysis as compared with bulk Ni composition and surface Zn/Ni ratio	66
4.5	Hydrogenation activity of the catalysts as compared with Ni dispersion, $D_{Ni}$ , Ni surface area, $SA_{Ni}$ and average pore diameter, $d_p$	69
4.6	Conversion of C18:2, selectivity of C18:0 over <i>trans</i> -C18:1 and selectivity of <i>trans</i> -C18:1 over <i>cis</i> -C18:1 of sunflower oil at specific iodine value upon undergoing partial hydrogenation (temperature: 180 °C, hydrogen pressure: 5 bar (g), agitation rate: 2000 rpm)	73
4.7	Comparison of <i>trans</i> -fats and saturated fats content with other works	77



## LIST OF FIGURES

Figures	Page
1.1 Structural formula of a triglyceride with fatty acids of varying chain length and number of double bonds (Fletcher, 2016)	1
1.2 Structural formula of <i>trans</i> -fatty acid and <i>cis</i> -fatty acid (King, 2016)	3
2.1 General hydrogenation scheme of C18 fatty acids (Veldsink et al., 1997)	7
2.2 Reaction mechanism of hydrogenation at the state of (a) $\pi$ -complex (b) half-hydrogenated intermediate (c) saturated (Hoffman, 1989)	8
2.3 Two-step hydrogenation scheme (Scrimgeour, 2009)	9
3.1 Catalyst samples after (a) oven-drying (b) hydrogen reduction and fats-coating	34
3.2 Oil samples collected at different time intervals with increasing solid fats content showing progress of partial hydrogenation	40
3.3 Oil samples from partial hydrogenation (a) before filtration (b) after filtration (c) after esterification and dissolved in dichloromethane	43
4.1 Ni 2p <sub>3/2</sub> , Zn 2p <sub>1/2</sub> and Zn 2p <sub>3/2</sub> XPS spectra for (a) Ni/Al <sub>2</sub> O <sub>3</sub> (b) ZnO/Al <sub>2</sub> O <sub>3</sub> (c)-(d) 2_Ni/ZnO/Al <sub>2</sub> O <sub>3</sub> (e)-(f) 3_Ni/ZnO/Al <sub>2</sub> O <sub>3</sub> (g)-(h) 1_Ni/ZnO/Al <sub>2</sub> O <sub>3</sub>	47
4.2 EDXS element mapping of 3_Ni/ZnO/Al <sub>2</sub> O <sub>3</sub> catalyst for elements of (a) nickel (b) zinc (c) aluminium and (d) oxygen	52
4.3 SEM images showing surface morphology of (a) Ni/Al <sub>2</sub> O <sub>3</sub> (b) 2_Ni/ZnO/Al <sub>2</sub> O <sub>3</sub> (c) 3_Ni/ZnO/Al <sub>2</sub> O <sub>3</sub> (d) 1_Ni/ZnO/Al <sub>2</sub> O <sub>3</sub> (e) ZnO/Al <sub>2</sub> O <sub>3</sub>	53
4.4 Pore size distribution curves	55
4.5 Comparison of XRD spectra for catalyst precursors before hydrogen reduction	57

4.6	Comparison of XRD spectra for the catalysts after hydrogen reduction	58
4.7	Contrast-enhanced and magnified TEM image of (a) 3_Ni/ZnO/Al <sub>2</sub> O <sub>3</sub> (b) Ni/Al <sub>2</sub> O <sub>3</sub> showing the crystalline planes of different species based on measured spacing between lattice fringes where $d_{\text{Ni}(111)} = 2.03 \text{ \AA}$ , $d_{\text{Ni}(200)} = 1.76 \text{ \AA}$ , $d_{\text{NiO}(101)} = 2.41 \text{ \AA}$ , $d_{\text{ZnO}(110)} = 2.29 \text{ \AA}$	61
4.8	Temperature programmed reduction profiles across temperatures from 100 – 1000 °C with inset showing amount of hydrogen consumed during H <sub>2</sub> -TPR	62
4.9	Change in iodine value in the course of partial hydrogenation of sunflower oil (temperature: 180 °C, hydrogen pressure: 5 bar (g), agitation rate: 2000 rpm) over respective catalyst samples	68
4.10	Change in oil composition with iodine value during partial hydrogenation of sunflower oil (temperature: 180 °C, pressure: 5 bar (g), stirring intensity: 2000 rpm) with the use of (a) Ni/Al <sub>2</sub> O <sub>3</sub> (b) 2_Ni/ZnO/Al <sub>2</sub> O <sub>3</sub> (c) 3_Ni/ZnO/Al <sub>2</sub> O <sub>3</sub> (d) 1_Ni/ZnO/Al <sub>2</sub> O <sub>3</sub> catalyst	72

## LIST OF ABBREVIATION AND NOMENCLATURE

### Abbreviation

IV	Iodine value
ICP-OES	Inductively-coupled plasma optical emission spectroscopy
XPS	X-ray photoelectron spectroscopy
BET	Brunauer-Emmett-Teller method
BJH	Barrett-Joyner-Halenda method
H <sub>2</sub> -TPR	Hydrogen temperature-programmed reduction
TEM	Transmission electron microscopy
GC	Gas chromatography
DFT	Density functional theory
SEM-EDXS	Scanning electron microscopy-electron dispersive X-ray spectroscopy

### Nomenclature

C18:0	Stearic acid
<i>Cis</i> -C18:1	Oleic acid
<i>Trans</i> -C18:1	Elaidic acid
C18:2	Linoleic acid
C18:3	Linolenic acid
C-C	Carbon-carbon single bonding
C=C	Carbon-carbon double bonding
$S_{BET}$	Specific surface area from BET method
$V_p$	Specific pore volume
$d_p$	Average pore diameter
$S_{BJH}$	Specific surface area from BJH method
$V_{BJH}$	Specific pore volume from BJH method
$B$	Volume of titrant of blank set
$S$	Volume of titrant of sample set
$N$	Normality
$D_{Ni}$	Nickel dispersion
$SA_{Ni}$	Nickel surface area
$T$	Temperature
$P$	Pressure

## CHAPTER ONE

### INTRODUCTION

#### 1.1 Background

Fats and oils (triglycerides) are one of the basic nutrients and biological building blocks required by human body. Each triglyceride molecule is made up of one glycerol bonded with three fatty acid chains as illustrated in Figure 1.1. The fatty acid chains come in different chain lengths and possess varying number of carbon-carbon double bonds. The number of double bonds determines the degree of saturation of the fatty acids.

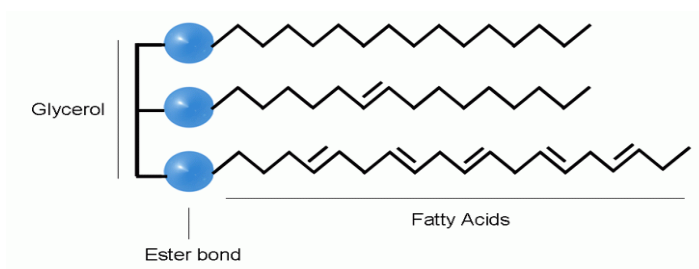


**Figure 1.1: Structural formula of a triglyceride with fatty acids of varying chain length and number of double bonds (Fletcher, 2016)**

Edible oil is most commonly extracted from vegetable sources such as oil palm, canola seed, soybean and sunflower seed. In their raw and natural form, these vegetable oils have low degree of saturation and low melting point (-17 °C to -10 °C) due to the presence of large number of double bonds (Nassu and Gonçalves, 1999). These oils can easily turn rancid due to oxidation,

resulting in short shelf-life which has limited its industrial applicability. Moreover, they are also unstable when repeatedly heated to high temperature for cooking or food processing (McArdle et al., 2011; Gutsche et al., 2004).

Therefore, partial hydrogenation of oil can be carried out to eliminate the double bonds in the fatty acid chains through addition of hydrogen atoms. This results in semi-solid oil products with higher melting point (37 °C to 43 °C) and steeper melting profile (Cepeda et al., 2016; Nassu and Gonçalves, 1999). Oil products with steep melting profile are important in controlling sensory enhancing properties in food such as the texture and flavour release. Due to their unique melting profile, partially hydrogenated oil products are highly demanded to make baking products, chocolate and confectionaries, ice cream fats, beverage creamer, deep-fried food and processed food (Dhaka et al., 2011). Cocoa butter substitute and milk fats replacer are two typical uses of partially hydrogenated vegetable oils due to its ability to remain in solid state at ambient temperature but melt and release flavour upon exposure to human body temperature (Cruz and Álvarez, 2016; Sekula and Tancibok, 2001).

Nevertheless, partial hydrogenation of oil also results in the formation of *trans*-fats. *Trans*-fatty acid has a linear configuration which differs from its *cis*- counterpart as shown in Figure 1.2. It was found that consumption of *trans*-fats is directly related to coronary heart diseases as it would not only increase low density cholesterol but also decrease high density cholesterol simultaneously (Zock and Katan, 1992; Mozaffarian et al., 2006). The deteriorating effect of *trans*-fats consumption to our body is of high concern

that in year 2004, Denmark banned the use of oils with more than 2 % *trans*-fats content (Leth et al., 2006).

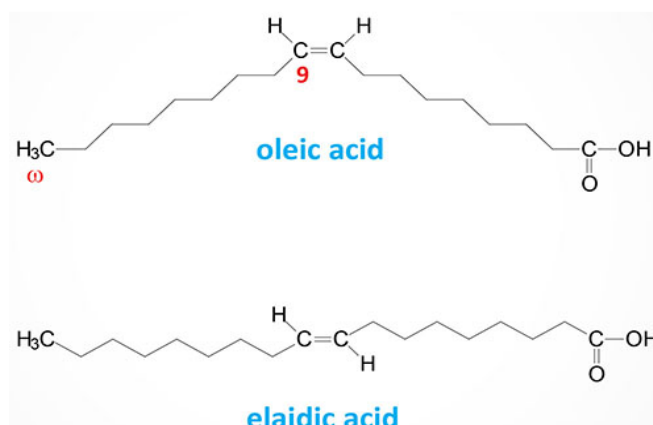


**Figure 1.2: Structural formula of *trans*-fatty acid (elaidic acid) and *cis*-fatty acid (oleic acid) (King, 2016)**

The deleterious effects of *trans*-fats to our health call for the need to decrease formation of *trans*-fats during partial hydrogenation. Various attempts have been reported including changes in reaction condition and the catalyst employed. As changes in reaction condition has limited effect and also practicability due to cost and mechanical constraints, more focus have been exerted on improving the catalyst. Ni-Zn catalyst was reported to show higher activity than Ni/SiO<sub>2</sub> in hydrogenation of fish oil (Feldhauser et al., 1997) and have high olefin selectivity in hydrogenation of acetylene (Studt et al., 2008). Incorporation of Zn in the form of ZnO into Ni catalyst was also found to increase activity in deoxygenation of oleic acid. However, the application of this catalyst in partial hydrogenation of vegetable oils has yet to be investigated in depth. In view of the potentials, this research studies the effect of

incorporating ZnO into Ni catalyst to form Ni/ZnO/Al<sub>2</sub>O<sub>3</sub> catalyst and its application in partial hydrogenation of sunflower oils.

## 1.2 Aim and Objectives

This work aims to synthesise, characterise and apply Ni/ZnO/Al<sub>2</sub>O<sub>3</sub> catalyst in partial hydrogenation of edible oils. Specific objectives are as listed below:

1. To synthesise Ni/ZnO/Al<sub>2</sub>O<sub>3</sub> catalyst with varying composition by co-precipitation method.
2. To characterise the synthesised catalysts with physical and chemical analyses.
3. To test and evaluate the activity and selectivity of synthesised catalysts in lab-scale hydrogenation reactor.

## 1.3 Problem Statement

Albeit partial hydrogenation of vegetable oils is an established and common industrial process, there remain persistent issues to be solved. One of the major problems faced is the formation of *trans*-fats which had raised concerns due to its impacts on human health. Commonly, the *trans*-fats content in margarine is 15 % to 26 % while those in shortenings are about 15 % to 33 % (Tarrago-Trani et al., 2006; Hunter, 2005). Although the conventional nickel catalyst enables high activity during hydrogenation process, its selectivity is not optimum for low-*trans* production.

The challenge would be to produce partially hydrogenated oil with low *trans*-fats content and possesses equivalent functionality at reasonable cost without drastic increase in saturated fats (Hunter, 2005). One promising solution is through the use of a novel catalyst that have high selectivity to *cis*- isomer and low selectivity to saturated fats (Stanković et al., 2015).

Besides the formation of *trans*-fats, nickel catalyst also tends to be deactivated by free fatty acids and radicals in the oil feeds, forming nickel soap complex (Henderson, 1994). The formation of nickel soap can result in contamination in the hydrogenated product. The tendency to form nickel soap can be lowered with the use of catalyst with less nickel content. Furthermore, the cost of nickel catalyst takes up substantial portion of the partial hydrogenation operating cost. Therefore, cost reduction could result from substitution of nickel with cheaper catalytic metals.

## CHAPTER TWO

### LITERATURE REVIEW

#### 2.1 Hydrogenation of Oils

The human body can synthesize most of the fats needed but there are some essential fatty acids vital to our body that could only be obtained from consumption of food. The most important dietary fats required by humans are those with fatty acid carbon chain of 18 carbons which are also the dominant components in vegetable oils (Bartholomew, 2006). Table 2.1 tabulates the common C18 fatty acids. The nomenclature for the fatty acids is based on C:X:Y where X designates the number of carbon atoms while Y shows the number of double bonds in the fatty acids.

**Table 2.1: Common fatty acids with 18-carbons**

Name	Nomenclature	Iodine Value
Stearic Acid	C18:0	0
Oleic Acid	<i>Cis</i> -C18:1	90
Elaidic Acid	<i>Trans</i> -C18:1	90
Linoleic Acid	C18:2	181
Linolenic Acid	C18:3	274



## 2.2 Reaction Mechanism

Based on Polanyi-Horiuti mechanism, the hydrogenation reaction starts by dissociative chemisorption of hydrogen molecule (H-H) to active sites on nickel catalyst (M) forming two polarised  $\sigma$ -bonded hydrogen on nickel (M-H). The carbon-carbon double bond also forms temporary  $\sigma$ -bond (M-C) by chemisorption at the catalyst active site through their  $\pi$ -system (C=C). When in close neighbourhood or adjacent to each other, the  $\sigma$ -bonded hydrogen on nickel (M-H) would react stepwise with the  $\sigma$ -bonded carbon (M-C) first forming a half-hydrogenated intermediate. Subsequently, if the other  $\sigma$ -bonded carbon atom in the half-hydrogenated intermediate becomes free, it can accept another  $\sigma$ -bonded hydrogen atom in the neighbourhood and the double bond of the carbon chain becomes saturated. The saturated compound is then desorbed due to lower adsorption strength compared to its previous unsaturated state. (Hoffmann, 1989; Dijkstra, 2006; Gutsche et al., 2004) The general scheme of this reaction mechanism is shown in Figure 2.2.

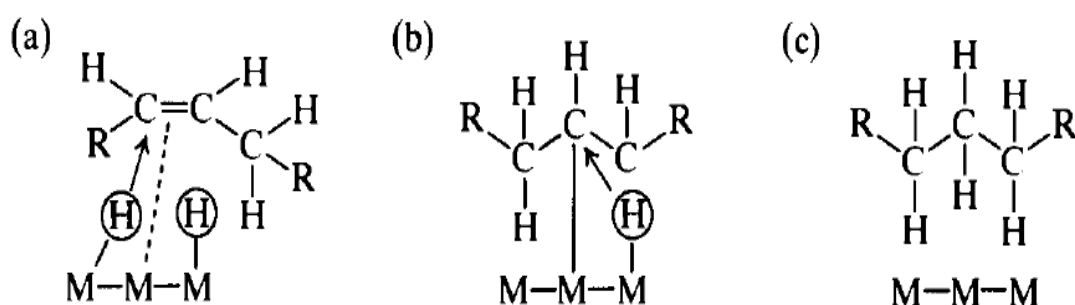


**Figure 2.2: Reaction mechanism of hydrogenation at the state of (a)  $\pi$ -complex (b) half-hydrogenated intermediate (c) saturated (Hoffman, 1989)**

In another explanation and illustration by Scrimgeour (2009), hydrogenation proceeds via two steps with a semi-hydrogenated intermediate as shown in Figure 2.3. The first step is the reversible addition of one hydrogen atom to form semi-hydrogenated intermediate. The semi-hydrogenated intermediate is unstable and tends to generate double bond with altered position or geometry through isomerisation (Step 2A). From the semi-hydrogenated intermediate, the reaction could also proceed via Step 2B, with the addition of the second hydrogen which is non-reversible and results in a saturated bond. It was reported that for saturation of dienes, the first step is the rate-limiting step while for saturation of monoenes, the rate-limiting step is the second step. In addition, low dissolved hydrogen concentrations favour isomerisation over saturation, hence allowing control of product composition by change in hydrogen pressure, agitation and reaction time.

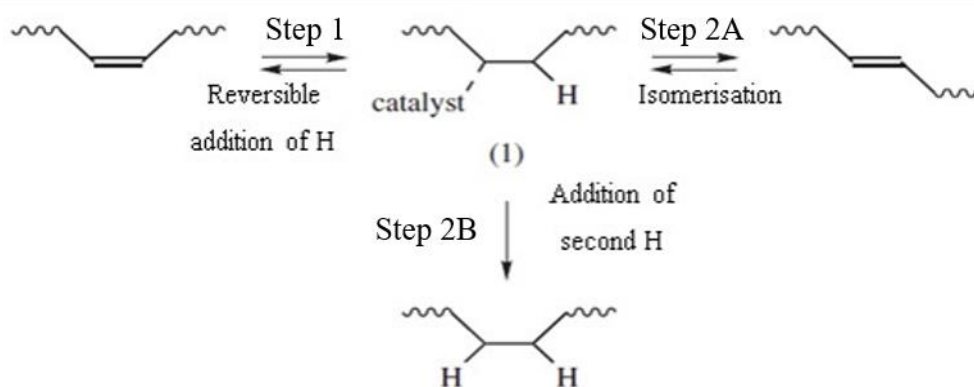


**Figure 2.3: Two-step hydrogenation scheme (Scrimgeour, 2009)**

### 2.3 Reaction Conditions

The typical conditions applied for partial hydrogenation of edible oils were reported in numerous journals as summarised in Table 2.2. Conventionally, nickel catalyst is employed in slurry reactor with temperature range of 140 – 230 °C and pressure range of 1 – 6 bar.

**Table 2.2: Typical partial hydrogenation conditions**

<b>Reference</b>	<b>Temperature (°C)</b>	<b>Pressure (bar)</b>	<b>Catalyst Type</b>	<b>Reactor Type</b>
Cepeda et al. (2016)	150 – 180	1 – 6	Nickel	-
Krstić et al. (2015)	140 – 230	low	Nickel	Slurry
McArdle et al. (2011)	170	1 – 6	Nickel	Semi-batch slurry
Tonetto et al. (2009)	180	1 – 6	Nickel	Semi-batch slurry
Schmidt and Schomacker (2007)	140 – 225	1 – 4	Nickel	Batch slurry
Fernández et al. (2007)	120 – 188	1 – 6	Nickel	Semi-batch slurry

## **2.4 Control of *Trans*-fats Formation**

The formation of *trans*-fats during hydrogenation could be controlled by adjusting reaction parameters including temperature, hydrogen pressure and mixing efficiency as well as modifying the type of catalyst used.

### **2.4.1 Change in Reaction Condition**

The conditions applied during hydrogenation would affect the concentration of hydrogen at the catalyst surface, which in turn, greatly influences the extent of hydrogenation and also *cis*- to *trans*- isomerisation (Dijkstra, 2006). *Cis*- to *trans*- isomerization is significant under hydrogen deficiency while formation of saturated C-C bonds is predominant under high surface hydrogen concentration (Simakova et al., 2008). Commonly studied parameters with critical influence on the reaction are temperature, pressure and stirring intensity.

#### **2.4.1.1 Temperature**

Beers (2007) showed that decrement of reaction temperature could significantly lower the *trans*-fatty acids formation of a reaction employing nickel catalyst. By lowering the reaction temperature to 40 – 60 °C, the *trans*-fatty acid content could be reduced to 6 %. However, the reaction activity would drop drastically and the percentage of saturates would increase. Temperature effect on *trans*-fats formation is more significant at high pressure condition. At high pressure, the

*trans*-fats content dropped with decrement of temperature from 15 % at 130 °C to 7 – 10 % at 100 °C (Belkacemi and Hamoudi, 2009).

#### **2.4.1.2 Pressure**

According to Beers (2007), hydrogen pressure could be increased to form wider coverage of hydrogen on the surface area of the catalyst. In order to achieve *trans*-fatty acid level of less than 10 %, hydrogen pressure more than 60 bar has to be applied at standard pressure conditions. This is not viable as the upper limit for existing edible oil plant facilities seldom reach more than 20 – 25 bar and also, under such high pressure, the saturated fats level can increase up to 30 %.

Cheng et al. (2014) tested the effect of changing pressure (2 bar and 5 bar) on hydrogenation of cottonseed oil and soybean oil respectively by using Ni, Pd and Pt catalysts. It was found that less *trans*-fatty acids were formed at higher pressure. The most significant reduction is from 41 % to 30 % which was achieved by using Pd catalyst in partial hydrogenation of soybean oil.

#### **2.4.1.3 Stirring Intensity**

The transport of hydrogen through the bulk liquid to the catalyst surface could be enhanced by increasing mixing efficiency. Increasing the stirrer speed to improve mixing efficiency could avoid hydrogen starvation on the catalyst surface and results in less *trans*-fatty acids formation (Beers, 2007). However,

the large step-up of stirrer speed would also require more powerful and robust mechanical facility.

Besides that, the impeller types used for stirring also affect the formation of *trans*-fats. Belkacemi and Hamoudi (2009) reported that when the sparger type impeller was used, *trans*-fats content was reduced down to 5 % while saturated fats content was as low as 3 %. Meanwhile when the traditional turbine type impeller was used, the *trans*-fats and saturated fats content were at 14 % and 9 % respectively.

#### **2.4.2 Change in Catalyst Type**

According to Dijkstra (2006), change in process conditions could only result in moderate reduction of *trans*-fats formation but it incurs large operating expenses. On the other hand, formulation of catalyst is one important factor affecting composition of *trans*-fats and saturated fats in the product (Stanković et al., 2015). Larger reduction of *trans*-fats formation is more likely to be achieved from development of new or novel catalysts. Other than nickel catalyst, the possibilities of employing or incorporating other catalytic materials including noble metal catalyst, multi-metallic catalyst and incorporation of Zn in Ni catalyst are explored.

### 2.4.2.1 Noble Metal Catalyst

It was reported by Fernández et al. (2005) and Savchenko and Makaryan (1999) that Pd is catalytically active at low temperatures unlike Ni, which enables hydrogenation to be carried out under low temperature to reduce *trans*-fats formation. With Pd catalyst, reaction temperature could be lowered to 50 °C with resulting *trans*-fatty acids content of 14.9 % (Liu et al., 2016). By increasing operating pressure up to 11 bar with Pd/C catalyst, *trans*-fatty acid level in the hydrogenation product could be further lowered down to 4 – 5 % (Simakova et al., 2008).

Nohair et al. (2004) added Cu to Pd catalyst but it reduced the activity and only slightly decreased *trans*-fats formation compared to Pd. Pd catalyst was also found to perform differently when the type of support was changed. It was reported that Pd supported on gamma-alumina ( $\gamma$ -Al<sub>2</sub>O<sub>3</sub>) showed the best activity compared to  $\alpha$ -Al<sub>2</sub>O<sub>3</sub>, ZSM-5 and MCM-22 supports. In addition, Pd/ $\gamma$ -Al<sub>2</sub>O<sub>3</sub> also slightly reduced *trans*-fats formation (18.6 %) compared to commercial nickel catalyst (21.7 %) (Fernández et al., 2009).

However, McArdle et al. (2011) reported that although Pd has higher activity than Ni, its effect on reduction of *trans*-fats formation is only comparable if not lower than Ni. The hydrogenation was carried out at 100°C, 10 bar and stirred at 600 rpm. It was highlighted that although Pt has lower activity than Pd, it has better *trans*-fat reduction effect than Pd and Ni. Cheng et al. (2014) also reported that Pt and Ni could achieve lower *trans*-fatty acids

content than Pd. Nonetheless, Pt catalyst is disadvantageous in terms of its high cost as compared to Ni catalyst.

#### **2.4.2.2 Multi-metallic Catalyst**

Incorporation of other catalytic metals into conventional metal catalysts to obtain synergistic effect remains a potential area to be explored. Hwang et al. (2013) opined that the use of dual metals in catalyst alters the electronic structure of the metals which helps to improve its catalytic performance. This is in agreement with Yu et al. (2013) which pointed out that bimetallic catalyst shows distinct electronic and chemical structure from their parent metal hence providing opportunity to obtain new catalyst with higher selectivity, activity and stability.

Addition of another catalytic metal benefits the parent metals in various ways. By combining noble and non-noble metals in a core-shell structure, high noble metal utilization could be achieved due to interposition with the non-noble metal core thus increasing the economics of the costly noble metal (Hwang et al., 2013). In addition, Persson et al. (2007) found that the incorporation of Pt into Pd catalyst could increase catalytic activity and the Pt would also improve stability of Pd during reaction.

The following subsections discuss different types of multi-metallic catalysts that have been employed to achieve higher selectivity in different reactions with emphasis on hydrogenation of fats.

#### **2.4.2.1.1 Nickel-Boron (Ni-B) Catalyst**

Li et al. (2009) showed that Ni-B alloy catalyst could achieve higher hydrogenation activity and lower *trans*-fatty acids formation as compared to Ni/SiO<sub>2</sub> catalyst. The *trans*-selectivity was low and the *trans*-fatty acids present in the hydrogenated product was around 7 % to 9 % which is much lower than the 15 % and 17 % obtained from the use of commercial Pd/C and Ni/SiO<sub>2</sub> catalyst respectively. However, the use of Ni-B resulted in significantly higher concentration of C18:0 and C18:2 and also lower *cis*-C18:1. Hunter (2005) opined that food products with low *trans*-fats but overly high saturated fats are not acceptable. Hence the goal of achieving very low *trans*-fats in partially hydrogenated oil remains challenging.

#### **2.4.2.1.2 Nickel-Magnesium-Silver Catalyst Supported on Diatomite (Ni-Mg-Ag/D)**

Stanković et al. (2009) compared Ni-Mg-Ag/D and Ni-Mg/D catalysts employed in partial hydrogenation of soybean oil. They reported that the addition of Ag reduced both the *trans*-selectivity and saturated fatty acids. Higher loadings of Ag on the catalyst produced the least amount of *trans*-fatty acids (26.3 %) while Ni-Mg/D produced 61.2 % of *trans*-fatty acids. However, the presence of Ag and higher loading of it decreased the hydrogenation activity. Despite that, reaction rate of the two catalysts were reported to be slightly higher compared to Ni/SiO<sub>2</sub> catalyst. Nevertheless, incorporation of Ag and higher loadings of it would incur higher cost, making it less favourable in the industry.

#### **2.4.2.1.3 Nickel-Cerium (Ni-Ce) Catalyst**

Konkol et al. (2016) reported that addition of low amount of cerium (0.65 wt %) could reduce *trans*-fats formation from 36.7 to 27.2 % with operating pressure at 2.5 bar. The figure could be further reduced to 18.7 % when the pressure is increased up to 21 bar. Level of saturated fats was also decreased with the addition of Ce. However, the activity dropped with the presence of Ce and the effect was more apparent with the increase of Ce concentration.

#### **2.4.2.3 Summary of Multi-metallic Catalysts**

In the effort to reduce *trans*-fats formation during hydrogenation of fats, various innovations of multi-metallic catalyst were reported. Table 2.3 summarises a few multi-metallic catalysts that were reported to show effective reduction of *trans*-fats formation as compared to Ni/SiO<sub>2</sub> catalyst. Albeit with the achievement of lower *trans*-fats formation, the catalysts were found to have their respective shortcomings in terms of overly high saturated fats formation, high cost and lower activity. The selection of multi-metallic catalyst for application in hydrogenation is dependent on the priority of requirement on the process performance. Comparisons of performance between the multi-metallic catalysts are difficult due to the difference in process conditions and slight variance in the basis of calculation used in quantifying the fats formation.

**Table 2.3: Performance of multi-metallic catalysts employed in hydrogenation of fats as compared to Ni/SiO<sub>2</sub> catalyst**

Catalyst	Activity	<i>Trans</i> -fats	Saturated Fats	Reference	Disadvantage
Ni-B	Higher	Lower	Significantly higher	Li et al. (2009)	Too high saturated fats
Ni-Mg-Ag/D	Slightly higher	Lower	Lower	Stanković et al. (2009)	High cost as it requires high Ag loading
Ni-Ce	Lower	Lower	Lower	Konkol et al. (2016)	Low activity

### 2.4.3 Incorporation of Zinc into Nickel Catalyst

The incorporation of Zn as ZnO in Cu/ZnO/Al<sub>2</sub>O<sub>3</sub> catalyst was widely studied and reported to significantly enhance the characteristics and catalytic performance of Cu/Al<sub>2</sub>O<sub>3</sub> catalyst, which is conventionally used for methanol synthesis. The addition of ZnO in Cu/Al<sub>2</sub>O<sub>3</sub> catalyst was reported to improve reducibility, increase surface area and pore volume as well as increase metal dispersion of the catalyst (Martin et al., 2015; Hoang et al., 2011). In view of the potentials and benefits, the effects of Zn or ZnO incorporation in Ni catalyst are reviewed in the following sub-sections.

#### **2.4.3.1 Incorporation of Zinc in Nickel Catalyst in Bulk**

Studt et al. (2008) employed density functional theory (DFT) calculations to screen numerous bimetallic compounds in their attempt of finding a new low-cost catalyst to replace Pd-Ag catalyst for hydrogenation of acetylene to ethylene. Ni-Zn alloy catalyst was found to stand out from the other candidates in terms of activity, selectivity, stability and low cost.

The superiority of Ni-Zn catalyst was also investigated and affirmed by Spanjers et al. (2014). The potential energy diagram obtained from DFT calculation showed that Ni-Zn has better activity and selectivity than Ni and comparable with the noble metal catalyst. This was verified by actual reaction results whereby in reaction employing Ni-Zn with higher Zn loading, the outlet ethane concentration (undesired product) was significantly lower than Ni catalyst. It was pointed out that the addition of Zn changed electronic properties of Ni on the surface, resulting changes in its adsorption properties.

Synthesis of the Ni-Zn catalyst was carried out by solid state diffusion method with a series of programmed-heating in a quartz tube. The catalyst was constantly stored in a glove box with argon gas environment to maintain the active metallic state of the catalyst. The synthesis and handling of the Ni-Zn catalyst appear to be more complex and more technically demanding as compared to the conventional Ni catalyst.

#### **2.4.3.2 Incorporation of Zinc in Trace Amount**

Addition of Zn in trace amount was found to improve the activity of Ni/SiO<sub>2</sub> catalysts for hydrogenation of fish oil and soybean oil (Feldhauser et al., 1997). However, the characteristics of the catalyst were not studied and the melting points of the hydrogenated fats were the only indicator of reaction selectivity with no analysis of fats composition.

#### **2.4.3.3 Incorporation of Zinc as Zinc Oxide**

Ni/ZnO/Al<sub>2</sub>O<sub>3</sub> catalyst was applied in deoxygenation of oleic acid to diesel-range alkanes by Chen et al. (2017). The catalyst was prepared at varying Zn/Al ratio by hydrothermal synthesis of ZnO/Al<sub>2</sub>O<sub>3</sub> followed by incipient wetness impregnation of Ni(NO)<sub>3</sub>. It was reported that at high Zn/Al ratio, the interaction between metal species and the support was weakened, hence resulting in higher reducibility but lower metal dispersion due to easier agglomeration. However, at low Zn/Al ratio, stronger interaction between the metal species and the support led to less presence of reduced Ni, which then decreased the deoxygenation activity. The optimum deoxygenation activity coupled with the highest alkane yield (95 %) was obtained at Zn/Al ratio of 2/1. Apart from that, the catalyst was reported to be mesoporous with pore size that decreased with increasing Zn/Al ratio.

#### **2.4.4 Other Alternatives**

Other than the change of process conditions and catalyst types, there are also attempts to reduce *trans*-fats formation by various other methods with their respective strengths and limitations.

##### **a) Use of Solvent**

Dijkstra (2006) reviewed that the use of super-critical propane which is a good solvent for oil and hydrogen could promote diffusivity of hydrogen during reaction and ensure that only fatty acids with high affinity would adsorb on the catalyst hence reducing *trans*-fats formation. However, the time needed to achieve adsorption equilibrium would need to be allocated by lowering the rate of hydrogenation and thus a lower production rate. It was also reviewed that treating Ni catalyst with ammonia before reaction could make it more selective and achieve *trans*-fats content of less than 1 %. Nevertheless, as useful as these additives may be, their usage is doubtful for food-grade product.

##### **b) Use of Additives**

Tonetto et al. (2009) reported that *trans*-fats formation could be controlled by modification of Pd catalyst with ethyl benzoate and magnesium glycinate which are edible additives. It was found that the additives could change the catalyst's electronic properties. Ethyl benzoate was found to increase *trans*-fats formation while magnesium glycinate was able to decrease *trans*-fats formation. The ab

initio calculation performed by them showed that Mg and Pd shared a short bond length which helped to promote attachment of hydrogens on the same side, forming *cis*- configuration.

#### **c) Use of Membrane Reactor**

Schmidt et al. (2007) attempted partial hydrogenation with membrane reactor that had Pd catalyst impregnated in the porous membrane. It was intended to avoid mass transfer limitation of the reactants to the catalyst and also to enable short contact time between reactants and catalyst. The short contact time was opined to be able to control and avoid complete hydrogenation to stearic acids. However, there was no observable reduction in *trans*-fats formation.

#### **d) Changing the Catalyst Form**

Boger et al. (2004) modified the catalyst configuration by using cordierite monolithic catalyst instead of powder form catalyst in slurry reactor. It was found that *trans*-fats formation was reduced as there was no mass transfer limitation. Despite higher manufacturing cost, the monolithic catalyst configuration was able to have repeated usage and easier to be separated from the products.

### e) **Inter-Esterification**

During inter-esterification, saturated fatty acids (15 %) were blended with non-hydrogenated liquid oil (85 %) that has no *trans*-fatty acids to yield products of intermediate characteristics and have no *trans*-fats. This is done through hydrolysis of triglycerides in liquid oils, followed by reformation of ester bonds between glycerol and mixed fatty acids (Tarragotrani et al., 2006). Hence, fatty acids of varying saturation would be randomly rearranged on the glycerol with the help of sodium methoxide catalyst or lipase enzyme (Hunter et al., 2005). The product formed would be free of *trans*-fats. However, this method requires complex equipment, long processing time and high cost (Hunter et al., 2005).

## 2.5 **Catalyst Synthesis**

Synthesis of catalysts is very diverse and each could follow a distinct route. Generally, three fundamental stages are involved during synthesis (Haber et al., 1995):

1. Preparation of precursory solids associating all the components required.
2. Processing of the solids to obtain catalyst precursor, most commonly by heat treatment.
3. Activation of precursors to get the active catalyst.

The synthesis of catalyst should be able to result in catalysts with high surface area, porosity, high mechanical strength and thermal stability. The following

subsections describe two common catalyst synthesis methods, namely co-precipitation and impregnation.

### **2.5.1 Co-Precipitation Method**

Synthesis of nickel catalyst on alumina support by co-precipitation for selective hydrogenation of fats and oils was demonstrated in a patent by Broecker et al. (1975). Metal precursor solution containing 2 M of nickel nitrate hexahydrate and aluminium nitrate nonahydrate were precipitated with 2 M of sodium carbonate at 80 °C while maintaining the pH at 6.5. This yielded precipitates which were the catalyst precursor in the form of hydrotalcites with the formula  $\text{Ni}_6\text{Al}_2(\text{OH})_{16}\text{CO}_3 \cdot 4\text{H}_2\text{O}$ . The slurry was then stirred at 80 °C for another 15 minutes before it was filtered and washed until no more nitrates could be detected in the filtrate. The precipitates were dried in oven at 110 °C and calcined at 350 °C for 20 hours followed by reduction by hydrogen for 20 hours in the range of 400 °C – 470 °C.

On a separate note, washing of the precipitates is a vital step. Thorough washing of the precipitates is required in order to remove the metal nitrates and other water soluble compounds on the precipitate such as sodium which originates from the use of sodium carbonate as a common precipitating agent. The presence of sodium was reported to block Ni surface sites, leading to loss of active metal surface area and greater sintering during reduction (Nemeth et al., 2017; Kondrat et al., 2017), demonstrating the importance of thorough washing of the precipitates.

According to Bouwman and Terorde (2011), for every 2 L of metal precursor solution employed in co-precipitation of catalyst, the precipitates have to be washed with approximately 30 L of water. The large volume of water used for washing is to ensure that metal nitrate salt is dissolved and removed before subsequent heat treatment as these water-soluble salts are unlikely to be properly removed during heat treatment. Acetone could also be used to wash off sodium residues on the precipitates as acetone is effective in solvating cations such as sodium ion due to the negative end of dipole and lone pair of electrons on its oxygen atom, which facilitate favourable interaction with the sodium ion (Brown et al., 2011; Weller et al., 1982).

Besides that, in another study by Ganguli et al. (1991), synthesis of alumina-supported nickel catalyst was reported to be a two-step process consisting of precipitation and ageing. Nickel nitrate was first precipitated with sodium carbonate at 20 °C and pH 9. The slurry was then simultaneously dosed with aluminium nitrate at 97 °C and pH 9.4 into an ageing reactor. The resulting slurry was stirred and aged for 90 minutes and filtered. The precipitates were washed with 4 L of distilled water followed by acetone. The wet cake was then dried in room temperature and reduced in hydrogen flow at 450 °C for 30 minutes. It was reported that the active nickel surface area achieved was 70 to 150 m<sup>2</sup>/g Ni and average pore size between 4 – 20 nm.

In comparison, Ganguli et al. (1991) used more severe conditions than Broecker et al. (1975). The results reported by Ganguli et al. (1991) were better in terms of lower stearic acids formation (8.2 %) and higher hydrogenation rate

(0.95 IV per minute), in contrast with Broecker et al. (1975) that had 8.9 % stearic acids formation and hydrogenation rate of 0.22 IV per minute.

Li et al. (2006) made comparison between Ni/Al<sub>2</sub>O<sub>3</sub> synthesised from co-precipitation method and impregnation method. Co-precipitation method resulted in formation of nickel aluminate surface spinel NiAl<sub>2</sub>O<sub>4</sub> after calcination which enables strong interaction between Ni<sup>2+</sup> and the support. This would lead to better stability and higher dispersion (> 7 %). On the other hand, NiO was formed alongside the nickel aluminate spinel on the catalyst prepared by impregnation method. Catalyst synthesised by impregnation method was easier to be reduced into active metals but they were easily sintered as well due to their weak bonding, resulting in lower dispersion and Ni surface area.

### **2.5.2 Impregnation Method**

During impregnation, a certain volume of solution containing the active phase precursor is made to be in contact with the solid support. For incipient wetness impregnation or dry impregnation, the volume of solution used is equal or slightly less than the pore volume of the support. Due to the limited impregnating solution in contact with the dry support, impregnation is carried out by capillary action hence enabling faster uptake of impregnating solution by the support. However, during subsequent drying and heat treatment, the capillary force also leads to rapid transport of impregnating solution to the surface of the pellets followed by deposition at the external edges, resulting in egg-shell like distribution of active phase (Geus, 2007). The maximum loading

of the active phase on the support is limited by the solubility of the precursor in the solution.

Dry impregnation method was used by Huang and Schwarz (1987) in their synthesis of alumina-supported nickel catalyst. The amount of metal deposited was controlled by the concentration of metal in the impregnation solution used. Huang and Schwarz used 2 g of gamma-alumina with 5 cm<sup>3</sup> of nickel nitrate hexahydrate as metal precursor solution. The pH of the solution was adjusted to the range of 1 – 5 by using nitric acid. The suspension was constantly shaken and allowed to dry completely. The solid samples were then dried at room temperature for 24 hours. It was found that at the same loading, the specific surface area and dispersion decreased with increasing pH of the impregnating solution. However, catalyst with loading of 0.9 wt% impregnated at pH 5 could achieve similar dispersion with catalyst with loading of 2.9 wt% impregnated at pH 1.

In another research by Bartholomew and Farrauto (1976), alumina-supported nickel catalyst was prepared by the dry impregnation method using pure nickel nitrate hexahydrate with gamma-alumina. The samples were dried in air at 80 °C to 100 °C. It was found that calcination at 400 °C for 1 hour is detrimental to the catalyst, causing reduction in surface area and dispersion. Hence it was suggested that the calcination was performed above 600 °C. It was subsequently reduced in hydrogen gas at heating rate of 5 °C/min to reach 230 °C and held at 230 °C for 1 hour. This was followed by heating slowly to 480 °C and hold for at least 10 hours. The slow heating during reduction was

required in order to prevent exothermic temperature that will badly sinter the catalyst.

Besides that, Espinosa-Alonso et al. (2008) also employed dry impregnation method in synthesising nickel catalyst supported on alumina with 3 wt% nickel. Ethylenediamine was introduced as chelating ligands in the precursor complex to be impregnated into pre-shaped alumina pellets. Beforehand, the alumina pellets were calcined at 450 °C for 8 hours and kept at 120 °C until use. The volume of precursor solution was equal to the support's pore volume and with a surplus of 10 %. The solution was added dropwise to the pellets and the pellets were shaken for 2 minutes for even distribution of solution. The 10 % excess solution was removed and the impregnated pellets were kept for 2 hours in a closed vessel and subsequently dried in preheated oven with static air at 100 °C for 8 hours. The use of chelating ligands was shown to influence the molecular interaction with the support and the macro-distribution of the active metal species.

### **2.5.3 Heat Treatment**

Typically, heat treatment is one of the most crucial steps in catalyst synthesis that adds the finishing touch to the catalyst to be ready for catalytic reaction. The first step of heat treatment is to remove the solvent (typically water) for the metal precursor. This is done by subjecting the wet catalyst precursor to static or flowing dry air at temperatures higher than the boiling point of the solvent or lower temperatures for gentler drying (Marceau et al., 2009). For solvent with

low viscosity, the movement of solvent away and out of the catalyst tends to drag along the metal precursors and results in segregation of metal precursors at pore mouths. However, this would only occur for nickel nitrate hexahydrate precursor if fast heating up to 200 °C is applied (Li et al., 1994).

After drying, the catalyst precursors would be subjected to prolonged high temperature heating to allow changes in solid phase to take place. The two common heat treatment for solid metal oxide catalysts are calcination and reduction, which could be carried out sequentially or in some cases, reduction is done directly without calcination. Calcination is carried out with presence of air at temperature ranging from 400 – 600 °C, generally to convert the metal precursors (salt) into metal oxides which could be activated into pure metal subsequently in reduction. During calcination, an array of processes occur in the catalyst, including loss of chemically bonded water or carbon dioxide molecules, sintering, modification of structure and stabilisation of mechanical properties (Perego and Villa, 1997).

For nickel catalyst supported on alumina, nickel aluminate spinel would also be formed alongside nickel oxide when heated at high temperature (Shalvoy et al., 1980). The strong interaction between  $\text{Ni}^{2+}$  and the support helps to maintain the position of the metals on the support, resulting in high dispersion (Li et al., 2006). However, the nickel aluminate spinel requires very high temperatures (700°C and above) to be reduced to the active nickel form. Meanwhile, nickel oxide have higher reducibility but it is easily sintered, causing a drop in dispersion.

Reduction is commonly carried out with flow of hydrogen gas which would react with the oxides to form water which is driven off with heat or flow of hydrogen gas, leaving behind pure and active metal sites on the catalyst. Reduction with increasing temperature for a same reduction time would increase catalyst metal dispersion whereas prolonging reduction time at a same temperature would give the opposite effect (Chen and Shiue, 1988). However, increase of either reduction temperature or time would increase sintering effect.

According to Bartholomew and Farrauto (1976), catalyst activation with hydrogen reduction without calcination was shown to produce catalyst with higher nickel surface area compared to those with prior calcination. However, care has to be taken when dealing with co-precipitated hydrotalcites in reduction without prior calcination as the substances liberated from the hydrotalcites such as CO and CO<sub>2</sub> might react exothermically with hydrogen, causing localised hot spots or uncontrolled rise in temperature on the solids. It could be prevented by heating the hydrotalcites in nitrogen gas flow prior to hydrogen gas, as to liberate and purge out the carbonates and hydroxyls (Lin et al., 2005) from the hydrotalcites before introduction of hydrogen gas.

## CHAPTER THREE

### METHODOLOGY

#### 3.1 Materials

The sunflower oil used for partial hydrogenation was Olife Sunflower Oil (Sime Darby Food and Marketing Sdn. Bhd., Malaysia). Iodine value and fats composition of the sunflower oil were analysed with the same method as the oil samples reported in Section 3.5. The sunflower oil has iodine value (IV) of 162 and its compositions as analysed with gas chromatography are listed in Table 3.1. All chemicals used were of analytical grade and obtained from Sigma Aldrich Malaysia, unless otherwise stated. Methylene chloride, methanol, hydrochloric acid and potassium hydroxide used for methylation of oil samples prior to gas chromatography analysis were obtained from Merck, Malaysia.

**Table 3.1: Fatty acids composition in Olife Sunflower Oil analysed by GC**

Compounds	Composition
Palmitic acid (C16:0)	6.0 %
Stearic acid (C18:0)	3.3 %
Oleic acid ( <i>cis</i> -C18:1)	42.0 %
Elaidic acid ( <i>trans</i> -C18:1)	0.0 %
Linoleic acid (C18:2)	48.4 %
Other C20 fatty acids	0.3%

### 3.2 Synthesis of Catalyst

The catalysts under study were synthesised by co-precipitation method with modifications from the patent by Ganguli et al. (1991). Catalysts with varying Ni and Zn molar ratio as shown in Table 3.2 were synthesised.

**Table 3.2: Designated stoichiometric molar ratio of synthesised catalysts**

Catalyst	Number of Moles			
	Nickel	Zinc	Aluminium	Sodium Carbonate
Ni/Al <sub>2</sub> O <sub>3</sub>	3	0	1	4.5
1_Ni/ZnO/Al <sub>2</sub> O <sub>3</sub>	1	2	1	4.5
2_Ni/ZnO/Al <sub>2</sub> O <sub>3</sub>	2	1	1	4.5
3_Ni/ZnO/Al <sub>2</sub> O <sub>3</sub>	1.5	1.5	1	4.5
ZnO/Al <sub>2</sub> O <sub>3</sub>	0	3	1	4.5

For synthesis of each sample, nickel nitrate, zinc nitrate, aluminium nitrate and sodium carbonate solutions were prepared respectively according to the designated Ni:Zn molar ratio of the respective sample in Table 3.2 with the use of nickel nitrate hexahydrate, zinc nitrate hexahydrate, aluminium nitrate nonahydrate and sodium carbonate. The mass of chemicals corresponding to the number of moles in Table 3.2 were uniformly scaled down with a factor of 60 to a lab-scale synthesis. The chemicals were dissolved in deionised water with the volume of deionised water calculated and adjusted to result in 0.3 M of nickel nitrate solution, 0.3 M of zinc nitrate solution, 0.94 M of aluminium nitrate solution and 1.79 M of sodium carbonate solution for synthesis of each

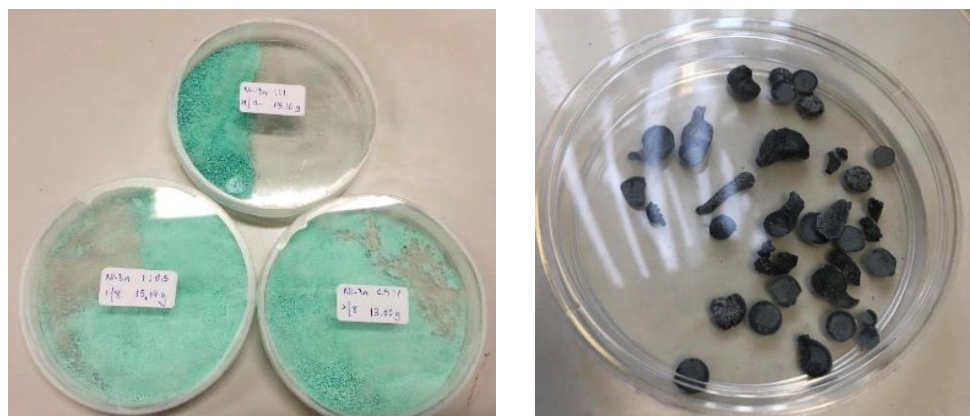
sample. The high molarity of sodium carbonate as a precipitating agent was required to ensure that the metal precursors were precipitated completely.

Each set of nickel nitrate and zinc nitrate solution were entirely mixed to form metal precursor solution. The metal precursor solution and sodium carbonate solution were added dropwise to a precipitating beaker. The pH of the slurry was maintained at 9.4, achieved by controlling the addition of sodium carbonate solution. The high pH reflects the presence of sodium carbonate in excess to facilitate precipitation. The slurry was vigorously stirred.

The slurry formed was then added dropwise into another beaker simultaneously with aluminium nitrate solution. The content was heated and maintained at 97 °C. The pH was also maintained at pH 9.0 by adding sodium carbonate solution when needed. The resulting slurry was aged by being stirred vigorously at 97°C and pH 9.0 for another 90 minutes. Sodium carbonate solution was added dropwise when necessary to maintain the pH. The slurry was filtered with the aid of filter paper and vacuum pump. The precipitate retained was washed with 1.5 L of hot deionised water followed by 335 ml of acetone. The washed precipitate was dried in oven at 100 °C for 1 hour.

The dried precipitate was reduced in 0.2 bar g hydrogen gas flow at 450 °C for 5 hours in a tube furnace. The tube furnace's temperature was ramped from room temperature at a rate of 10 °C/min in 0.8 bar g nitrogen gas flow prior to commencement of hydrogen gas flow. To prevent oxidation of reduced

Ni, samples intended to be used in hydrogenation reaction were coated with pure stearic acid to form pellets with 22 wt% of Ni.



(a)

(b)

**Figure 3.1: Catalyst samples after (a) oven-drying (b) hydrogen reduction and fats-coating**

### 3.3 Characterisation of Catalyst

All the synthesised catalysts without fats-coating were subjected to various analyses in order to determine their physical and chemical characteristics. The characterisation data could be interpreted to help in understanding the catalytic process.

#### 3.3.1 Inductively-Coupled Plasma Optical Emission Spectroscopy (ICP-OES) Analysis

The analysis on bulk composition of inorganic elements was performed on Inductively-Coupled Plasma-Optical Emission Spectrometer (Perkin Elmer Optima 7000 DV). Three replications of measurement were taken for each sample and a wash time of 120 seconds was allocated between analyses. The

synthesised catalysts were analysed for the presence of Ni, Zn, Al and Na. Prior to ICP-OES analysis, 0.01 g of each catalyst samples were completely digested in 100 ml of 2 M nitric acid at 100 °C in a reflux system for 2 hours. The solution was vigorously stirred throughout. For analysis of sodium content, 50 ppm of potassium was added into the calibration standards and samples by using KNO<sub>3</sub> solution in order to prevent ionisation interference. Calibration standards of 6.25 ppm, 12.5 ppm, 25ppm, 50 ppm and 100 ppm were prepared by using Ni(NO<sub>3</sub>)<sub>2</sub>·6H<sub>2</sub>O, Zn(NO<sub>3</sub>)<sub>2</sub>·6H<sub>2</sub>O, Al(NO<sub>3</sub>)<sub>3</sub>·9H<sub>2</sub>O, Na<sub>2</sub>SiO<sub>3</sub>, Mg(NO<sub>3</sub>)<sub>2</sub> and NaNO<sub>3</sub> dissolved in 2 M nitric acid respectively. Calculations involved in preparation of standards and samples for ICP-OES analysis are presented in Appendix A.

### **3.3.2 X-ray Photoelectron Spectroscopy (XPS) Analysis**

The analysis was conducted to determine the surface (1 – 12 nm depth) elemental composition as well as to determine the compound species present on the surface of the samples. Thermo Fisher Scientific K-Alpha X-ray Photoelectron Spectrometer was employed for the analysis at the excitation energy of Al Ka (1486.6 eV). Charge correction was performed by calibrating the C-C peak to 285 eV in the C 1s spectra. The spectra background were also subtracted by applying Shirley baseline. The XPS spectra were de-convoluted and fitted with OriginPro 8.5 graphing software to determine peaks corresponding to bonding between elements in the sample.

### **3.3.3 Scanning Electron Microscopy and Energy Dispersive X-ray Spectroscopy (SEM-EDXS) Analysis**

The SEM-EDXS analysis was carried out to determine the surface morphology and investigate the sub-surface (1  $\mu\text{m}$  depth) elemental composition of the sample. Hitachi S-3400N was employed with electron beam of 20 kV energy. Results from five different spots on the catalyst was obtained and the average reading was calculated.

### **3.3.4 Nitrogen Adsorption-Desorption Analysis**

The analysis was performed to determine the specific surface area, pore size and specific pore volume of the catalysts. The instrument employed was Thermo Scientific Sorptomatic. Samples were degassed at 200  $^{\circ}\text{C}$  overnight prior to analysis and the analysis was carried out at -196  $^{\circ}\text{C}$  (77 K). Specific surface area,  $S_{\text{BET}}$  was computed by Brunauer-Emmett-Teller (BET) method and specific pore volume,  $V_{\text{p}}$  was measured at  $P/P_0 = 0.99$ , both with reference to the adsorption branch. Pore size distribution was determined using Barrett-Joyner-Halenda (BJH) method with reference to the desorption branch of isotherm. Average pore diameter was calculated assuming cylindrical pores,  $d_{\text{p}} = 4V_{\text{BJH}}/S_{\text{BJH}}$ , where  $V_{\text{BJH}}$  is the pore volume and  $S_{\text{BJH}}$  is the surface area, both obtained from the desorption branch.

### **3.3.5 Hydrogen Temperature-Programmed Reduction (H<sub>2</sub>-TPR) Analysis**

The analysis was conducted to study the catalyst reducibility and type of reducible compound present in the catalyst. It determined the amount of hydrogen gas consumed during reaction and liberation of oxygen atoms from the compounds in the catalyst sample, along with increase in temperature. Thermo Scientific TPDRO 1100 with built-in thermal conductivity detector (TCD) was employed in this analysis. Pre-treatment was carried out before the analysis in which the samples were cleaned with nitrogen gas flow of 20 cm<sup>3</sup>/min starting from room temperature to 200 °C with heating ramp of 10 °C/min and held for 10 minutes. During TPR analysis, the sample was purged with 5.47% hydrogen in nitrogen gas flow of 25 cm<sup>3</sup>/min and heating from room temperature to 1000 °C with heating ramp of 5 °C/min.

### **3.3.6 Pulse Chemisorption Analysis**

The analysis was conducted to determine the amount of hydrogen chemically adsorbed on the metal active sites. Thermo Scientific TPDRO 1100 with built-in thermal conductivity detector (TCD) was employed in this analysis. The sample undergone 3 stages of conditioning in-situ, prior to pulse chemisorption as summarised in Table 3.3. The analysis was conducted at room temperature with 20 pulses of hydrogen gas (loop load: 3; loop volume: 0.351 cm<sup>3</sup>) with 10 minutes interval between pulses. Nitrogen gas flow of 20 cm<sup>3</sup>/min flow was used as the carrier gas.

**Table 3.3: In-situ conditioning stages prior to pulse chemisorption**

Stage	Gas	Flow Rate (cm <sup>3</sup> /min)	Ramp (°C/min)	Temperature (°C)	Holding Time (min)
Degassing	N <sub>2</sub>	20	10	120	60
Reduction	5.47% H <sub>2</sub> /N <sub>2</sub>	20	20	450	300
Degassing	N <sub>2</sub>	20	-	400	120

### 3.3.7 X-ray Diffraction (XRD) Analysis

The analysis was used to determine the crystallite phases, crystallinity and Scherrer's crystallite size of the catalyst. The catalyst sample in powder form was packed evenly in the sample holder until a smooth surface was obtained. The analysis employed Shimadzu LabX XRD-6000 with Cu K $\alpha$  radiation ( $\lambda = 1.54 \text{ \AA}$ ) operated at 30 mA and 40 kV. The scan was carried out from 3° to 80° at scanning rate of 2° per second at room temperature. Scherrer's crystallite size was calculated with Scherrer's equation based on the results obtained from XRD analysis, as presented in Appendix B1.

### 3.3.8 Transmission Electron Microscopy (TEM) Analysis

The analysis was carried out to obtain lattice fringe images of the catalyst surface. The analysis was conducted on the synthesised catalyst samples that showed the best results from hydrogenation (3\_Ni/ZnO/Al<sub>2</sub>O<sub>3</sub> and Ni/Al<sub>2</sub>O<sub>3</sub>). Prior to analysis, the sample powder was dispersed in ethanol with the use of

direct probe ultra-sonicator for 2 minutes and immediately transferred dropwise onto a carbon film on copper 300 mesh. The excess ethanol was then let to dry off. The analysis employed JEOL JEM-ARM200F Transmission Electron Microscope at 200 kV. The lattice spacing in the TEM images obtained were measured with ImageJ to identify the crystal lattices. In ImageJ, measurement were conducted across ten lattice fringes to obtain the single lattice spacing. The reference lattice spacing for each species under study were calculated with Miller Indices as demonstrated in Appendix B2.

### **3.4 Partial Hydrogenation**

Partial hydrogenation was carried out in a 1 L batch slurry reactor (Buchiglasuster Eco-Clave). The reactor temperature was regulated by Huber Unistat Tango Nuevo with the use of silicone oil jacket around the reactor and temperature probe in the reactor. For all the samples, the reaction conditions were set at 180 °C, 5 bar g and 2000 rpm similar to the typical industrial condition used.

For a set of reaction, 1 L of sunflower oil was added into the reactor with the aid of vacuum pump. The oil was heated by the heating jacket with set-point temperature of 180 °C. The reactor was vacuumed and then purged with nitrogen gas to remove the air present in the reactor. Any water content present in the feed was also removed in the process as it will poison the catalyst.

When the slurry temperature reached 180 °C, 2 g of catalyst was introduced and hydrogen gas at 5 bar g was charged in to start the reaction. The slurry was vigorously stirred by impeller at 2000 rpm. Oil samples were taken at intervals of 10 minutes. The reaction was stopped when the iodine value exceeded 70 or when reaction time reached 480 minutes, whichever came first.

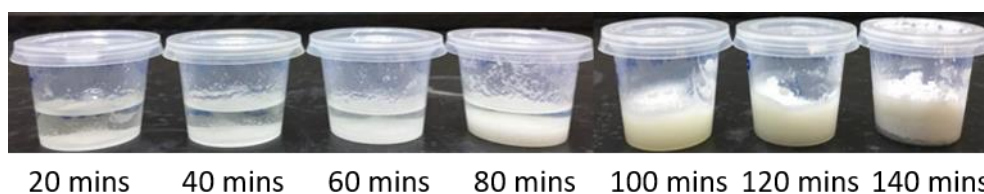


**Figure 3.2: Oil samples collected at different time intervals with increasing solid fats content showing progress of partial hydrogenation**

### **3.5 Partial Hydrogenation Product Analyses**

Oil samples taken from the reactor were subjected to iodine value test and gas chromatography (GC) analysis to determine the extent of hydrogenation and study the resulting change in oil composition.

#### **3.5.1 Iodine Value (IV) Test**

Oil samples collected from the reactor were subjected to iodine value test according to American Oil Chemist's Society (AOCS) Official Method Tg 1a-64 (AOCS, 2003). The oil sample was melted, if it was not already liquid, and filtered through filter paper to remove impurities and traces of moisture. The sample was weighed into a conical flask according to the recommended mass for each IV range attached in Appendix C. The weighed sample was added with

15 ml of cyclohexane and acetic acid mixture with 1:1, v/v ratio which served as a solvent to dissolve the oil sample.

The flask was added with 25 ml of Wijs solution (iodine monochloride, ICl), stoppered and swirled until an intimate mixture was formed to enable addition reaction between the C=C double bonds present in the oil sample and the ICl. Simultaneously, a blank set was prepared with steps c – d without the addition of oil sample. Both sets of flasks were stored in a dark place for 30 minutes at room temperature. The flasks were removed from the dark place and added with 20 ml of 15 % potassium iodide solution to convert the remaining unreacted ICl into I<sub>2</sub>. 100 ml of distilled water was added to the lip of the flasks to absorb any iodine that may leak past the stopper.

The flasks were each titrated with sodium thiosulphate solution of 0.1 normality until a pale yellow colour appeared as the dark yellow I<sub>2</sub> solution was reduced by sodium thiosulphate into I<sup>-</sup> which was colourless. Concurrently, I<sub>3</sub><sup>-</sup> species was formed from combination of I<sub>2</sub> and I<sup>-</sup> in the solution. The pale yellow colour solution was added with 1 – 2 ml of 1 % starch solution to form a blue-black colour solution due to the formation of starch tri-iodide complex, which served as an endpoint indicator. The titration was continued until the blue-black colour disappeared, indicating that all the I<sub>2</sub> and I<sub>3</sub><sup>-</sup> species were reduced into I<sup>-</sup>. The resulting iodine value was calculated with the following formula and sample calculations were demonstrated in Appendix C.:

$$\text{Iodine Value} = \frac{(B - S) \times N \times 12.691}{\text{mass of sample, g}}$$

Where B = volume of titrant of blank set, in ml

S = volume of titrant of sample set, in ml

N = normality of sodium thiosulphate solution

### 3.5.2 Gas Chromatography (GC) Analysis

The analysis was conducted with Perkin Elmer Clarus 500 Gas Chromatography to analyse the fatty acids composition in the samples. The column used was Perkin Elmer COL-ELITE-2560 (100 m × 0.25 mm ID × 0.20 μm df). Helium gas was used as the carrier gas with flowrate of 2 ml/min at 1.7 bar (24.7 psi). The detector temperature was set at 220°C, the injector temperature at 250°C and flame ionization temperature at 270°C. Pure fatty acids standards were used to determine the retention time for each fatty acids species. The fatty acids composition was determined by the relative area under the corresponding peaks in GC chromatogram, with sample calculation shown in Appendix D1.

The oil samples obtained from reactor were esterified to fatty acid methyl esters (FAME) prior to GC analysis according to the steps as reported by Jham et al. (1982). The oil sample was melted, if it was not already liquid, and filtered through filter paper to remove impurities and traces of moisture. Subsequently, 0.2 ml of oil sample was heated in reflux with 4 ml of 0.5 M potassium hydroxide in absolute methanol (KOH/MeOH) at 100°C for 5 minutes.

Following that, 1.6 ml of aqueous hydrochloric acid in absolute methanol (HCl/MeOH, 4:1, v/v) was added into the mixture and heated in reflux at 100°C for 15 minutes. The mixture was cooled down followed by addition of 5 ml distilled water and 10 ml dichloromethane into the mixture. The mixture was poured into a separatory funnel and the lower layer of organic solution was extracted.

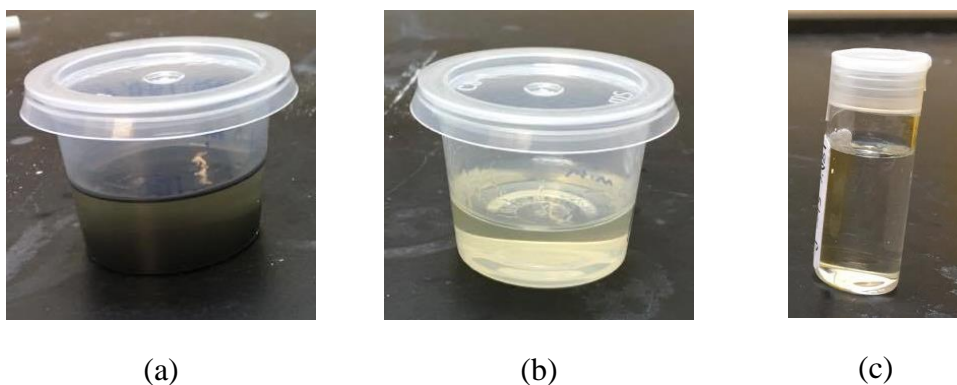


**Figure 3.3: Oil samples from partial hydrogenation (a) before filtration (b) after filtration (c) after esterification and dissolved in dichloromethane**

### 3.5.3 Evaluation of Catalyst Activity and Selectivity

The activity of catalyst samples in the reaction was calculated by the following formula with sample calculation demonstrated in Appendix D2:

$$\text{Activity} = \frac{\text{Initial iodine value} - \text{Final iodine value}}{\text{Reaction time taken to reach IV 70, minutes}}$$

Selectivity of the catalyst samples towards saturated fats and *trans*-fats were calculated respectively at IV 70 with the following formula:

Selectivity of *trans* C18: 1

$$= \frac{\text{Composition of } \textit{trans} \text{ C18: 1}}{\text{Total composition of } \textit{trans} \text{ and } \textit{cis} \text{ C18: 1}} \times 100\%$$

Selectivity of C18: 0

$$= \frac{\text{Composition of C18: 0}}{\text{Total composition of } \textit{trans} \text{ C18: 1 and C18: 0}} \times 100\%$$

## **CHAPTER FOUR**

### **RESULTS AND DISCUSSION**

#### **4.1 Catalyst Characterisation**

The physical and chemical characteristics of the samples were determined through a series of analyses. Knowledge of the catalyst characteristics is important to study its performance-determining factors, which enables further understanding of its catalytic performance.

##### **4.1.1 Catalyst Composition**

The composition of elements in the synthesised catalysts are summarised in Table 4.1 while the peak-fittings of XPS spectra are shown in Figure 4.1. Assessment of the catalysts under ICP-OES analysis shows the bulk composition while XPS and EDXS analyses show results corresponding to the composition at the surface and sub-surface respectively due to their difference in penetration depth during analysis. It is noted that the bulk composition of synthesised catalysts matched their designated molar ratio set during synthesis, confirming the successful synthesis of the specified catalysts with varying molar ratio.

**Table 4.1: Elemental composition for synthesised catalyst samples from XPS, EDXS and ICP-OES analyses**

<b>Catalyst Sample</b>	Ni/Al <sub>2</sub> O <sub>3</sub>	2_Ni/ZnO/Al <sub>2</sub> O <sub>3</sub>	3_Ni/ZnO/Al <sub>2</sub> O <sub>3</sub>	1_Ni/ZnO/Al <sub>2</sub> O <sub>3</sub>	ZnO/Al <sub>2</sub> O <sub>3</sub>	
<b>Designated Molar Ratio (Ni:Zn:Al)</b>	3: 0: 1	2: 1: 1	1.5: 1.5: 1	1: 2: 1	0: 3: 1	
<b>ICP -OES (At %)</b>	Ni	32.37	22.17	9.83	15.73	-
	Zn	-	11.94	21.71	17.20	32.05
	Al	9.50	10.37	9.95	11.47	12.31
	Na	0.40	0.42	0.80	0.79	0.74
	Ni+Zn	32.37	34.11	31.54	32.93	32.05
	Ni+Zn+Al	41.87	44.48	41.49	44.40	44.36
	Zn/Ni ratio	-	0.54	2.21	1.09	-
<b>XPS (At %)</b>	Ni 2p <sub>3/2</sub>	11.67	11.53	6.82	10.00	-
	Zn 2p <sub>3/2</sub>	-	9.80	15.78	12.66	24.97
	Al 2p	9.77	11.77	13.98	9.06	9.21
	Na	-	-	-	-	-
	Ni+Zn	11.67	21.33	22.60	22.66	24.97
	Ni+Zn+Al	21.44	33.10	36.58	31.72	34.18
	Zn/Ni ratio	-	0.85	2.31	1.27	-
<b>EDXS (At %)</b>	Ni	46.66	26.10	16.44	27.19	-
	Zn	-	10.37	22.87	14.97	43.96
	Al	9.70	15.98	11.14	13.89	9.55
	Na	-	-	-	-	-
	Ni+Zn+Al	56.36	52.45	50.45	56.05	53.51
Zn/Ni ratio	-	0.40	1.39	0.55	-	
<b>Degree of ZnO Migration <sup>a</sup></b>	-	1.57	1.17	1.05	-	

<sup>a</sup> Ratio of surface Zn/Ni ratio (from XPS) to bulk Zn/Ni ratio (from ICP-OES).

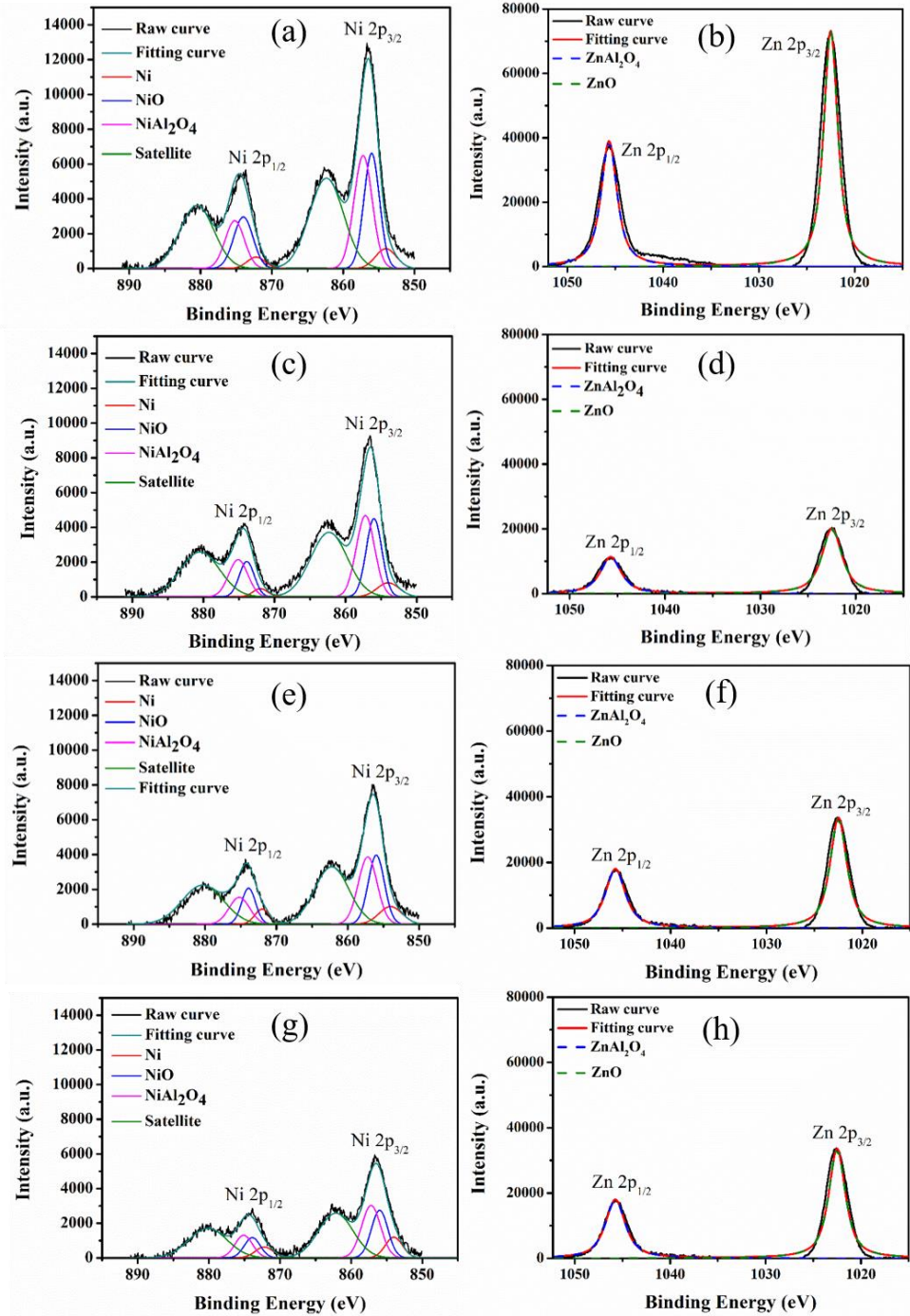


**Figure 4.1:** Ni 2p<sub>1/2</sub>, Ni 2p<sub>3/2</sub>, Zn 2p<sub>1/2</sub> and Zn 2p<sub>3/2</sub> XPS spectra for (a) Ni/Al<sub>2</sub>O<sub>3</sub> (b) ZnO/Al<sub>2</sub>O<sub>3</sub> (c)-(d) 2\_Ni/ZnO/Al<sub>2</sub>O<sub>3</sub> (e)-(f) 3\_Ni/ZnO/Al<sub>2</sub>O<sub>3</sub> (g)-(h) 1\_Ni/ZnO/Al<sub>2</sub>O<sub>3</sub>

It could be observed from Table 4.1 that the total elemental metal percentage (Ni+Zn+Al) are consistent between the synthesised samples. However, this consistency was not shown at the surface for Ni/Al<sub>2</sub>O<sub>3</sub>, whereby

the total metal atomic percentage (21.44 At %) deviated from the other samples (31.72 – 36.58 At %). This deviation on the surface of Ni/Al<sub>2</sub>O<sub>3</sub> is caused by attenuation of metal species composition by the inevitable formation of oxygen-rich compounds such as metal oxides and organic contaminants on the surface when exposed to the ambient environment (Hoffer et al., 2000). With reference to the C 1s spectra (Appendix E) obtained from XPS analysis, the notably high intensity HCOOH peak indicates that higher level of carbon-oxygen contaminants were present on the surface of Ni/Al<sub>2</sub>O<sub>3</sub> compared to the other samples and contributed in the seemingly high oxygen composition.

Apart from that, there are also extensive formation of NiO and NiAl<sub>2</sub>O<sub>4</sub> species on the surface of Ni/Al<sub>2</sub>O<sub>3</sub>, as observed from the high intensity and area of NiO and NiAl<sub>2</sub>O<sub>4</sub> peaks in the de-convoluted XPS fitting curve (Figure 4.1(a)). The extensive formation of NiAl<sub>2</sub>O<sub>4</sub> species on the surface of Ni/Al<sub>2</sub>O<sub>3</sub> rather than Ni/ZnO/Al<sub>2</sub>O<sub>3</sub> could be attributed to the difference in site preference energy between Zn<sup>2+</sup> (32 kJ/mol) and Ni<sup>2+</sup> (50 kJ/mol), based on the theory postulated by Bolt et al. (1998) on the rate of aluminate spinel formation. It was reported that Zn<sup>2+</sup> which has lower site preference energy, could diffuse through vacancies in the lattices of alumina with more mobility than Ni<sup>2+</sup>, and resulted in its higher rate of aluminate spinel formation (Bolt et al., 1998).

In this case, the presence of Zn<sup>2+</sup> in Ni/ZnO/Al<sub>2</sub>O<sub>3</sub> catalyst has dominance over Ni<sup>2+</sup> in the formation of aluminate spinel, hence indirectly helped to suppress the formation of NiAl<sub>2</sub>O<sub>4</sub> in Ni/ZnO/Al<sub>2</sub>O<sub>3</sub> catalyst, which is in contrast with the higher NiAl<sub>2</sub>O<sub>4</sub> formation on the surface of the Ni/Al<sub>2</sub>O<sub>3</sub>

catalyst. The suppression of  $\text{NiAl}_2\text{O}_4$  formation by Zn helped to maintain more Ni in the active state for reaction or in the NiO state which is more reducible than  $\text{NiAl}_2\text{O}_4$ . Similarly, the presence of Zn in the precursor of Ni/ZnO/ $\text{Al}_2\text{O}_3$  catalyst is also deduced to help suppress formation of NiO species. As Zn has higher affinity towards oxygen compared to Ni based on the metal reactivity series, more oxygen would be reacted with Zn to form ZnO during heat treatment, hence resulting in less NiO formation compared to Ni/ $\text{Al}_2\text{O}_3$  catalyst.

Despite the consistency of total metal percentage between the samples, there are notable variations when compared between the catalyst structures (surface, sub-surface and bulk). It can be seen that the Ni+Zn+Al percentage at the surface (21.44 – 36.58 At % in XPS) is lower than at the bulk (41.49 – 44.48 At % in ICP-OES) while the sub-surface (50.45 – 56.36 At % in EDXS) is higher than the bulk. It is deduced that there was movement of elemental species between the catalyst surface and sub-surface during reduction. When the hydrotalcites were being reduced at high temperature, the layered  $\text{Ni}_3\text{Zn}_3\text{Al}_2(\text{OH})_{16}\text{CO}_3 \cdot 4\text{H}_2\text{O}$  structure collapsed with the removal of carbonate ions and hydroxide ions while the metal atoms gained mobility and changed from multi-cationic compounds to supported metal species (Lin et al., 2005).

The movement of species in the catalyst could be further validated from the ratio of Zn to Ni of the samples at each catalyst structure (i.e. surface, sub-surface, bulk). It can be seen that the Zn/Ni ratios at bulk are in agreement with their respective designated molar ratio. However, the Zn/Ni ratios at the surface and sub-surface deviate from the ratio at bulk and increase from the sub-surface

to the surface. This implies that there were enrichment of Zn at the surface and deficiency of Zn at the sub-surface, resulted by migration of Zn species (zinc oxide) from the sub-surface to the surface.

Similar observations of Zn enrichment at the surface were also reported for Cu/ZnO catalyst (Behrens et al., 2012; Naumann d'Alnoncourt et al., 2006; Viitanen et al., 1999), in which the migration was attributed to the difference in surface energy between Zn and Cu. It was also reported that Zn has a negative segregation energy in Ni-Zn alloys as calculated by density functional theory (DFT) and tends to segregate outwards (Yu et al., 2016). In present case, the surface free energy of ZnO ( $0.74 \text{ J/m}^2$ ) (Rasmussen et al., 2012) is significantly lower than  $\text{Al}_2\text{O}_3$  ( $1.54 \text{ J/m}^2$ ) (Castro et al., 2006; Castro and Quach, 2012) and Ni ( $2.080 \text{ J/m}^2$ ) (Tyson and Miller 1977), which inevitably acts as a driving force of ZnO migration to the surface.

The migration of ZnO is interpreted with the degree of ZnO migration, calculated by the ratio of surface Zn/Ni (from XPS) to bulk Zn/Ni (from ICP-OES). It is apparent that the degree of ZnO migration decreased with higher bulk ZnO content in the catalyst, showing that ZnO migration is more prevalent when the presence of ZnO is in low quantity. Conversely, ZnO migration becomes limited when ZnO is the major constituent. It is inferred that when ZnO is the major constituent, the difference in surface energy is less prominent throughout the body of molecules as more ZnO molecules are surrounded by likewise species. With a lower contrast of surface energy, the driving force of ZnO migration diminished (Behrens et al., 2012).

Elemental composition of the catalysts in Table 4.1 also showed a small atomic percentage of sodium which originated from the use of sodium carbonate as the precipitating agent during synthesis. It is present in the bulk as detected by ICP-OES analysis but found absent on the surface and sub-surface by XPS and EDXS analyses. This could be due to the thorough washing of wet precipitates with hot deionised water and acetone, which are good solvents of sodium ions (Brown et al., 2011; Weller et al., 1982). Nonetheless, the sodium residing in the inner cores of the catalysts might be more difficult to remove by washing, hence resulting in the residual sodium detected.

Further analysis of the peaks from XPS analysis with peak deconvolution and fitting in Figure 4.1 shows that the species present in Ni-containing samples are Ni (854 eV), NiO (856 eV) and NiAl<sub>2</sub>O<sub>4</sub> (857.2 eV), while in samples containing ZnO, the species present are ZnO (1022.5 eV) and ZnAl<sub>2</sub>O<sub>4</sub> (1045.9 eV). The species detected in the main Ni 2p<sub>3/2</sub> peak could also be seen in the Ni 2p<sub>1/2</sub> peak with an area ratio of 2:1, which further validates the peak-fitting in the Ni 2p<sub>3/2</sub> peak. Concurrently, satellite peaks due to presence of Ni<sup>2+</sup> species in paramagnetic state are also observed in the Ni 2p spectra, which is typical for samples containing NiO and NiAl<sub>2</sub>O<sub>4</sub> species (Cheng et al., 2015; Molina and Poncelet, 1999).

Besides that, the XPS peak-fitting shows that ZnO is present in the sample rather than Zn after hydrogen reduction as at the present reduction temperature of 450 °C, reduction of ZnO to Zn could not take place. Hydrogen reduction of ZnO to Zn was reported to only occur at temperatures above 600 °C

(de Siqueira et al., 2014). The presence of Ni-O, Zn-O, Ni-Al, Al<sub>2</sub>O<sub>3</sub> and Al<sub>2</sub>O<sub>4</sub> bonding in the samples are also supported by the XPS peak-fitting for the spectra of Al 2p, C 1s and O 1s appended in Appendix E.

On the other hand, elemental mapping of 3\_Ni/ZnO/Al<sub>2</sub>O<sub>3</sub> catalyst for each element are shown in Figure 4.2. It is deduced that the distribution of Ni, Zn and Al in the catalyst are even, consistent and homogeneous in spite of employing 2-step co-precipitation method during synthesis. Elemental mapping of the other samples attached in Appendix F are also noted to share similar observation.

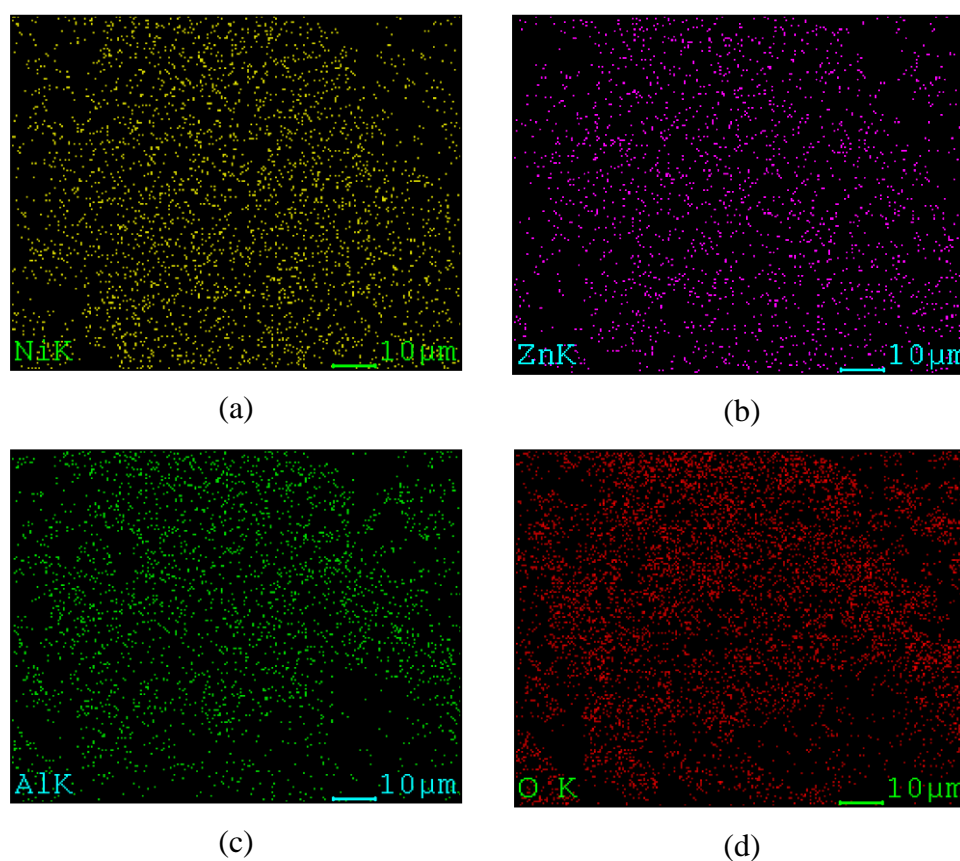


**Figure 4.2: EDXS element mapping of 3\_Ni/ZnO/Al<sub>2</sub>O<sub>3</sub> catalyst for elements of (a) nickel (b) zinc (c) aluminium and (d) oxygen**

The surface morphology of the catalysts as visualised with SEM analysis are shown respectively in Figure 4.3. It can be observed that Ni/Al<sub>2</sub>O<sub>3</sub> catalyst showed a comparable flat and blunt surface while ZnO/Al<sub>2</sub>O<sub>3</sub> catalyst showed a rough surface blanketed with small, sharp folds. Interestingly, the small, sharp folds are seen to be prominent in 1\_Ni/ZnO/Al<sub>2</sub>O<sub>3</sub> and 3\_Ni/ZnO/Al<sub>2</sub>O<sub>3</sub> catalysts in which ZnO is a major constituent. When ZnO is a minor constituent, they are barely visible as observed in 2\_Ni/ZnO/Al<sub>2</sub>O<sub>3</sub> catalyst, indicating that the morphology of small, sharp folds on a rough surface are characteristic to the presence of ZnO in the catalyst.

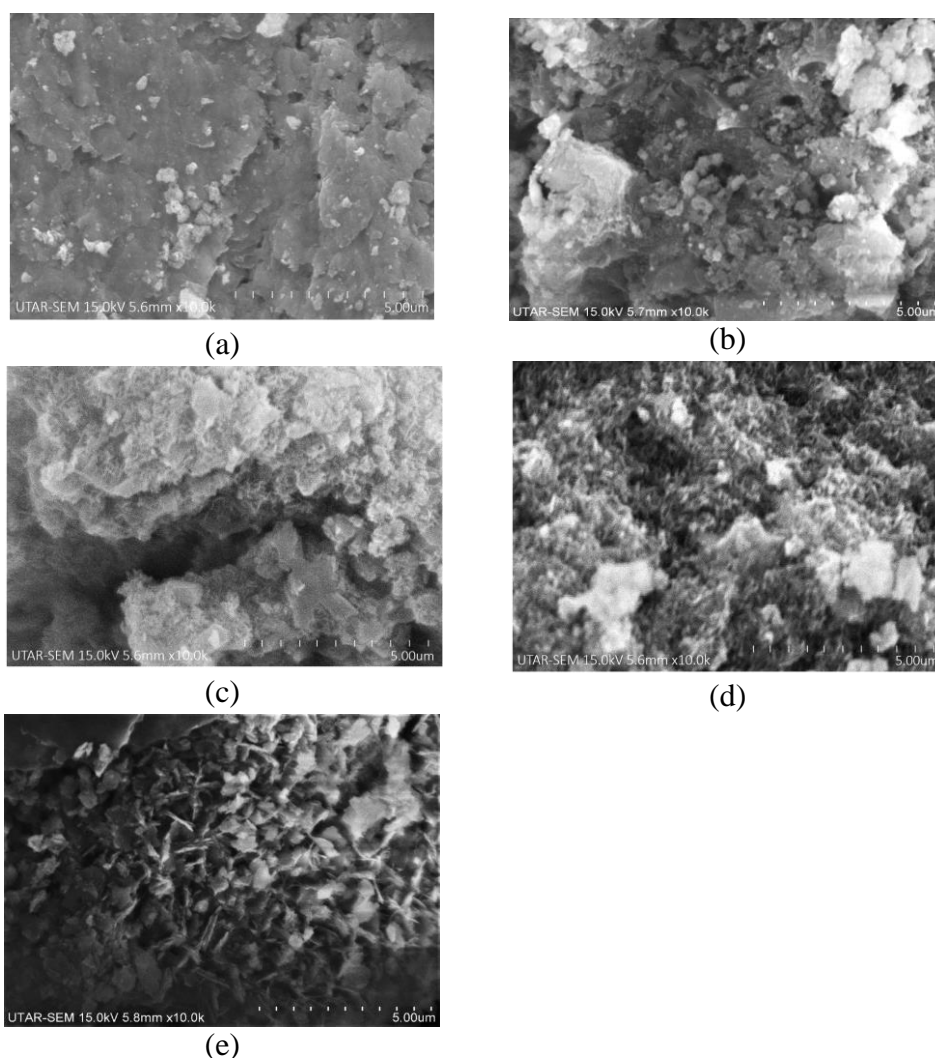


**Figure 4.3: SEM images showing surface morphology of (a) Ni/Al<sub>2</sub>O<sub>3</sub> (b) 2\_Ni/ZnO/Al<sub>2</sub>O<sub>3</sub> (c) 3\_Ni/ZnO/Al<sub>2</sub>O<sub>3</sub> (d) 1\_Ni/ZnO/Al<sub>2</sub>O<sub>3</sub> (e) ZnO/Al<sub>2</sub>O<sub>3</sub>**

### 4.1.2 Pore Structure

The pore characteristics of the catalysts under study are shown in Table 4.2 while the pore size distribution curves are shown in Figure 4.4. It is apparent that the pore characteristics were affected by the incorporation of ZnO into Ni/Al<sub>2</sub>O<sub>3</sub> at varying composition. The pore characteristics were found to follow the ratio of surface Zn/Ni to sub-surface Zn/Ni in the catalysts, in which a higher ratio led to larger specific surface area, specific pore volume and average pore diameter. A higher ratio of surface Zn/Ni to sub-surface Zn/Ni indicates a larger contrast of ZnO content between the two surfaces. It is deduced that the shortage of ZnO in the interior of the catalyst following ZnO migration to the surface, resulted in the creation of more pores and also wider pores, as the migration left behind cavities or more loosely packed structure in the interior of the catalyst.

**Table 4.2: Specific surface area,  $S_{BET}$ , specific pore volume,  $V_p$  and average pore diameter,  $d_p$  of the catalysts obtained from nitrogen adsorption-desorption analysis**

Catalyst	$\frac{(Zn/Ni)_{surface}}{(Zn/Ni)_{Sub-surface}}$ <sup>a</sup>	$S_{BET}$ (m <sup>2</sup> /g)	$V_p$ <sup>b</sup> (cm <sup>3</sup> /g)	$d_p$ <sup>c</sup> (nm)
Ni/Al <sub>2</sub> O <sub>3</sub>	-	42.94	0.244	15.55
2_Ni/ZnO/Al <sub>2</sub> O <sub>3</sub>	2.13	98.05	0.393	11.31
3_Ni/ZnO/Al <sub>2</sub> O <sub>3</sub>	2.31	112.66	0.860	27.95
1_Ni/ZnO/Al <sub>2</sub> O <sub>3</sub>	1.67	24.86	0.065	10.89
ZnO/Al <sub>2</sub> O <sub>3</sub>	-	67.63	0.387	17.17

<sup>a</sup> Ratio of Zn/Ni from XPS analysis over Zn/Ni from EDXS analysis.

<sup>b</sup> Specific pore volume measured at  $P/P_0 = 0.99$

<sup>c</sup> Average pore size calculated by  $d_p = 4V_{BJH}/S_{BJH}$

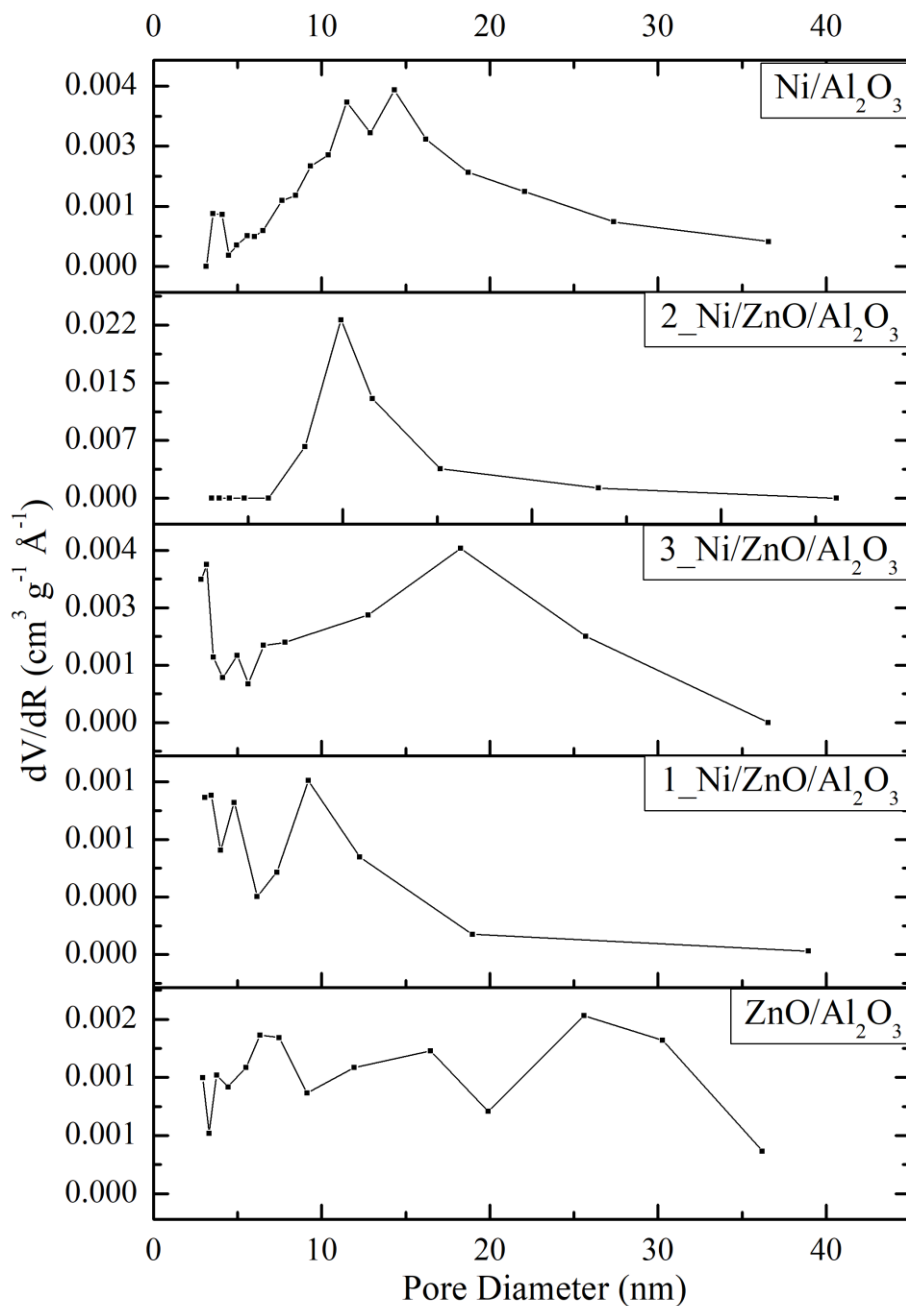


**Figure 4.4: Pore size distribution curves**

It is interesting to note that sample 3\_Ni/ZnO/Al<sub>2</sub>O<sub>3</sub> showed pore characteristics that surpassed the single-metal catalyst of Ni/Al<sub>2</sub>O<sub>3</sub>, demonstrating the strong influence of ZnO in modifying the Ni catalysts. On the other hand, sample 1\_Ni/ZnO/Al<sub>2</sub>O<sub>3</sub> which experienced the least ZnO migration,

showed the smallest specific surface area, specific pore volume and average pore diameter. This could also be observed in the pore size distribution curve where there is incremental distribution of large pores from sample 1\_Ni/ZnO/Al<sub>2</sub>O<sub>3</sub> to 2\_Ni/ZnO/Al<sub>2</sub>O<sub>3</sub> and 3\_Ni/ZnO/Al<sub>2</sub>O<sub>3</sub>.

The size of pores will imperatively influence the diffusion and access of reactants to the active sites on the catalyst as partial hydrogenation of oils involves large and bulky molecules of triglycerides. It was demonstrated by Coenen (1986) that pores narrower than 2 nm prohibit the diffusion of triglycerides, while pores wider than 3.5 nm are necessary to allow access to the nickel active sites. Diffusion of triglycerides at this pore size is possible but is still limited by the frequent collision with the pore walls. In a more recent study by Witoon et al. (2014), diffusion limitation of palm oil was still observed for catalysts with average pore size around 12 nm. In contrast with the current work, wide pores in 3\_Ni/ZnO/Al<sub>2</sub>O<sub>3</sub> catalyst alleviates diffusion limitation and facilitates the diffusion of triglyceride molecules in pores, which may enhance the hydrogenation activity. The relationship between hydrogenation activity and pore size will be discussed in Section 4.2.1.

### **4.1.3 XRD and TEM Analyses**

Figure 4.5 shows the XRD spectra for the hydrotalcites obtained from coprecipitation before hydrogen reduction to show the change in crystalline structure before and after reduction. The common peaks exhibited by all the samples at 11.8°, 23.2°, 35.2°, 39.3°, 46.9° and 62° verify the presence of

hydrotalcite-like structure or double-layered hydroxides which are in good agreement with those reported in literature (Abelló et al., 2014, 2016; Rudolf et al., 2014). Additional peaks were detected on the Zn-Al precursor corresponding to intensified characteristic peaks of Zn-Al hydrotalcite due to larger presence of Zn compared to the other samples.

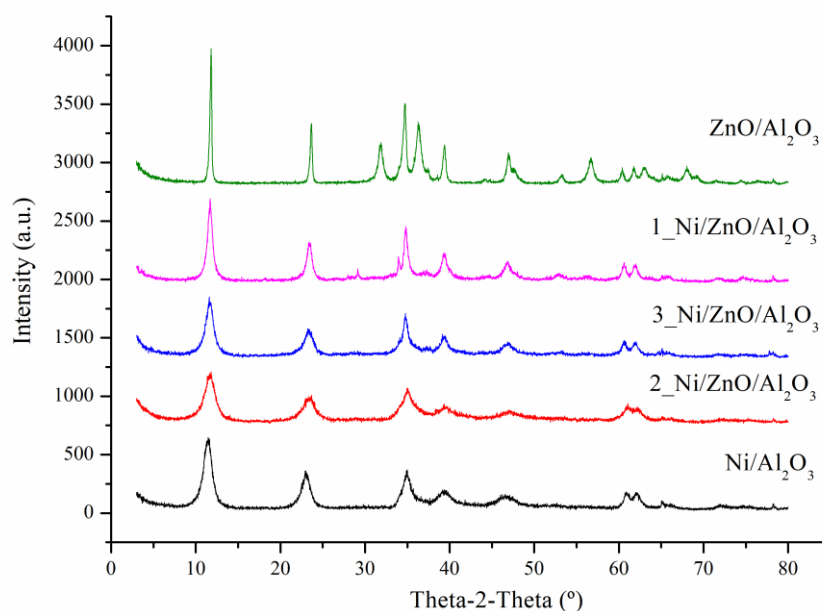


**Figure 4.5: Comparison of XRD spectra for catalyst precursors before hydrogen reduction**

For comparison, the XRD spectra for catalysts after hydrogen reduction are shown in Figure 4.6. It is clear that the XRD spectra changed significantly after the catalyst undergo hydrogen reduction. Peaks at 11.8° and 23.2° which were prominent in the spectra of hydrotalcites before reduction have disappeared and the peaks for Ni and ZnO become sharper and more prominent, showing that the catalyst experienced changes in phase upon reduction to form crystalline Ni and ZnO.

Sharp and defined peaks in Figure 4.6 indicate the presence of crystalline Ni (ICDD card No. 00-004-0805), NiO (ICDD Card No. 00-044-1159), NiAl<sub>2</sub>O<sub>4</sub> (ICDD Card No. 00-010-0339) and ZnO (ICDD Card No. 00-036-1451) after reduction. The XRD spectra of the samples also greatly resemble the spectra of Ni/ZnO/Al<sub>2</sub>O<sub>3</sub> catalyst reported in literature (Fuentes and Rangel, 2011). The Ni(111), Ni(200), NiO(101) and ZnO(110) lattices respectively represented by peaks at 44.5°, 51.7°, 63° and 37.3° could also be visualised in TEM image (Figure 4.7). The peak corresponding to NiAl<sub>2</sub>O<sub>4</sub> at 37° appeared to be absent in the spectra of sample 1\_Ni/ZnO/Al<sub>2</sub>O<sub>3</sub> and 3\_Ni/ZnO/Al<sub>2</sub>O<sub>3</sub>, which is deduced to be a result of being overshadowed by the highly crystalline ZnO peaks that are present in large amount in those samples.

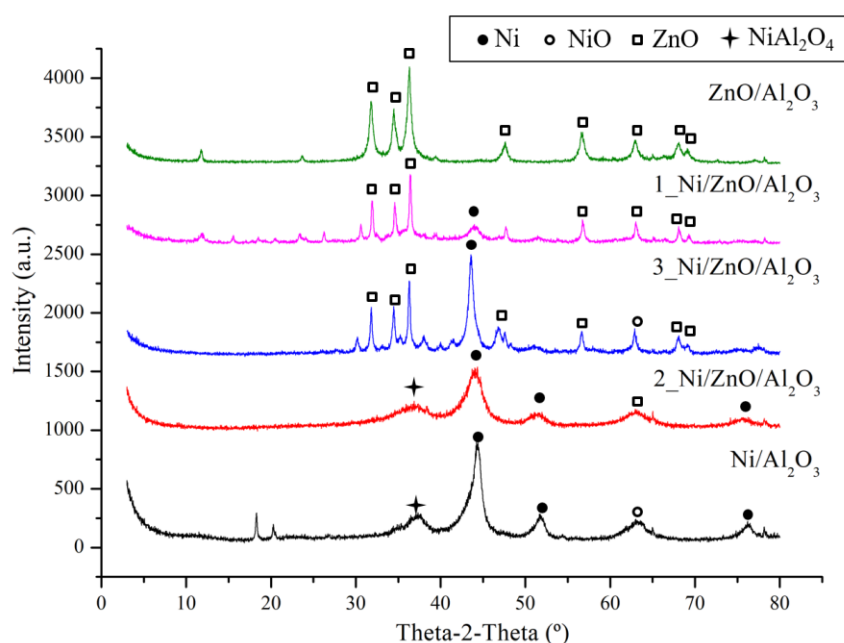


**Figure 4.6: Comparison of XRD spectra for the catalysts after hydrogen reduction**

Based on Figure 4.6, the peaks corresponding to Ni species greatly diminished in the spectra of sample 1\_Ni/ZnO/Al<sub>2</sub>O<sub>3</sub> due to its very high ZnO content, resulting in only a tiny peak of Ni(111) being visible. Conversely, when ZnO becomes the minor constituent in sample 2\_Ni/ZnO/Al<sub>2</sub>O<sub>3</sub>, the peaks representing ZnO species are hardly visible and the spectra closely resembles the spectra of Ni/Al<sub>2</sub>O<sub>3</sub>. The absence of peaks representing ZnO in this sample could be due to the limit of detection for species in small amount or being overshadowed by the prominent peaks of Ni and NiO with high crystallinities, resulting in a seemingly amorphous ZnO state. As for sample 3\_Ni/ZnO/Al<sub>2</sub>O<sub>3</sub>, peaks corresponding to both Ni and ZnO species are sharp and prominent, which is attributed to its equimolar Ni and ZnO content.

The crystallite size of Ni(111) lattice in the samples were calculated with the Scherrer's equation as demonstrated in Appendix B1. Table 4.3 shows the calculated crystallite size for each sample. It is apparent that the crystallite size decreased by more than half from 6.8 nm in Ni/Al<sub>2</sub>O<sub>3</sub> catalyst to 3.2 nm in 2\_Ni/ZnO/Al<sub>2</sub>O<sub>3</sub> catalyst, which could be attributed to the presence of ZnO in small amount that act as a physical spacer between Ni crystallites, thus preventing formation of large Ni crystallites. Nonetheless, the effect of ZnO being a physical spacer diminished with increasing ZnO content in the catalyst, as observed in the increase of crystallite size to 11.9 nm in 3\_Ni/ZnO/Al<sub>2</sub>O<sub>3</sub> catalyst. On the contrary, 1\_Ni/ZnO/Al<sub>2</sub>O<sub>3</sub> catalyst showed slightly smaller crystallite size than Ni/Al<sub>2</sub>O<sub>3</sub> catalyst, possibly due to its significantly lower Ni content which limited the Ni crystallite growth.

**Table 4.3: Crystallite size of Ni(111) lattice based on XRD spectra of reduced catalysts as calculated by Scherrer's equation**

Catalyst	Ni(111) Crystallite Size (nm)
Ni/Al <sub>2</sub> O <sub>3</sub>	6.8
2_Ni/ZnO/Al <sub>2</sub> O <sub>3</sub>	3.2
3_Ni/ZnO/Al <sub>2</sub> O <sub>3</sub>	11.9
1_Ni/ZnO/Al <sub>2</sub> O <sub>3</sub>	4.9
ZnO/Al <sub>2</sub> O <sub>3</sub>	-

On the other hand, the crystalline planes of Ni/Al<sub>2</sub>O<sub>3</sub> and 3\_Ni/ZnO/Al<sub>2</sub>O<sub>3</sub> catalysts could be visualised in their TEM images shown in Figure 4.7. Evidently, the catalyst surfaces are crystalline as seen from the lattice fringes which form crystallites approximately in the size range of 5 – 10 nm. Measurement of lattice spacing on each cluster of lattice fringes with uniform parallel lines shows the presence of Ni(111), Ni(200), NiO(101) and ZnO(110) crystal lattices, which resonates with the lattices detected in XRD spectra. In the TEM image of 3\_Ni/ZnO/Al<sub>2</sub>O<sub>3</sub> catalyst (catalyst showing best results in hydrogenation), ZnO crystallites are observed to be sandwiched between Ni crystallites, which corroborates the role of ZnO as a physical spacer. It is also implied that ZnO could act as a structural promoter which potentially stabilise the active Ni phase in a dispersed state and improve the dispersion of Ni in the catalyst.

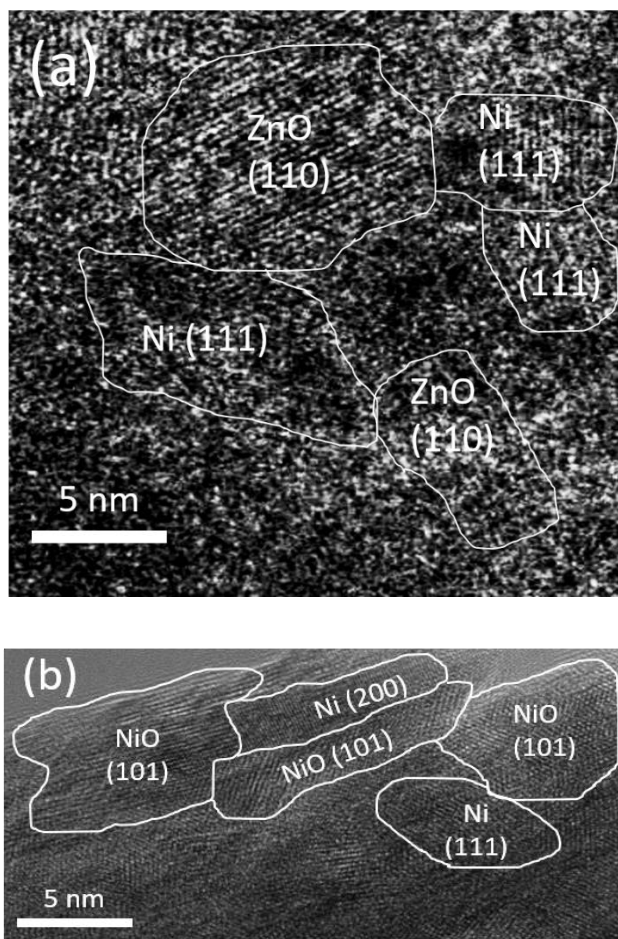


**Figure 4.7: Contrast-enhanced and magnified TEM image of (a) 3\_Ni/ZnO/Al<sub>2</sub>O<sub>3</sub> (b) Ni/Al<sub>2</sub>O<sub>3</sub> showing the crystalline planes of different species based on measured spacing between lattice fringes by ImageJ where  $d_{\text{Ni}(111)} = 2.03 \text{ \AA}$ ,  $d_{\text{Ni}(200)} = 1.76 \text{ \AA}$ ,  $d_{\text{NiO}(101)} = 2.41 \text{ \AA}$ ,  $d_{\text{ZnO}(110)} = 2.29 \text{ \AA}$**

#### 4.1.4 Temperature-Programmed Reduction Profiles

The H<sub>2</sub>-TPR profiles of the catalyst samples are compared in Figure 4.8. To serve as reference, the TPR profile of NiO obtained by calcination of unsupported metal precursor is also included, in which a distinct peak at 290 °C indicates the reduction of NiO species. Generally, the TPR profiles of Ni-

bearing catalysts exhibit two reduction peaks: a prominent peak at low temperature and a broad peak at high temperature.

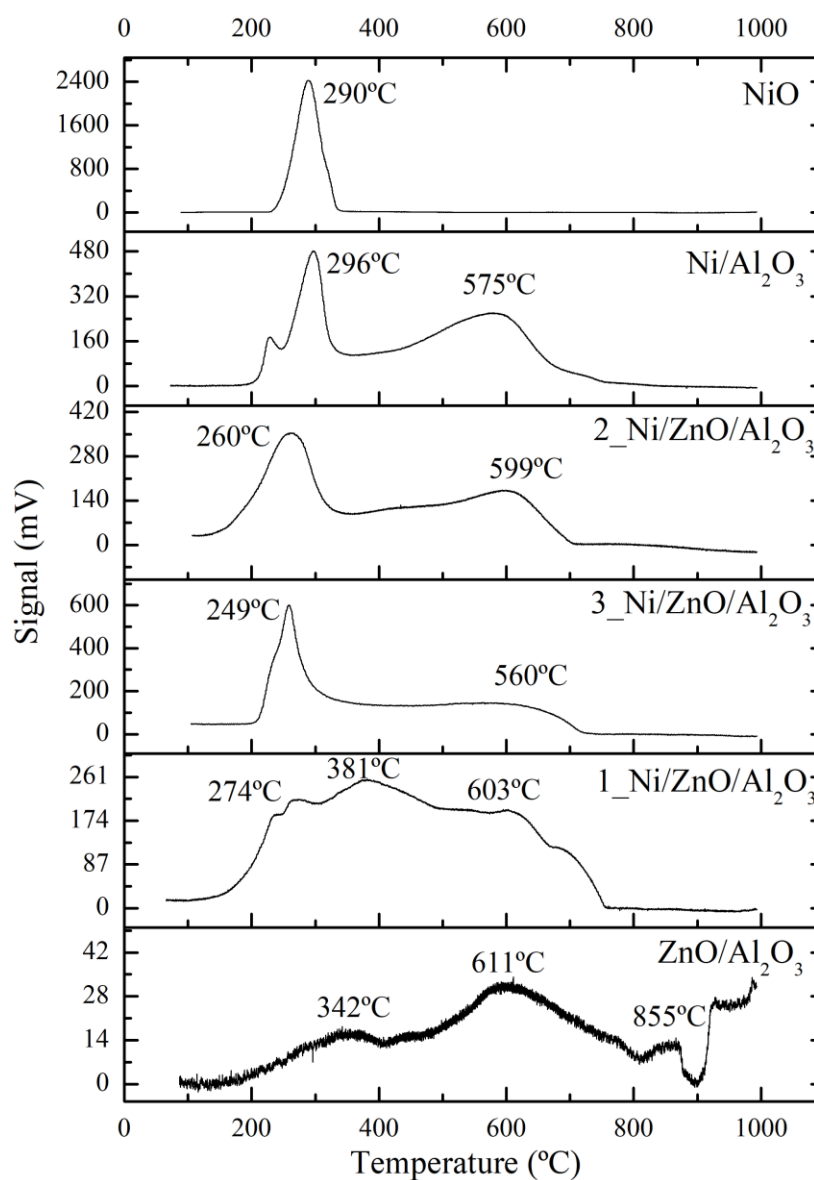


**Figure 4.8: Temperature programmed reduction profiles across temperatures from 100 – 1000 °C with inset showing amount of hydrogen consumed during H<sub>2</sub>-TPR**

The low-temperature peak corresponds to reduction of NiO that has weak interaction with the Al<sub>2</sub>O<sub>3</sub> support in the samples. On the other hand, the high-temperature peak represents reduction of metal aluminate spinel (Jiao et al., 2016) which were formed through intimate contact between the metal and

support (Chang et al., 2004). Metal aluminate has very low reducibility and high stability due to the incorporation of the metal ion into alumina crystallite structure (Jiao et al., 2016).

The metal aluminate spinel species found to be present in the synthesised samples are  $\text{NiAl}_2\text{O}_4$  and  $\text{ZnAl}_2\text{O}_4$  as shown in the XPS fittings (Figure 4.1). Nevertheless, it is deduced that the high-temperature peaks in the TPR profiles are contributed by reduction of  $\text{NiAl}_2\text{O}_4$  instead of  $\text{ZnAl}_2\text{O}_4$ , as there is barely any reduction peak detected in the profile of  $\text{ZnO}/\text{Al}_2\text{O}_3$  catalyst where  $\text{ZnAl}_2\text{O}_4$  is the only metal aluminate spinel species. The TPR profile of  $\text{ZnO}/\text{Al}_2\text{O}_3$  catalyst is noted to be stunted, broad and shows low intensity. Therefore, it can be deduced that the high-temperature peak corresponds to reduction of  $\text{NiAl}_2\text{O}_4$  species in all the synthesised samples.

It is also evident that the reducibility of  $\text{Ni}/\text{Al}_2\text{O}_3$  catalyst improved with the incorporation of  $\text{ZnO}$ , as observed from the drop in temperature of the TPR peaks from  $\text{Ni}/\text{Al}_2\text{O}_3$  to 1\_ $\text{Ni}/\text{ZnO}/\text{Al}_2\text{O}_3$ , 2\_ $\text{Ni}/\text{ZnO}/\text{Al}_2\text{O}_3$  and 3\_ $\text{Ni}/\text{ZnO}/\text{Al}_2\text{O}_3$  catalyst. A reduction peak at lower temperature signifies a higher reducibility. Similar effect of  $\text{ZnO}$  in enhancing reducibility was also reported for  $\text{Cu}/\text{ZnO}/\text{Al}_2\text{O}_3$  catalysts in past literature (Hoang et al., 2011; Lopez et al., 2008; Agrell et al., 2003). The higher reducibility was correlated to a larger fraction of  $\text{Cu}$  sites being in close vicinity with  $\text{ZnO}$  sites in the system (Martin et al., 2015).

In this case, it is deduced that 3\_Ni/ZnO/Al<sub>2</sub>O<sub>3</sub> catalyst showed higher reducibility than 2\_Ni/ZnO/Al<sub>2</sub>O<sub>3</sub> catalyst because there are more ZnO sites present in the 3\_Ni/ZnO/Al<sub>2</sub>O<sub>3</sub> catalyst system, hence enabling more Ni sites to be neighbouring the ZnO sites than in the 2\_Ni/ZnO/Al<sub>2</sub>O<sub>3</sub> catalyst. Amongst the ZnO-bearing catalysts, 1\_Ni/ZnO/Al<sub>2</sub>O<sub>3</sub> catalyst showed the lowest reducibility due to its high ZnO content, as ZnO became the main constituent instead of spacers in close vicinity between Ni sites.

In terms of peak shapes, 1\_Ni/ZnO/Al<sub>2</sub>O<sub>3</sub> catalyst showed a broad and convoluted profile, sharing similarities with the profile of ZnO/Al<sub>2</sub>O<sub>3</sub> catalyst. This is due to the high ZnO content in 1\_Ni/ZnO/Al<sub>2</sub>O<sub>3</sub> catalyst, resulting in more prominent effect of the broad ZnO reduction peaks in overlapping and interfering with the NiO and NiAl<sub>2</sub>O<sub>4</sub> reduction peaks. Meanwhile, 2\_Ni/ZnO/Al<sub>2</sub>O<sub>3</sub> and 3\_Ni/ZnO/Al<sub>2</sub>O<sub>3</sub> catalyst exhibit profiles that resemble the profile of Ni/Al<sub>2</sub>O<sub>3</sub> catalyst.

Besides that, the hydrogen consumption during TPR is shown in the inset of Figure 4.8 for each catalyst. They are generally correlated with their bulk Ni content, where higher Ni content leads to higher hydrogen consumption. However, the hydrogen consumption level is significantly higher for Ni/Al<sub>2</sub>O<sub>3</sub> catalyst than the others, as the Ni/Al<sub>2</sub>O<sub>3</sub> catalyst is dominated by NiO and NiAl<sub>2</sub>O<sub>4</sub> species as seen from its high intensity peaks shown in XPS fittings in Figure 4.1(a).

#### 4.1.5 Hydrogen Pulse Chemisorption

The amount of hydrogen adsorbed during pulse chemisorption analysis was utilised to compute the Ni dispersion and Ni surface area as demonstrated in Appendix G. The results are shown in Table 4.4 alongside the bulk Ni composition and surface Zn/Ni ratio for easier comparison. Generally the synthesised catalysts show high Ni dispersion and Ni surface area, which could be attributed to the two-step precipitation method employed in this work.

With reference to Table 4.4, the Ni dispersion and Ni surface area of the catalysts decrease in the order of  $2\_Ni/ZnO/Al_2O_3 > 3\_Ni/ZnO/Al_2O_3 > Ni/Al_2O_3 > 1\_Ni/ZnO/Al_2O_3$ . Conventionally, high Ni surface area would stem from high Ni composition, but in this case, it is interesting to see  $2\_Ni/ZnO/Al_2O_3$  and  $3\_Ni/ZnO/Al_2O_3$  catalysts showing higher Ni surface area and Ni dispersion despite their lower bulk Ni content than  $Ni/Al_2O_3$ . This suggests that the incorporation of ZnO helps in enhancement of Ni dispersion, followed by increment of Ni surface area. However, with ZnO becoming the main constituent in  $1\_Ni/ZnO/Al_2O_3$  catalyst, the effect diminished.

Several studies in the past have demonstrated that the presence of ZnO increased the Cu surface area and dispersion in  $Cu/ZnO/Al_2O_3$  catalyst by functioning as physical spacer for the Cu nanoparticles (Behrens et al., 2012; Phongamwong et al., 2017; Witoon et al., 2018; Ajamein and Haghghi, 2016). In the present work, it is inferred that the enrichment of ZnO at the catalyst surface encouraged its spacer effect between Ni particles. The Ni particles

became more spread out and dispersed on the catalyst surface, hence exposing more active surfaces for hydrogen adsorption. Conversely, in the absence of ZnO as a spacer, the Ni particles are less spaced out from each other on the support, resulting in smaller active surfaces.

**Table 4.4: Amount of hydrogen adsorbed, Ni dispersion,  $D_{Ni}$  and Ni specific surface area,  $SA_{Ni}$  of the catalysts obtained from hydrogen pulse chemisorption analysis as compared with bulk Ni composition and surface Zn/Ni ratio**

Catalyst	H <sub>2</sub> Adsorbed (μmol/g)	$D_{Ni}$ <sup>a</sup> (%)	$SA_{Ni}$ <sup>b</sup> (m <sup>2</sup> /g <sub>Ni</sub> )	Bulk Ni Composition <sup>c</sup> (At%)	Surface Zn/Ni ratio <sup>d</sup>
Ni/Al <sub>2</sub> O <sub>3</sub>	624.33	19.38	129.05	32.36	-
2_Ni/ZnO/Al <sub>2</sub> O <sub>3</sub>	736.74	35.13	233.99	22.17	0.85
3_Ni/ZnO/Al <sub>2</sub> O <sub>3</sub>	304.10	21.17	140.98	15.73	1.27
1_Ni/ZnO/Al <sub>2</sub> O <sub>3</sub>	87.10	9.84	65.53	9.83	2.31
ZnO/Al <sub>2</sub> O <sub>3</sub>	6.45	-	-	-	-

<sup>a</sup> Calculated by dividing the amount of hydrogen adsorbed per gram of Ni (assuming 1 H<sub>2</sub> molecule dissociates and adsorbs on 2 Ni atoms) by the bulk Ni content. Adsorption of H<sub>2</sub> on ZnO and other species is assumed to be negligible.

<sup>b</sup> Calculated based on Ni dispersion, and by assuming Ni has the proportion of low index plane fcc (111):(100):(110) = 1:1:1, with a single Ni atom occupying 0.0649 nm<sup>2</sup> (Bergeret and Gallezot, 2008).

<sup>c</sup> Obtained from ICP-OES analysis.

<sup>d</sup> Obtained from XPS analysis.

For Ni/ZnO/Al<sub>2</sub>O<sub>3</sub> catalysts, the Ni surface area and Ni dispersion are also influenced by their surface Zn/Ni ratio, where a lower ratio leads to higher surface area and dispersion. It can be inferred that the effect of ZnO as a spacer

is most prominent when ZnO is in low quantity as seen in 2\_Ni/ZnO/Al<sub>2</sub>O<sub>3</sub> catalyst which showed significantly higher surface area and dispersion. The spacer effect diminishes when the quantity of ZnO becomes higher, as observed in the lower surface area and dispersion in 3\_Ni/ZnO/Al<sub>2</sub>O<sub>3</sub> followed by 1\_Ni/ZnO/Al<sub>2</sub>O<sub>3</sub> catalyst, with ZnO becoming the main constituent. These findings are in agreement with the work of Chen et al. (2017) which also shown that increasing ZnO content for Ni/ZnO/Al<sub>2</sub>O<sub>3</sub> catalysts led to declining Ni dispersion and bigger Ni crystallites.

## **4.2 Catalyst Test in Partial Hydrogenation**

The catalysts under study were applied in lab-scale partial hydrogenation of sunflower oil in order to assess their catalytic performance in terms of activity and selectivity. Through correlations between their characteristics and catalytic performance, specific characteristics that are beneficial for enhancement of catalytic performance could be identified, leading on further to the design of an optimum catalyst.

### **4.2.1 Hydrogenation Activity**

The change in iodine value (IV) throughout the reaction time for each catalyst was traced and plotted in Figure 4.9. The sunflower oil employed as reactant has an initial IV of 162 which decreases as hydrogenation proceeds and saturates the sunflower oil. The rate of IV decrement is represented by the gradient of the graph, where a steeper gradient indicates greater activity. The

end-point of reaction was set at IV 70 as it is the most common target IV for partial hydrogenation of vegetable oil to form margarine (Cepeda et al., 2016).

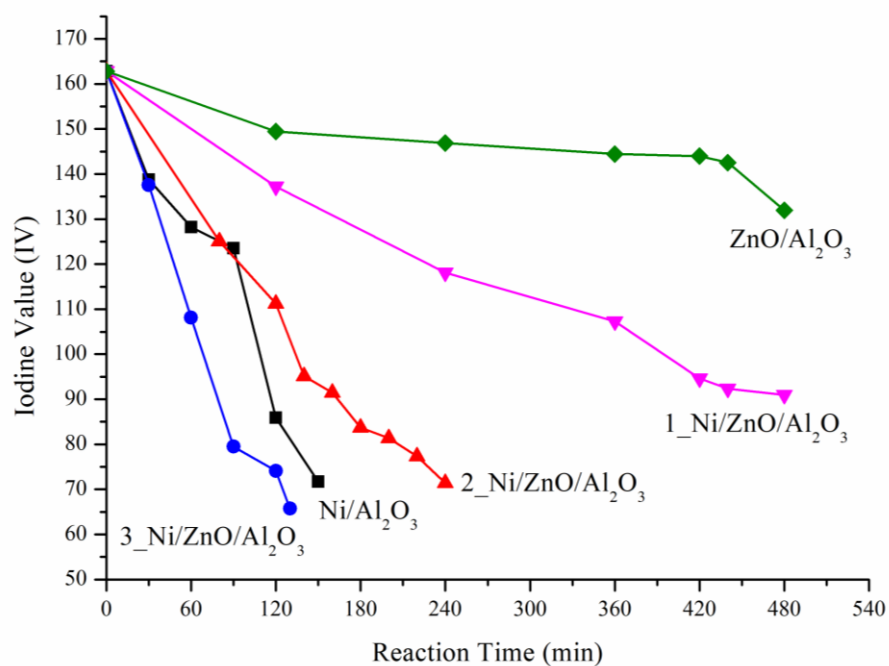


**Figure 4.9: Change in iodine value in the course of partial hydrogenation of sunflower oil (temperature: 180 °C, hydrogen pressure: 5 bar (g), agitation rate: 2000 rpm) over respective catalyst samples**

It can be seen from Figure 4.9 that the hydrogenation activity decreases in the order of 3\_Ni/ZnO/Al<sub>2</sub>O<sub>3</sub> > Ni/Al<sub>2</sub>O<sub>3</sub> > 2\_Ni/ZnO/Al<sub>2</sub>O<sub>3</sub> > 1\_Ni/ZnO/Al<sub>2</sub>O<sub>3</sub> > ZnO/Al<sub>2</sub>O<sub>3</sub>. To shed light on the factors affecting hydrogenation activity, comparison of hydrogenation activity with Ni surface area, Ni dispersion and average pore diameter of the catalysts are shown in Table 4.5 for easier analysis.

Higher hydrogenation activity is found to be generally linked to larger Ni surface area and higher Ni dispersion with the exception of 2\_Ni/ZnO/Al<sub>2</sub>O<sub>3</sub>. For instance, 2\_Ni/ZnO/Al<sub>2</sub>O<sub>3</sub> exhibits the highest Ni surface area and Ni dispersion, but shown notably lower hydrogenation activity than

3\_Ni/ZnO/Al<sub>2</sub>O<sub>3</sub> and Ni/Al<sub>2</sub>O<sub>3</sub>. In addition, 3\_Ni/ZnO/Al<sub>2</sub>O<sub>3</sub> also shows higher hydrogenation activity compared to Ni/Al<sub>2</sub>O<sub>3</sub> despite them having a similar range of Ni surface area. These observations suggest that hydrogenation activity in this study is not directly related to Ni dispersion and Ni surface area. Instead, it is apparent that the hydrogenation activity is well-correlated with the average pore size, where the use of catalyst with larger pore size leads to higher hydrogenation activity, with the exception of ZnO/Al<sub>2</sub>O<sub>3</sub> due to the low intrinsic activity of ZnO towards hydrogenation.

**Table 4.5: Hydrogenation activity of the catalysts as compared with Ni dispersion,  $D_{Ni}$ , Ni surface area,  $SA_{Ni}$  and average pore diameter,  $d_p$**

Catalyst	$D_{Ni}$ <sup>a</sup> (%)	$SA_{Ni}$ <sup>b</sup> (m <sup>2</sup> /g)	Hydrogenation Rate <sup>c</sup> (IV/min)	$d_p$ (nm)
Ni/Al <sub>2</sub> O <sub>3</sub>	19.38	129.05	0.60	15.55
2_Ni/ZnO/Al <sub>2</sub> O <sub>3</sub>	35.13	233.99	0.38	11.31
3_Ni/ZnO/Al <sub>2</sub> O <sub>3</sub>	21.17	140.98	0.74	27.95
1_Ni/ZnO/Al <sub>2</sub> O <sub>3</sub>	9.84	65.53	0.15	10.89
ZnO/Al <sub>2</sub> O <sub>3</sub>	-	-	0.06	17.17

<sup>a</sup> Calculated by dividing the amount of hydrogen adsorbed per gram of Ni (assuming 1 H<sub>2</sub> result in adsorption on 2 Ni atoms) by the bulk Ni content. Adsorption of H<sub>2</sub> on ZnO and other species is assumed to be negligible.

<sup>b</sup> Calculated based on Ni dispersion, and by assuming Ni has the proportion of low index plane fcc (111):(100):(110) = 1:1:1, with a single Ni atom occupying 0.0649 nm<sup>2</sup> (Bergeret and Gallezot, 2008).

<sup>c</sup> Calculated by the difference between final and initial iodine value divided over the total reaction time used to reach the final iodine value.

It is evident from Table 4.5 that sample 3\_Ni/ZnO/Al<sub>2</sub>O<sub>3</sub>, which possessed the largest average pore size, showed the highest hydrogenation activity among all the synthesised catalysts. Accordingly, 1\_Ni/ZnO/Al<sub>2</sub>O<sub>3</sub> which has the smallest average pore size and lowest pore volume, showed the lowest hydrogenation activity. Meanwhile, 2\_Ni/ZnO/Al<sub>2</sub>O<sub>3</sub> catalyst did not show the highest activity despite possessing the highest Ni dispersion and Ni surface area, as its pore size is notably smaller than 3\_Ni/ZnO/Al<sub>2</sub>O<sub>3</sub> and Ni/Al<sub>2</sub>O<sub>3</sub>, demonstrating the impact of limited pore accessibility on the hydrogenation activity.

On the other hand, among the ZnO-bearing catalysts, the hydrogenation activity appeared to increase with larger specific surface area and pore volume (Table 4.2), as more surface area and spaces would be available for occupancy by triglycerides in the pores, enabling higher chances of adsorption on the active sites for reaction. However, when compared with Ni/Al<sub>2</sub>O<sub>3</sub> catalyst, it is interesting to note that Ni/Al<sub>2</sub>O<sub>3</sub> exhibited higher hydrogenation activity than 2\_Ni/ZnO/Al<sub>2</sub>O<sub>3</sub> despite having a smaller specific surface area and pore volume. This is attributed to the larger pore diameter of Ni/Al<sub>2</sub>O<sub>3</sub> catalyst as compared to 2\_Ni/ZnO/Al<sub>2</sub>O<sub>3</sub>, which enabled less restriction of triglycerides diffusion into the pores. A small pore diameter particularly near the pore opening would impose restrictions on diffusion of triglycerides (Witton et al., 2014).

Therefore, this further supports the widely held view that pore size plays a vital role in contributing to hydrogenation activity, as it controls the accessibility of triglycerides to the active sites in the pores. From the

observations, it is clear that the incorporation of ZnO indirectly affects the hydrogenation activity by changing the availability of wide pores, which could either result in an enhancement (3\_Ni/ZnO/Al<sub>2</sub>O<sub>3</sub>) or impediment (2\_Ni/ZnO/Al<sub>2</sub>O<sub>3</sub> and 1\_Ni/ZnO/Al<sub>2</sub>O<sub>3</sub>) of hydrogenation activity as compared to Ni catalyst without presence of ZnO. The hydrogenation activity was increased by 23 % with the use of 3\_Ni/ZnO/Al<sub>2</sub>O<sub>3</sub> catalyst compared to Ni/Al<sub>2</sub>O<sub>3</sub> catalyst.

#### 4.2.2 Hydrogenation Selectivity

As shown previously in Table 3.1, the raw material for partial hydrogenation used in this work is sunflower oil, which contains 3.3 wt% of saturated fats and no *trans*-fat. Partial hydrogenation was performed by employing each of the catalyst under study. Catalytic performance of the catalysts was evaluated based on the formation of saturated fat (C18:0), *trans*-C18:1 and *cis*-C18:1 in the hydrogenation products at specific IV values, as shown in Figure 4.10. Interpretation of the results in terms of conversion and selectivity are also shown in Table 4.6. With the exception of 1\_Ni/ZnO/Al<sub>2</sub>O<sub>3</sub> and ZnO/Al<sub>2</sub>O<sub>3</sub>, which had low hydrogenation activity and products beyond targeted IV limit (> IV 70) even after 8 hours of reaction time, the other catalyst samples showed distinctive differences in the formation of both *trans*- and saturated fats at various IV intervals.

Comparing between the reaction dynamics in Figure 4.10(a) – (d), it is clear that the reactions showed similar overall trend – where the increase in

C18:0 and *trans*-C18:1 are contributed by decrease in *cis*-C18:1 and C18:2 respectively. The elimination of double bonds and the isomerisation process during the reaction can be tracked through the plots and it appears to be in agreement with the hydrogenation scheme postulated in Figure 2.1. For Ni/Al<sub>2</sub>O<sub>3</sub> and 3\_Ni/ZnO/Al<sub>2</sub>O<sub>3</sub>, it can be seen that the significant increment of *cis*-C18:1 at the beginning of hydrogenation coincides with the drastic decrement of C18:2, which implies that C18:2 are hydrogenated to form *cis*-C18:1. Nonetheless, *cis*-C18:1 has shown smaller increment compared to the decrement of C18:2, and this is due to the simultaneous hydrogenation of *cis*-C18:1 to C18:0 or *trans*-C18:1. The level of *cis*-C18:1 reached a maximum when C18:2 is almost depleted, and then decreased thereafter to produce *trans*-C18:1 and C18:0, via isomerisation and hydrogenation respectively.

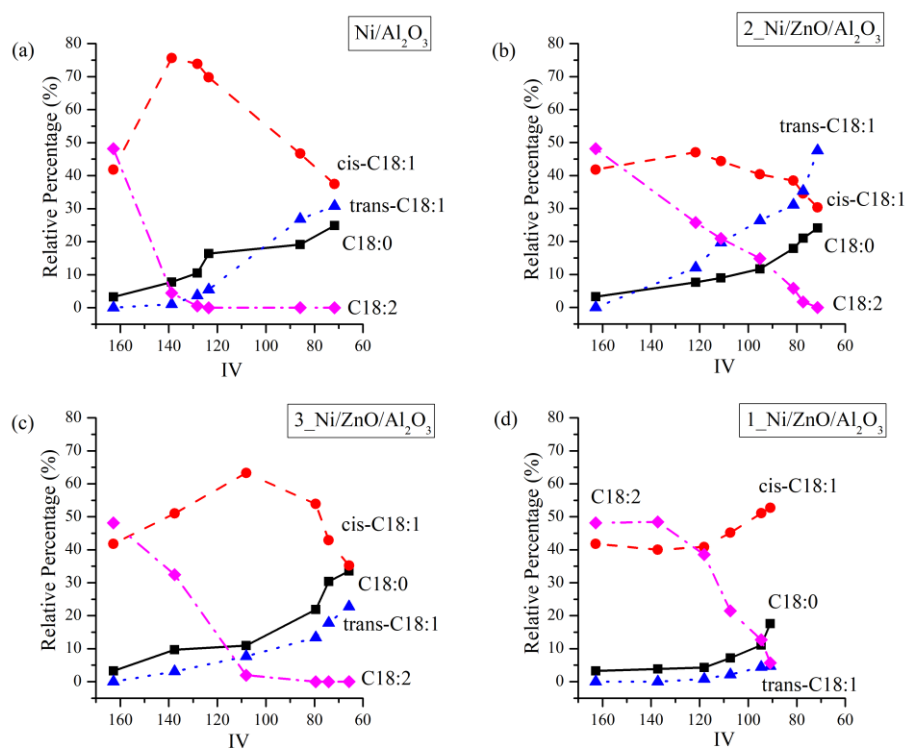


**Figure 4.10: Change in oil composition with iodine value during partial hydrogenation of sunflower oil (temperature: 180 °C, pressure: 5 bar (g), stirring intensity: 2000 rpm) with the use of (a) Ni/Al<sub>2</sub>O<sub>3</sub> (b) 2\_Ni/ZnO/Al<sub>2</sub>O<sub>3</sub> (c) 3\_Ni/ZnO/Al<sub>2</sub>O<sub>3</sub> (d) 1\_Ni/ZnO/Al<sub>2</sub>O<sub>3</sub> catalyst**

**Table 4.6: Conversion of C18:2, selectivity of C18:0 over *trans*-C18:1 and selectivity of *trans*-C18:1 over *cis*-C18:1 of sunflower oil at specific iodine value upon undergoing partial hydrogenation (temperature: 180 °C, hydrogen pressure: 5 bar (g), agitation rate: 2000 rpm)**

IV values	Conversion of C18:2 (%)			Selectivity of C18:0 over <i>trans</i> -C18:1 (%)		Selectivity of <i>trans</i> -C18:1 over <i>cis</i> -18:1 (%)	
	120	90	70	90	70	90	70
Ni/Al <sub>2</sub> O <sub>3</sub>	100	100	100	43.5	45	33.2	46.2
2_Ni/ZnO /Al <sub>2</sub> O <sub>3</sub>	48.0	76.2	100	33.2	33.6	41.4	61.0
3_Ni/ZnO /Al <sub>2</sub> O <sub>3</sub>	70.4	98.5	100	61.3	61.2	16.9	34.1
1_Ni/ZnO /Al <sub>2</sub> O <sub>3</sub>	18.0	88.2	-	78.8	-	8.2	-

Moreover, Table 4.6 shows that catalyst with lower *trans*-C18:1/*cis*-C18:1 selectivity would have higher C18:0/*trans*-C18:1 selectivity and vice versa. This indicates that when *trans*-C18:1 selectivity is low, subsequent hydrogenation of *trans*-C18:1 to C18:0 and direct hydrogenation of *cis*-C18:1 to C18:0 instead of isomerisation to *trans*-C18:1 tend to occur, which leads to high C18:0 formation. Conversely, when *trans*-C18:1 selectivity is high, isomerisation of *cis*-C18:1 to *trans*-C18:1 is favoured and subsequent hydrogenation of *trans*-C18:1 to C18:0 is less inclined, which results in lower C18:0 formation.

With reference to the C18:0/*trans*-C18:1 selectivity at IV 90, it can be seen that the increase of ZnO content in the Ni/ZnO/Al<sub>2</sub>O<sub>3</sub> catalysts from 2\_Ni/ZnO/Al<sub>2</sub>O<sub>3</sub> to 3\_Ni/ZnO/Al<sub>2</sub>O<sub>3</sub> and 1\_Ni/ZnO/Al<sub>2</sub>O<sub>3</sub>, led to increased selectivity for the saturated C18:0. When compared in terms of *trans*-C18:1/*cis*-C18:1, increasing ZnO content resulted in decreasing selectivity for *trans*-C18:1. Coupling of these two trends suggests that increasing ZnO content tends to suppress the formation of *trans*-C18:1 and promote the formation of saturated C18:0.

Nevertheless, it is also noted that despite the absence of ZnO, Ni/Al<sub>2</sub>O<sub>3</sub> catalyst showed higher C18:0/*trans*-C18:1 selectivity and lower *trans*-C18:1/*cis*-C18:1 selectivity than 2\_Ni/ZnO/Al<sub>2</sub>O<sub>3</sub>. This is thought to be closely related to 2\_Ni/ZnO/Al<sub>2</sub>O<sub>3</sub> having narrower distribution of pores in the range of 10 – 15 nm, which is probably large enough for triglycerides to diffuse in and avoiding low hydrogenation activity, but also small enough to retard the outward diffusion of *cis*-C18:1 molecules with a bent structure. A study by Balakos and Hernandez (1997) showed that pores with intermediate width favour the formation of *trans*-isomers where they desorb from active sites without being hydrogenated. As exit of *cis*-C18:1 from the pores is restricted due to its bent structure, they are trapped in the pores near the active sites and have high tendency to proceed with isomerisation or full-hydrogenation. In general, isomerisation is thermodynamically more favourable than full-hydrogenation, this would produce high level of *trans*-C18:1 with a linear structure and allow their easy escape from the intermediate-width pores.

On the other hand, Ni/Al<sub>2</sub>O<sub>3</sub> which shows significantly broader distribution of pores up to 30 nm would allow better access in and out of the pores for both bent *cis*-C18:1 and linear *trans*-C18:1. Hydrogenation with such wide pores will allow *cis*-C18:1 and *trans*-C18:1 to re-enter the pores for further hydrogenation and therefore result in higher conversion to saturated C18:0. Similarly, 1\_Ni/ZnO/Al<sub>2</sub>O<sub>3</sub> catalyst showed high saturated C18:0 formation due to its higher distribution of small pores in the range of 2 – 10 nm. The small pores would restrict the exit of both *cis*-C18:1 and *trans*-C18:1 from the pores, causing them to be trapped and to proceed with hydrogenation until full saturation, alongside a very low catalytic activity.

Interestingly, 3\_Ni/ZnO/Al<sub>2</sub>O<sub>3</sub> exhibits lower *trans*-C18:1 formation and lower *trans*-selectivity compared to Ni/Al<sub>2</sub>O<sub>3</sub> although they have similar range of Ni surface area (Table 4.5). As shown in Table 4.6, with the use of 3\_Ni/ZnO/Al<sub>2</sub>O<sub>3</sub> catalyst, the *trans*-selectivity at IV 70 was reduced by 26.2 % compared to Ni/Al<sub>2</sub>O<sub>3</sub>. This is attributed to the promotional effect of ZnO that functions as a selectivity modifier for Ni catalyst. It is thought that the presence of ZnO changed the electronic structure of the catalyst, which either increased the energy barrier for isomerisation or lowered the energy barrier for hydrogenation, resulting in faster conversion from *cis*-C18:1 to C18:0, thus affecting the selectivity of the reaction.

### 4.2.3 Comparison of Results with Literature

In order to have a better gauge and understanding on the performance of the synthesised catalysts, 3\_Ni/ZnO/Al<sub>2</sub>O<sub>3</sub> and Ni/Al<sub>2</sub>O<sub>3</sub> catalysts are selected to be compared with other catalysts from literature as shown in Table 4.7. The 3\_Ni/ZnO/Al<sub>2</sub>O<sub>3</sub> catalyst is chosen as it emerges to be the best-performing catalyst among the synthesised catalysts with consideration of its activity being the highest among the synthesised catalysts and also its ability to achieve lower *trans*-C18:1 selectivity than Ni/Al<sub>2</sub>O<sub>3</sub> catalyst.

Through comparison with catalysts reported in the literature for the same application, it can be seen that 3\_Ni/ZnO/Al<sub>2</sub>O<sub>3</sub> has yielded comparable saturated fat percentage as the Ni-B catalyst (Li et al., 2009), albeit forming more *trans*-fat, which may be resulted from operating at higher hydrogenation temperature. Besides that, Ni/Al<sub>2</sub>O<sub>3</sub> and 3\_Ni/ZnO/Al<sub>2</sub>O<sub>3</sub> have yielded lower *trans*-fat and higher saturated fat, as compared to precious metal catalysts Pt/Al<sub>2</sub>O<sub>3</sub> and Pd/Al<sub>2</sub>O<sub>3</sub> (Cepeda et al., 2016) which was performed using sunflower oil, albeit a lower activity.

When compared with hydrogenation process of other vegetable oils using Ni-based catalyst, such as Ni-Mg-Ag/D (Stanković et al., 2009), Ni-Ce (Konkol et al., 2016) and Ni-B (Li et al., 2009), this work has demonstrated comparable if not lower *trans*-fat formation, though it should be noted that the reaction conditions and types of oils vary slightly from one another, which may have subsequently affected the overall *trans*- and saturated fat contents. Therefore, this work has managed to demonstrate the potential of incorporating

ZnO onto Ni/Al<sub>2</sub>O<sub>3</sub> catalysts through the positive results it may provide in enhancing the hydrogenation activity and balancing between the formation of both *trans*- and saturated fats, depending on the fats product applications and requirements.

**Table 4.7: Comparison of *trans*-fats and saturated fats content with other works**

Catalyst	<i>T, P</i>	IV	Time (min)	<i>Trans</i> -C18:1 (%)	C18:0 (%)	Type of Oil
Pd/Al <sub>2</sub> O <sub>3</sub> Pt/Al <sub>2</sub> O <sub>3</sub>	150 °C, 3.5 bar	70	49 102	44.7 33.0	16.3 21.8	Sunflower (Cepeda et al., 2016)
Ni-Mg-Ag/D	160 °C, 1.6 bar	90	255	26.3	5.8	Soybean (Stanković et al., 2009)
Ni-Ce	180 °C, 6 bar	70	33	26.4	16.6	Canola (Konkol et al., 2016)
Ni-B	120 °C, 5 bar	77	80	8.0	34.0	Soybean (Li et al., 2009)
3_Ni/ZnO/Al <sub>2</sub> O <sub>3</sub> Ni/Al <sub>2</sub> O <sub>3</sub>	180 °C, 5 bar	70	130 150	22.8 30.8	33.5 24.9	Sunflower (present work)

## CHAPTER FIVE

### CONCLUSION

#### 5.1 Conclusion

Ni/ZnO/Al<sub>2</sub>O<sub>3</sub> catalysts with varying stoichiometric molar ratio were synthesised, characterised and evaluated in partial hydrogenation of sunflower oil. It has been demonstrated that the incorporation of ZnO in alumina-supported Ni catalyst lead to the following conclusions:

- a) Reducibility of Ni catalyst was improved with incorporation of ZnO and further increased with higher ZnO content, enabling reduction during synthesis of catalyst to be conducted at milder conditions.
- b) Presence of ZnO significantly changed the pore structure of the catalysts due to ZnO migration, in which higher ZnO content on the surface resulted in catalysts that have wider pores and higher surface area.
- c) Availability of wide pores was shown to be necessary for high hydrogenation activity.
- d) Higher ZnO content in the Ni/ZnO/Al<sub>2</sub>O<sub>3</sub> catalyst was shown to suppress *trans*-C18:1 formation and promote saturated C18:0 formation.
- e) The combined effect of larger pore size and higher ZnO content enabled the 3\_Ni/ZnO/Al<sub>2</sub>O<sub>3</sub> catalyst with the optimum Ni:Zn ratio of 1.5:1.5 to achieve 23 % higher activity and 26 % lower *trans*-C18:1 formation albeit forming higher saturated C18:0 than Ni/Al<sub>2</sub>O<sub>3</sub>.

The *trans*- and saturated fats content in specialty fats could be better adjusted to achieve the melting profile requirement without the expense of our health and efficiency of this industrial reaction.

## 5.2 Recommendation

This work has laid the path towards the use of Ni/ZnO/Al<sub>2</sub>O<sub>3</sub> as a promising alternative catalyst for partial hydrogenation of oils. Nonetheless, there are more areas yet to be explored in order to optimise this catalyst and achieve industrial utilisation. Future work on this catalyst may include and address the following areas:

- a) The influence of ZnO when added in smaller incremental amount to fine-tune the optimum Ni:Zn ratio by investigating smaller ratio step-size.
- b) The potential of Ni/ZnO/Al<sub>2</sub>O<sub>3</sub> catalyst when synthesised with other methods, i.e. impregnation.
- c) The optimisation of reaction parameters when employing Ni/ZnO/Al<sub>2</sub>O<sub>3</sub> catalyst to achieve further reduction in *trans*-fats formation.

## LIST OF REFERENCES

Abello, S., Berrueco, C., Gispert-Guirado, F. and Montane, D., 2016. Synthetic natural gas by direct CO<sub>2</sub> hydrogenation on activated takovites: effect of Ni/Al molar ratio. *Catalysis Science & Technology*, 6, pp.2305–2317.

Abelló, S., Bolshak, E., Gispert-Guirado, F., Farriol, X. and Montané, D., 2014. Ternary Ni–Al–Fe catalysts for ethanol steam reforming. *Catalysis Science & Technology*, 4, pp.1111.

Agrell, J., Birgersson, H., Boutonnet, M., Melián-Cabrera, I., Navarro, R.M. and Fierro, J.L.G., 2003. Production of hydrogen from methanol over Cu/ZnO catalysts promoted by ZrO<sub>2</sub> and Al<sub>2</sub>O<sub>3</sub>. *Journal of Catalysis*, 219, pp.389–403.

Ajamein, H. and Haghghi, M., 2016. On the microwave enhanced combustion synthesis of CuO–ZnO–Al<sub>2</sub>O<sub>3</sub> nanocatalyst used in methanol steam reforming for fuel cell grade hydrogen production: Effect of microwave irradiation and fuel ratio. *Energy Conversion and Management*, 118, pp.231–242.

American Oil Chemists' Society, 2017. Iodine Value of Fatty Acids, Wijs Method. *AOCS Official Method Tg 1a-64*.

Balakos, M.W. and Hernandez, E.E., 1997. Catalyst characteristics and performance in edible oil hydrogenation. *Catalysis Today*, 35, pp.415–425.

Bartholomew, C.H. and Farrauto, R.J., 1976. Chemistry of nickel-alumina catalysts. *Journal of Catalysis*, 45, pp.41–53.

Beers, A.E.W., 2007. Low Trans hydrogenation of edible oils. *Technology*, 19, pp.56–58.

Behrens, M., Studt, F., Kasatkin, I., Kühl, S., Hävecker, M., Abild-Pedersen, F., Zander, S., Girgsdies, F., Kurr, P., Kniep, B.-L., Tovar, M., Fischer, R.W., Nørskov, J.K. and Schlögl, R., 2012. The Active Site of Methanol Synthesis over Cu/ZnO/Al<sub>2</sub>O<sub>3</sub> Industrial Catalysts. *Science*, 336, pp.893.

Belkacemi, K. and Hamoudi, S., 2009. Low trans and saturated vegetable oil hydrogenation over nanostructured Pd/silica catalysts: Process parameters and mass-transfer features effects. *Industrial and Engineering Chemistry Research*, 48, pp.1081–1089.

Bergeret, G. and Gallezot, P., 2008. Particle Size and Dispersion Measurements, in: *Handbook of Heterogeneous Catalysis*. Weinheim: Wiley-VCH Verlag GmbH & Co. KGaA, pp. 738–764.

Boger, T., Zieverink, M.M.P., Kreutzer, M.T., Kapteijn, F., Moulijn, J. a. and Addiego, W.P., 2004. Monolithic Catalysts as an Alternative to Slurry Systems: Hydrogenation of Edible Oil. *Industrial & Engineering Chemistry Research*, 43, pp.2337–2344.

Bolt, P.H., Habraken, F.H.P.M. and Geus, J.W., 1998. Formation of Nickel, Cobalt, Copper, and Iron Aluminates from  $\alpha$ - and  $\gamma$ -Alumina-Supported Oxides: A Comparative Study. *Journal of Solid State Chemistry*, 135, pp.59–69.

Bouwman, H.J. and Terorde, R.J.A.M., 2011. Hydrogenation of fatty acids using a promoted supported nickel catalyst. EP 2 380 953 A1.

Broecker, F.J., Heners, J., Marosi, L., Schwarzmann, M. and Laurer, P.R., 1975. Nickel-Containing Hydrogenation Catalysts for the Selective Hydrogenation of Fats and Oils. US 3 896 053.

Brown, W.H., Foote, C.S., Iverson, B.L. and Anslyn, E., 2011. *Organic Chemistry*, 6th ed. Boston: Cengage Learning.

Castro, R.H.R. and Quach, D. V, 2012. Analysis of Anhydrous and Hydrated Surface Energies of  $\gamma$ -Al<sub>2</sub>O<sub>3</sub> by Water Adsorption Microcalorimetry. *The Journal of Physical Chemistry C*, 116, pp.24726–24733.

Castro, R.H.R., Ushakov, S. V, Gengembre, L., Gouvêa, D. and Navrotsky, A., 2006. Surface Energy and Thermodynamic Stability of  $\gamma$ -Alumina: Effect of Dopants and Water. *Chemistry of Materials* 18, pp.1867–1872.

Cepeda, E., Calvo, B., Sierra, I. and Iriarte-Velasco, U., 2016. Selective hydrogenation of sunflower oil over Ni catalysts. *Korean Journal of Chemical Engineering*, 33, pp.80–89.

Cepeda, E.A., Iriarte-Velasco, U., Calvo, B. and Sierra, I., 2016. Hydrogenation of Sunflower Oil over M/SiO<sub>2</sub> and M/Al<sub>2</sub>O<sub>3</sub> (M = Ni, Pd, Pt, Co, Cu) Catalysts. *Journal of the American Oil Chemists' Society*, 93, pp.731–741.

- Chang, F.-W., Kuo, M.-S., Tsay, M.-T. and Hsieh, M.-C., 2004. Effect of calcination temperature on catalyst reducibility and hydrogenation reactivity in rice husk ash–alumina supported nickel systems. *Journal of Chemical Technology & Biotechnology*, 79, pp.691–699.
- Chen, I. and Shiue, D.W., 1988. Reduction of nickel-alumina catalysts. *Industrial & Engineering Chemistry Research*, 27, pp.429–434.
- Chen, L., Zhang, F., Li, G. and Li, X., 2017. Effect of Zn/Al ratio of Ni/ZnO-Al<sub>2</sub>O<sub>3</sub> catalysts on the catalytic deoxygenation of oleic acid into alkane. *Applied Catalysis A: General*, 529, pp.175–184.
- Cheng, H., Su, Y.-Z., Kuang, P.-Y., Chen, G.-F. and Liu, Z.-Q., 2015. Hierarchical NiCo<sub>2</sub>O<sub>4</sub> nanosheet-decorated carbon nanotubes towards highly efficient electrocatalyst for water oxidation. *Journal of Materials Chemistry A*, 3, pp.19314–19321.
- Cheng, H.N., Rau, M.W., Dowd, M.K., Easson, M.W. and Condon, B.D., 2014. Comparison of soybean and cottonseed oils upon hydrogenation with nickel, palladium and platinum catalysts. *Journal of the American Oil Chemists' Society*, 91, pp.1461–1469.
- Coenen, J.W.E., 1986. Catalytic hydrogenation of fatty oils. *Industrial & Engineering Chemistry Fundamentals*, 25, pp.43–52.
- Cruz, A.F. and Álvarez, C.A., 2016. Cocoa butter substitute. EP 2822392 B1.
- de Siqueira, R.N.C., de Albuquerque Brocchi, E., de Oliveira, P.F. and Motta, M.S., 2014. Hydrogen Reduction of Zinc and Iron Oxides Containing Mixtures. *Metallurgical and Materials Transactions B*, 45, pp.66–75.
- Dhaka, V., Gulia, N., Ahlawat, K.S. and Khatkar, B.S., 2011. Trans fats-sources, health risks and alternative approach - A review. *Journal of Food Science and Technology*, 48, pp.534–541.
- Dhaka, V., Gulia, N., Ahlawat, K.S. and Khatkar, B.S., 2011. Trans fats sources, health risks and alternative approach - A review. *Journal of Food Science and Technology*, 48, pp.534–541.
- Dijkstra, A.J., 2006. Revisiting the formation of trans-isomers during partial hydrogenation of triacylglycerol oils. *European Journal of Lipid Science and Technology*, 108, pp.249–264.

Espinosa-Alonso, L., De Jong, K.P. and Weckhuysen, B.M., 2008. Effect of the nickel precursor on the impregnation and drying of  $\gamma$ -Al<sub>2</sub>O<sub>3</sub> catalyst bodies: A UV-vis and IR microspectroscopic study. *Journal of Physical Chemistry C*, 112, pp.7201–7209.

Feldhauser, B., Koetsier, W.T. and Lok, C.M., 1997. Nickel/silica catalyst for hydrotreating unsaturated organic compounds. US 5616531 A.

Fernández, M.B., Sánchez M., J.F., Tonetto, G.M. and Damiani, D.E., 2009. Hydrogenation of sunflower oil over different palladium supported catalysts: Activity and selectivity. *Chemical Engineering Journal*, 155, pp.941–949.

Fernández, M.B., Tonetto, G.M., Crapiste, G.H. and Damiani, D.E., 2007. Revisiting the hydrogenation of sunflower oil over a Ni catalyst. *Journal of Food Engineering*, 82, pp.199–208.

Fernández, M.B., Tonetto, G.M., Crapiste, G.H., Ferreira, M.L. and Damiani, D.E., 2005. Hydrogenation of edible oil over Pd catalysts: A combined theoretical and experimental study. *Journal of Molecular Catalysis A: Chemical*, 237, pp.67–79.

Fletcher, K., 2016. *Lipids* [Online]. Available at: <http://slideplayer.com/slide/8926361/> [Accessed: 7 March 2018]

Fuentes, E. and Rangel, M., 2011. Synthesis of Ni/ZnO/Al<sub>2</sub>O<sub>3</sub> Catalysts for the WGS Reaction from the Study of Structural and Catalytic Properties of Ni/ZnO and Ni/ Al<sub>2</sub>O<sub>3</sub>. *Revista Colombiana de Química*, 40, pp.105–123.

Ganguli, K.L., Nootenboom, P. and Lok, C.K., 1991. Nickel/Alumina Catalyst, Its Preparation and Use. US 5047178 A.

Geus, J.W., 2007. Production of Supported Catalysts by Impregnation and (Viscous) Drying. In: Regalbuto, J. (ed.). *Catalyst Preparation Science and Engineering*. Florida: CRC Press, pp. 341–370.

Gutsche, B., Robler, H. and Wurfert, S., 2008. Heterogeneous Catalysis in Oleochemistry. In: Ertl, G., Knözinger, H. and Weitkamp, J. (eds.). *Handbook of Heterogeneous Catalysis*. Weinheim: Wiley-VCH Verlag GmbH & Co. KGaA, pp. 3329–3356.

Haber, J., Black, J.H. and Delmon, B., 1995. Manual of methods and procedures for catalyst characterization (Technical Report). *Pure and Applied Chemistry*, 67, pp.1257–1306.

Henderson, J.H., 1994. Nickel Catalyst. US 5356847 A.

Hoang, D.L., Dang, T.T.H., Engeldinger, J., Schneider, M., Radnik, J., Richter, M. and Martin, A., 2011. TPR investigations on the reducibility of Cu supported on Al<sub>2</sub>O<sub>3</sub>, zeolite Y and SAPO-5. *Journal of Solid State Chemistry*, 184, pp.1915–1923.

Hoffer, B.W., Dick van Langeveld, A., Janssens, J.-P., Bonn , R.L.C., Lok, C.M. and Moulijn, J.A., 2000. Stability of highly dispersed Ni/Al<sub>2</sub>O<sub>3</sub> catalysts: Effects of pretreatment. *Journal of Catalysis*, 192, pp.432–440.

Hoffmann, G., 1989. Edible Oils and Fats. In: *The Chemistry and Technology of Edible Oils and Fats and Their High Fat Products*. London: Academic Press Limited, pp. 204.

Huang, Y.J. and Schwarz, J.A., 1987. The Effect of Catalyst Preparation on Catalytic Activity III: The Catalytic Activity of Ni/Al<sub>2</sub>O<sub>3</sub> Catalysts Prepared by Incipient Wetness. *Applied Catalysis*, 32, pp.45–57.

Hunter, J.E., 2005. Dietary levels of trans-fatty acids: Basis for health concerns and industry efforts to limit use. *Nutrition Research*, 25, pp.499–513.

Hwang, S.J., Yoo, S.J., Shin, J., Cho, Y.-H., Jang, J.H., Cho, E., Sung, Y.-E., Nam, S.W., Lim, T.-H., Lee, S.-C. and Kim, S.-K., 2013. Supported core@shell electrocatalysts for fuel cells: close encounter with reality. *Scientific Reports*, 3, pp.1309.

Jham, G.N., Teles, F.F.F. and Campos, L.G., 1982. Use of aqueous HCl/MeOH as esterification reagent for analysis of fatty acids derived from soybean lipids. *Journal of the American Oil Chemists' Society*, 59, pp.132–133.

Jiao, Y., Sun, D., Zhang, J., Du, Y., Kang, J., Li, C., Lu, J., Wang, J. and Chen, Y., 2016. Steam reforming of n-decane toward H<sub>2</sub> production over Ni/Ce-Al<sub>2</sub>O<sub>3</sub> composite catalysts: Effects of M (M = Fe, Co, Cu, Zn) promoters. *Journal of Analytical and Applied Pyrolysis*, 120, pp.238–246.

King, M.W., 2016. *Major Roles of Biological of Lipids* [Online]. Available at: <https://themedicalbiochemistrypage.org/lipids.php> [Accessed: 5 April 2018].

Kondrat, S.A., Smith, P.J., Carter, J.H., Hayward, J.S., Pudge, G.J., Shaw, G., Spencer, M.S., Bartley, J.K., Taylor, S.H. and Hutchings, G.J., 2017. The effect of sodium species on methanol synthesis and water-gas shift Cu/ZnO catalysts: utilising high purity zincian georgeite. *Faraday Discussions*, 197, pp.287–307.

Konkol, M., Bicki, R., Kondracka, M., Antoniak-Jurak, K., Wiercioch, P. and Próchniak, W., 2016. Characteristics and catalytic behavior of NiAlCe catalysts in the hydrogenation of canola oil: the effect of cerium on cis/trans selectivity. *Reaction Kinetics, Mechanisms and Catalysis*, 119, pp.595–613.

Krstić, J., Gabrovska, M., Lončarević, D., Nikolova, D., Radonjić, V., Vukelić, N. and Jovanović, D.M., 2015. Influence of Ni/SiO<sub>2</sub> activity on the reaction pathway in sunflower oil hydrogenation. *Chemical Engineering Research and Design*, 100, pp.72–80.

Leth, T., Jensen, H.G., Mikkelsen, A. E. and Bysted, A., 2006. The effect of the regulation on trans fatty acid content in Danish food. *Atherosclerosis Supplements*, 7, pp.53–56.

Li, G., Hu, L. and Hill, J.M., 2006. Comparison of reducibility and stability of alumina-supported Ni catalysts prepared by impregnation and co-precipitation. *Applied Catalysis A: General*, 301, pp.16–24.

Li, T., Zhang, W., Zhenhu, R. and Zhong, Q., 2009. Nickel – boron alloy catalysts reduce the formation of trans fatty acids in hydrogenated soybean oil. *Food Chemistry*, 114, pp.447–452.

Li, W.D., Li, Y.W., Qin, Z.F. and Chen, S.Y., 1994. Theoretical prediction and experimental validation of the egg-shell distribution of Ni for supported Ni/Al<sub>2</sub>O<sub>3</sub> catalysts. *Chemical Engineering Science*, 49, pp.4889–4895.

Lin, Y.-H., Adebajo, M.O., Frost, R.L. and Klopogge, J.T., 2005. Thermogravimetric analysis of hydrotalcites based on the takovite formula Ni<sub>x</sub>Zn<sub>6-x</sub>Al<sub>2</sub>(OH)<sub>16</sub>(CO<sub>3</sub>)·4H<sub>2</sub>O. *Journal of Thermal Analysis and Calorimetry*, 81, pp.83–89.

Liu, W., Tian, F., Yu, J. and Bi, Y., 2016. Magnetic Mesoporous Palladium Catalyzed Selective Hydrogenation of Sunflower Oil. *Journal of Oleo Science*, 458, pp.451–458.

Lopez, F., Bueno-López, A. and José Illán Gómez, M., 2008. Cu/Al<sub>2</sub>O<sub>3</sub> catalysts for soot oxidation: Copper loading effect. *Applied Catalysis B Environmental*, 84, pp.651–658.

Marceau, E., Carrier, X. and Che, M., 2009. Impregnation and Drying. In: *Synthesis of Solid Catalysts*. Weinheim: Wiley-VCH Verlag GmbH & Co. KGaA, pp. 59–82.

Martin, O., Mondelli, C., Curulla-Ferré, D., Drouilly, C., Hauert, R. and Pérez-Ramírez, J., 2015. Zinc-Rich Copper Catalysts Promoted by Gold for Methanol Synthesis. *ACS Catalysis*, 5, pp.5607–5616.

McArdle, S., Girish, S., Leahy, J.J. and Curtin, T., 2011. Selective hydrogenation of sunflower oil over noble metal catalysts. *Journal of Molecular Catalysis A: Chemical*, 351, pp.179–187.

Molina, R. and Poncelet, G., 1999.  $\alpha$ -Alumina-Supported Nickel Catalysts Prepared with Nickel Acetylacetonate. 2. A Study of the Thermolysis of the Metal Precursor. *The Journal of Physical Chemistry B*, 103, pp.11290–11296.

Mozaffarian, D., Katan, M.B., Ascherio, A., Stampfer, M.J. and Willett, W.C., 2006. Trans fatty acids and cardiovascular disease. *The New England journal of Medicine*, 354, pp.1601–1613.

Nassu, R.T. and Gonçalves, L. a. G., 1999. Determination of melting points of vegetable oil and fats by differential scanning calorimetry (DSC) technique. *Grasas y Aceites*, 50, pp.16–21.

Naumann d'Alnoncourt, R., Xia, X., Strunk, J., Löffler, E., Hinrichsen, O. and Muhler, M., 2006. The influence of strongly reducing conditions on strong metal-support interactions in Cu/ZnO catalysts used for methanol synthesis. *Physical Chemistry Chemical Physics*, 8, pp.1525–1538.

Nemeth, M., Sranko, D., Karolyi, J., Somodi, F., Schay, Z., Safran, G., Sajo, I. and Horvath, A., 2017. Na-promoted Ni/ZrO<sub>2</sub> dry reforming catalyst with high efficiency: details of Na<sub>2</sub>O-ZrO<sub>2</sub>-Ni interaction controlling activity and coke formation. *Catalysis Science & Technology*, 7, pp.5386-5401.

Nohair, B., Especel, C., Marécot, P., Montassier, C., Hoang, L.C. and Barbier, J., 2004. Selective hydrogenation of sunflower oil over supported precious metals. *Comptes Rendus Chimie*, 7, pp.113–118.

Perego, C., and Villa, P., 1997. Catalyst preparation methods. *Catalysis Today*, 34, pp.281–305.

Persson, K., Jansson, K., and Järås, S.G., 2007. Characterisation and microstructure of Pd and bimetallic Pd-Pt catalysts during methane oxidation. *Journal of Catalysis*, 245, pp.401–414.

Phongamwong, T., Chantaprasertporn, U., Witoon, T., Numpilai, T., Poo-arporn, Y., Limphirat, W., Donphai, W., Dittanet, P., Chareonpanich, M. and Limtrakul, J., 2017. CO<sub>2</sub> hydrogenation to methanol over CuO–ZnO–ZrO<sub>2</sub>–SiO<sub>2</sub> catalysts: Effects of SiO<sub>2</sub> contents. *Chemical Engineering Journal*, 316, pp.692–703.

Rasmussen, D.B., Janssens, T.V.W., Temel, B., Bligaard, T., Hinnemann, B., Helveg, S. and Sehested, J., 2012. The energies of formation and mobilities of Cu surface species on Cu and ZnO in methanol and water gas shift atmospheres studied by DFT. *Journal of Catalysis*, 293, pp.205–214.

Rudolf, C., Dragoi, B., Ungureanu, A., Chiriac, A., Royer, S., Nastro, A. and Dumitriu, E., 2014. NiAl and CoAl Materials Derived from Takovite-like LDHs and Related Structures as Efficient Chemoselective Hydrogenation Catalysts. *Catalysis Science & Technology*, 4, pp.179.

Savchenko, B.V.I. and Makaryan, I.A., 1999. Palladium Catalyst for the Production of Pure Margarine. *Platinum Metals Review*, 43, pp.74–82.

Schmidt, A., and Schomacker, R., 2007. Partial hydrogenation of sunflower oil in a membrane reactor. *Journal of Molecular Catalysis A: Chemical*, 271, pp.192–199.

Scrimgeour, C., 2009. Chemistry of Fatty Acids. In: Shahidi, F. (ed.) *Bailey's Industrial Oil and Fat*. New Jersey: Wiley Interscience, pp. 1–39.

Sekula, B.C. and Tancibok, K.U., 2001. Method of making a reduced calorie reconstituted milk composition. US 6235335 B1.

Shalvoy, R.B., Reucroft, P.J. and Davis, B.H., 1980. Summary Abstract: Investigation of the metal - support interaction in coprecipitated nickel on alumina methanation catalysts using x-ray photoelectron spectroscopy. *Journal of Vacuum Science and Technology*, 17, pp.209–210.

Simakova, I.L., Simakova, O.A., Romanenko, A. V. and Murzin, D.Y., 2008. Hydrogenation of vegetable oils over Pd on nanocomposite carbon catalysts. *Industrial and Engineering Chemistry Research*, 47, pp.7219–7225.

Spanjers, C.S., Held, J.T., Jones, M.J., Stanley, D.D., Sim, R.S., Janik, M.J. and Rioux, R.M., 2014. Zinc inclusion to heterogeneous nickel catalysts reduces oligomerization during the semi-hydrogenation of acetylene. *Journal Of Catalysis*, 316, pp.164–173.

Stanković, M., Čupić, Ž., Gabrovska, M., Banković, P., Nikolova, D. and Jovanović, D., 2015. Characteristics and catalytic behavior of supported NiMgAg/D catalysts in the partial hydrogenation of soybean oil. *Reaction Kinetics, Mechanisms and Catalysis*, 115, pp.105–127.

Stanković, M., Gabrovska, M., Krstić, J., Tzvetkov, P., Shopska, M., Tsacheva, T., Banković, P., Edreva-Kardjieva, R. and Jovanović, D., 2009. Effect of silver modification on structure and catalytic performance of Ni-Mg/diatomite catalysts for edible oil hydrogenation. *Journal of Molecular Catalysis A: Chemical*, 297, pp.54–62.

Studt, F., Ablid-Pedersen, F., Bligaard, T., Ramus Z., S., Clause H., C. and Norskov, J.K., 2008. Identification of Non-Precious Metal Alloy Catalysts for Selective Hydrogenation of Acetylene. *Science*, 320, pp.1320–1322.

Tarrago-Trani, M.T., Phillips, K.M., Lemar, L.E. and Holden, J.M., 2006. New and Existing Oils and Fats Used in Products with Reduced Trans-Fatty Acid Content. *Journal of the American Dietetic Association*, 106, pp.867–880.

Tonetto, G.M., Sánchez M., J.F., Ferreira, M.L. and Damiani, D.D., 2009. Partial hydrogenation of sunflower oil: Use of edible modifiers of the cis/trans-selectivity. *Journal of Molecular Catalysis A: Chemical*, 299, pp.88–92.

Tyson, W.R. and Miller, W.A., 1977. Surface free energies of solid metals: Estimation from liquid surface tension measurements. *Surface Science*, 62, pp.267–276.

Veldsink, J.W., Bouma, M.J., Schöön, N.H. and Beenackers, A.C.M., 1997. Heterogeneous Hydrogenation of Vegetable Oils: A Literature Review. *Catalysis Reviews*, 39, pp.253–318.

Viitanen, M.M., Jansen, W.P.A., van Welzenis, R.G., Brongersma, H.H., Brands, D.S., Poels, E.K. and Blik, A., 1999. Cu/ZnO and Cu/ZnO/SiO<sub>2</sub> Catalysts Studied by Low-Energy Ion Scattering. *The Journal of Physical Chemistry B*, 103, pp.6025–6029.

Weller, T., Lochmann, R., Meiler, W. and Köhler, H.-J., 1982. Theoretical investigations of the interaction of acetone with a sodium ion. *Journal of Molecular Structure*, 90, pp.81–87.

Witoon, T., Bumrungsalee, S., Vathavanichkul, P., Palitsakun, S., Saisriyoot, M. and Faungnawakij, K., 2014. Biodiesel production from transesterification

of palm oil with methanol over CaO supported on bimodal meso-macroporous silica catalyst. *Bioresource Technology*, 156, pp.329–334.

Witoon, T., Numpilai, T., Phongamwong, T., Donphai, W., Boonyuen, C., Warakulwit, C., Chareonpanich, M. and Limtrakul, J., 2018. Enhanced activity, selectivity and stability of a CuO-ZnO-ZrO<sub>2</sub> catalyst by adding graphene oxide for CO<sub>2</sub> hydrogenation to methanol. *Chemical Engineering Journal*, 334, pp.1781–1791.

Yu, M., Hu, J., Liu, J. and Li, S., 2013. Particles by Homogeneous Coprecipitation. *Materials Science Forum*, 746, pp.293–297.

Yu, Y., Xiao, W., Wang, J. and Wang, L., 2016. Understanding the surface segregation behavior of transition metals on Ni(111): a first-principles study. *Physical Chemistry Chemical Physics*, 18, pp.26616–26622.

Zock, P.L. and Katan, M.B., 1992. Hydrogenation alternatives: effects of trans fatty acids and stearic acid versus linoleic acid on serum lipids and lipoproteins in humans. *Journal of Lipid Research*, 33, pp.399–410.

## APPENDIX A

### ICP-OES ANALYSIS

#### 1.0 Preparation of Standards

Preparation of 100 ppm Ni standard by using  $\text{Ni}(\text{NO}_3)_2 \cdot 6\text{H}_2\text{O}$ :

$$\frac{0.01 \text{ g Ni}}{100 \text{ ml HNO}_3} = 100 \frac{\text{mg}}{\text{L}} = 100 \text{ ppm Ni}$$

$$\frac{0.01 \text{ g Ni}}{58.6934 \text{ g/mol Ni}} = 0.00017 \text{ mol Ni}$$

$$0.00017 \text{ mol Ni} = 0.00017 \text{ mol Ni}(\text{NO}_3)_2 \cdot 6\text{H}_2\text{O}$$

$$0.00017 \text{ mol Ni}(\text{NO}_3)_2 \cdot 6\text{H}_2\text{O} \times 290.79 \frac{\text{g}}{\text{mol}} = 0.04954 \text{ g Ni}(\text{NO}_3)_2 \cdot 6\text{H}_2\text{O}$$

$\therefore$  0.04954 g of  $\text{Ni}(\text{NO}_3)_2 \cdot 6\text{H}_2\text{O}$  was dissolved in 100 ml of 2 M  $\text{HNO}_3$  to prepare 100 ppm Ni standard. Calculation was repeated to prepare standard solutions of Zn, Al, Na, Si and Mg.

Dilution of 100 ppm Ni standard to 50 ppm:

$$M_1V_1 = M_2V_2$$

$$(100 \text{ ppm})(V_1) = (50 \text{ ppm})(50 \text{ ml})$$

$$V_1 = 25 \text{ ml}$$

$\therefore$  25 ml of 100 ppm Ni standard solution was topped up to 50 ml with 2 M  $\text{HNO}_3$  to prepare 50 ppm Ni standard. Calculation was repeated to prepare standard solutions with concentration of 25 ppm, 12.5 ppm and 6.25 ppm respectively.

## 2.0 Preparation of Samples

Preparation of 100 ppm catalyst sample solution:

$$\frac{0.01 \text{ g catalyst}}{100 \text{ ml HNO}_3} = 100 \frac{\text{mg}}{\text{L}} = 100 \text{ ppm catalyst}$$

∴ 0.01 g of catalyst was dissolved in 100 ml of 2 M HNO<sub>3</sub> to prepare 100 ppm catalyst sample solution. Preparation was repeated for each catalyst sample.

## 3.0 Conversion of Results to Atomic Percentage

ICP-OES results for catalyst sample 1\_Ni/ZnO/Al<sub>2</sub>O<sub>3</sub> analysed with 100 ppm sample solution:

Element	Concentration (ppm or mg/L)	Weight Percentage (wt%)
Zn	44.26	44.26
Ni	18.00	18.00
Al	8.37	8.37
Na	0.57	0.57
O	28.796	28.796

Note: Concentration of oxygen was calculated with the assumption that the remaining elemental composition are made up of oxygen. Weight percentage was based on total concentration of 100 ppm.

With basis of 100 g of catalyst, the number of moles were calculated:

<b>Element</b>	<b>Mass (g)</b>	<b>Atomic Mass (g/mol)</b>	<b>Number of Moles (mol)</b>
Zn	44.26	65.3820	0.677
Ni	18.00	58.6934	0.307
Al	8.37	26.9815	0.310
Na	0.57	22.9898	0.025
O	28.796	15.9990	1.799

Subsequently, the number of atoms was calculated with reference to the Avogadro's number ( $6.02 \times 10^{23}$  atom/mol), from which the atomic percentage was calculated:

<b>Element</b>	<b>Number of Atoms (<math>\times 10^{23}</math> atom)</b>	<b>Atomic Percentage (At%)</b>
Zn	4.077	21.71
Ni	1.850	9.83
Al	1.870	9.95
Na	0.149	0.80
O	10.800	57.7

Similar calculations were repeated for other catalyst samples.

## APPENDIX B1

### XRD ANALYSIS

#### 1.0 Calculation of Scherrer's Crystallite Size

Scherrer's equation:

$$\tau = \frac{K\lambda}{\beta \cos \theta}$$

Where

$\tau$  is the mean crystallite size, in angstroms, Å.

$K$  is a dimensionless shape factor, with value of 0.89.

$\lambda$  is the X-ray wavelength, with value of 1.54 Å.

$\beta$  is the full width at half maximum (FWHM) of the peak, in radians.

$\theta$  is the diffraction angle, in degree.

Diffraction peak of nickel(111) in catalyst sample 2\_Ni/ZnO/Al<sub>2</sub>O<sub>3</sub> showed that

FWHM = 2.66° and 2 $\theta$  = 44.34°.

$$\beta = 2.66^\circ \times \frac{\pi}{180^\circ} = 0.046 \text{ radian}$$

$$\tau = \frac{K\lambda}{\beta \cos \theta}$$

$$\tau = \frac{0.89(1.54)}{0.046 \cos 22.17} = 31.88 \text{ Å}$$

$$31.88 \text{ Å} \times \frac{1 \text{ nm}}{10 \text{ Å}} = 3.188 \text{ nm}$$

Similar calculation was repeated for other samples.

## APPENDIX B2

### TEM ANALYSIS

#### 1.0 Calculation of Reference Lattice Spacing

The following equation for inter-planar spacing using Miller Indices was applied:

$$d_{hkl} = \frac{a}{\sqrt{h^2 + k^2 + l^2}}$$

Where

$d_{hkl}$  is the inter-planar lattice spacing, in angstrom, Å.

$a$  is lattice constant.

$h, k, l$  is the Miller Indices.

For Ni(111) lattice:

$$d_{hkl} = \frac{3.524}{\sqrt{1^2 + 1^2 + 1^2}}$$
$$d_{hkl} = 2.03 \text{ \AA}$$

Similar calculation was repeated for other species.

## APPENDIX C

### IODINE VALUE TEST

#### 1.0 Recommended Sample Mass

The recommended mass of oil samples for respective expected iodine value ranges are listed below:

<b>Iodine Value Range</b>	<b>Sample Mass (g)</b>
< 3	> 10.576
3	8.4613 - 10.576
5	5.0770 - 6.3460
10	2.5384 - 3.1730
20	0.8461 - 1.5865
40	0.6346 - 0.7935
60	0.4321 - 0.5288
80	0.3175 - 0.3969
90	0.2822 - 0.3528
100	0.2540 - 0.3175
110	0.2309 - 0.2886
120	0.2117 - 0.2646
130	0.1954 - 0.2442
140	0.1814 - 0.2268
150	0.1693 - 0.2116
160	0.1587 - 0.1984
170	0.1494 - 0.1868
180	0.1411 - 0.1764
190	0.1337 - 0.1671
200	0.1270 - 0.1587
210	0.1210 - 0.1547
220	0.1155 - 0.1443

## 2.0 Iodine Value Calculation

The resulting iodine value was calculated with the following formula:

$$\text{Iodine Value} = \frac{(B - S) \times N \times 12.691}{\text{mass of sample, g}}$$

Where B = volume of titrant of blank set, in ml

S = volume of titrant of sample set, in ml

N = normality of sodium thiosulphate solution

For the oil sample obtained from reaction employing Ni/Al<sub>2</sub>O<sub>3</sub> catalyst at reaction time of 120 minute:

$$\text{Iodine Value} = \frac{(47.3 - 24.9) \times 0.1 \times 12.691}{0.3312}$$

Iodine Value = 85

## APPENDIX D1

### GAS CHROMATOGRAPHY ANALYSIS

#### 1.0 Fatty Acids Composition

Calculation of fatty acids composition for the oil sample collected at 120 minutes of reaction time in the reaction employing Ni/Al<sub>2</sub>O<sub>3</sub> catalyst is demonstrated below. The area of peaks corresponding to each fatty acid species are as follows:

Retention Time (min)	Fatty Acids	Area of Peak	Composition (%)
22	C16:0	5584.89	7.34
30	C18:0	14568.11	19.14
32	<i>Trans</i> -C18:1	20441.93	26.85
33 – 34	<i>Cis</i> -C18:1	35528.02	46.67
39	C18:2	-	-
40	C18:3	-	-
	<b>TOTAL</b>	<b>76122.95</b>	<b>100</b>

The composition was calculated by the relative area of a peak with the total peak area of the sample. E.g.:

$$\text{C18:0 (\%)} = \frac{14568.11}{76122.95} \times 100 \%$$

$$\text{C18:0 (\%)} = 19.14 \%$$

## APPENDIX D2

### ACTIVITY AND SELECTIVITY OF CATALYST

#### 1.0 Activity

The activity of catalyst samples in the reaction was calculated by the following formula:

$$\text{Activity} = \frac{\text{Initial iodine value} - \text{Final iodine value}}{\text{Reaction time taken to reach IV 70, minutes}}$$

Where Initial iodine value = 162

Final iodine value = 70

For Ni/Al<sub>2</sub>O<sub>3</sub> sample, the reaction time taken was 150 minutes, hence

$$\text{Activity} = \frac{162 - 70}{150 \text{ minutes}}$$

$$\text{Activity} = 0.6 \text{ IV per minute}$$

Calculation for the other samples are tabulated as follows:

Sample	Reaction Time (min)	Normalised Activity (IV/min)
2_Ni/ZnO/Al <sub>2</sub> O <sub>3</sub>	240	0.38
3_Ni/ZnO/Al <sub>2</sub> O <sub>3</sub>	130	0.74
1_Ni/ZnO/Al <sub>2</sub> O <sub>3</sub>	480	0.15
ZnO/Al <sub>2</sub> O <sub>3</sub>	480	0.06

## 2.0 Selectivity

Selectivity of the catalyst samples towards saturated fats and *trans*-fats were calculated respectively at IV 70 with the following formula:

Selectivity of *trans* C18: 1

$$= \frac{\text{Composition of } \textit{trans} \text{ C18: 1}}{\text{Total composition of } \textit{trans} \text{ and } \textit{cis} \text{ C18: 1}} \times 100\%$$

Selectivity of C18: 0

$$= \frac{\text{Composition of C18: 0}}{\text{Total composition of } \textit{trans} \text{ C18: 1 and C18: 0}} \times 100\%$$

For Ni/Al<sub>2</sub>O<sub>3</sub> sample,

$$\text{Selectivity of } \textit{trans} \text{ C18: 1} = \frac{31.2}{31.2 + 36.3} \times 100\%$$

$$\text{Selectivity of } \textit{trans} \text{ C18: 1} = 45\%$$

Similar calculations were performed for the other samples.

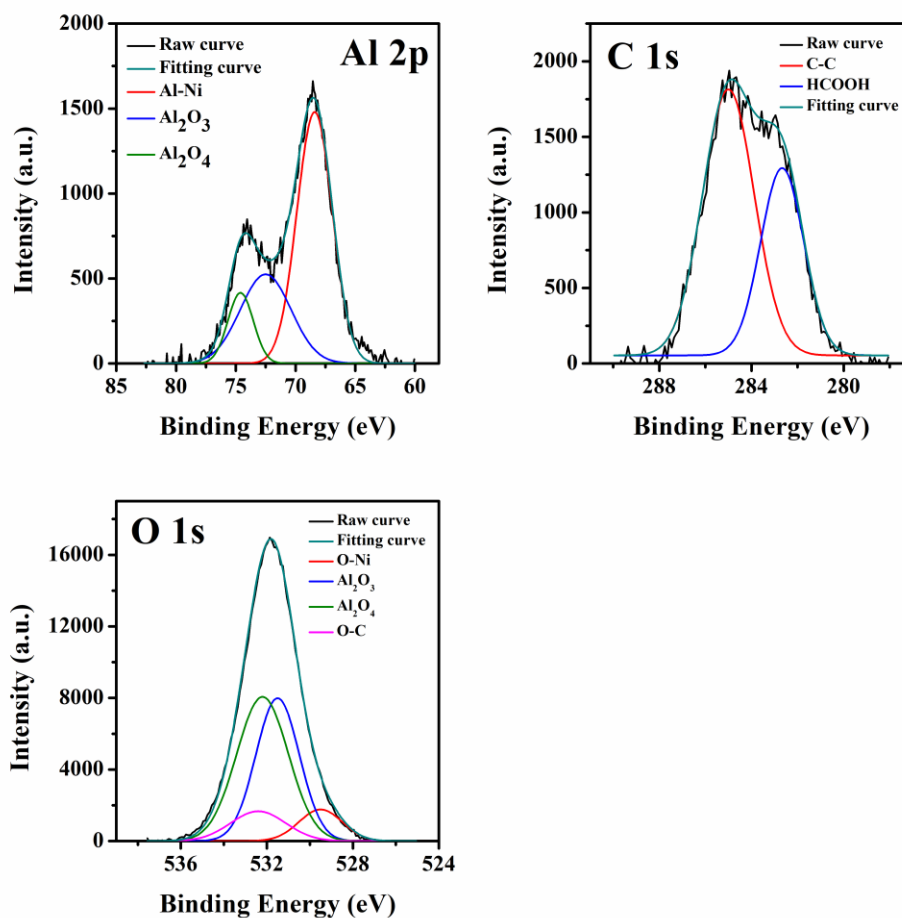
## APPENDIX E

### XPS CURVE-FITTING

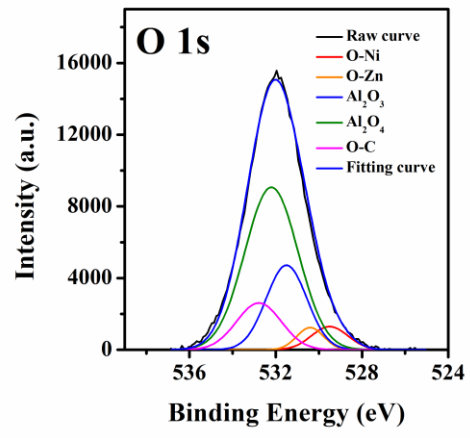
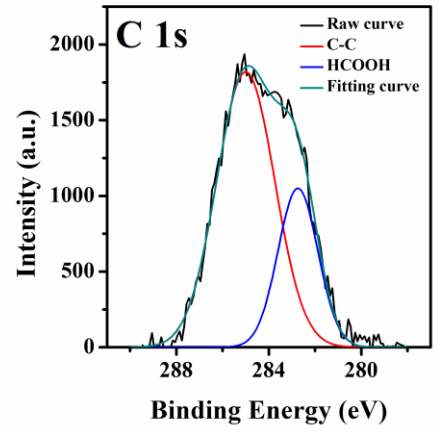
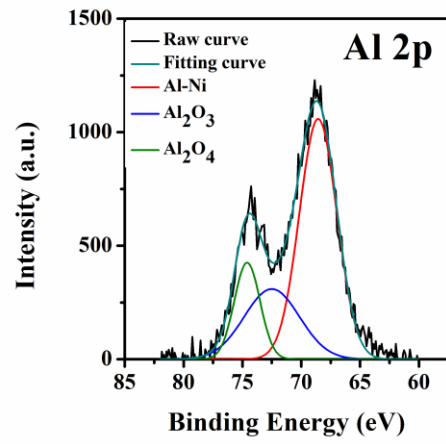
#### 1.0 XPS Fitted Curves

XPS spectra with fitted curve of each sample are presented as follows:

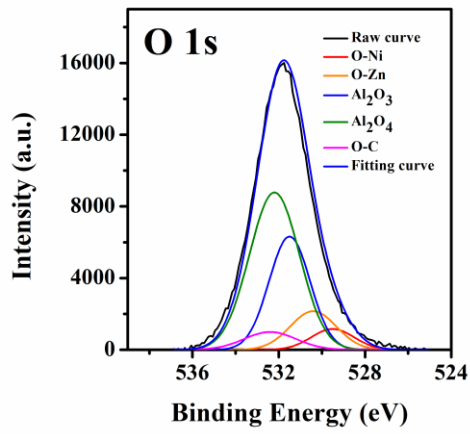
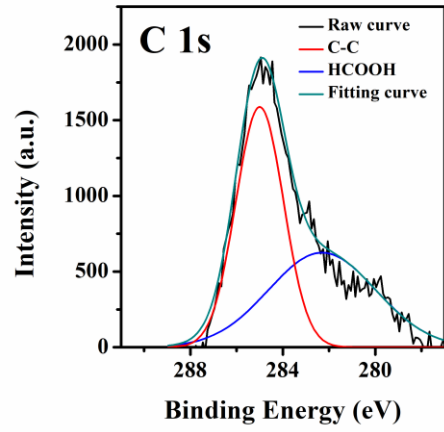
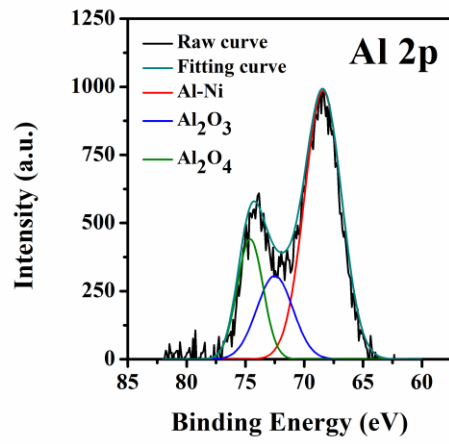
##### 1. Ni/Al<sub>2</sub>O<sub>3</sub> catalyst



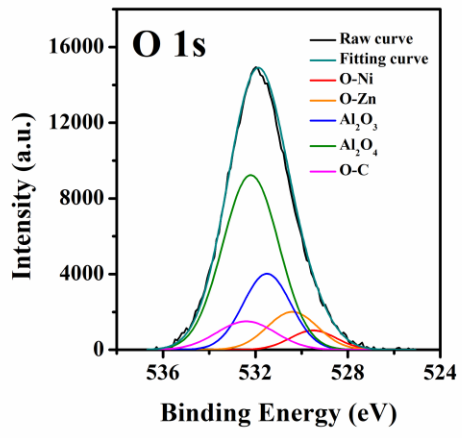
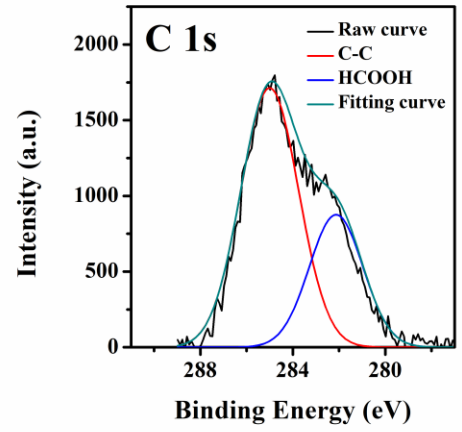
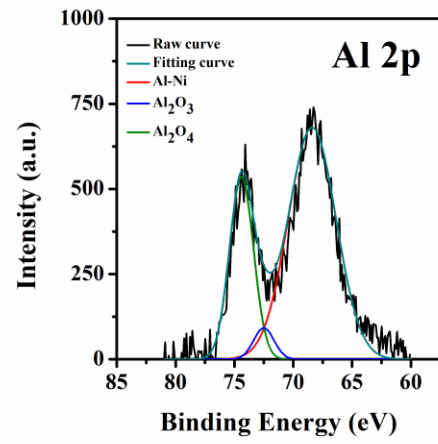
2. 2\_Ni/ZnO/Al<sub>2</sub>O<sub>3</sub> catalyst



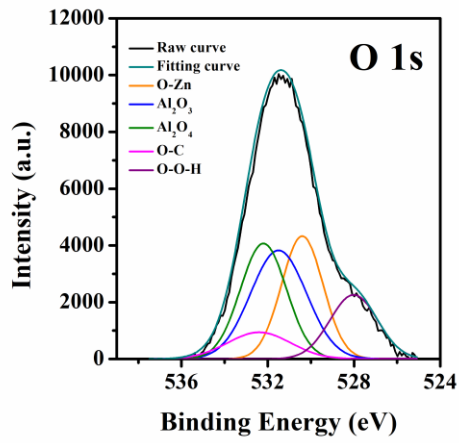
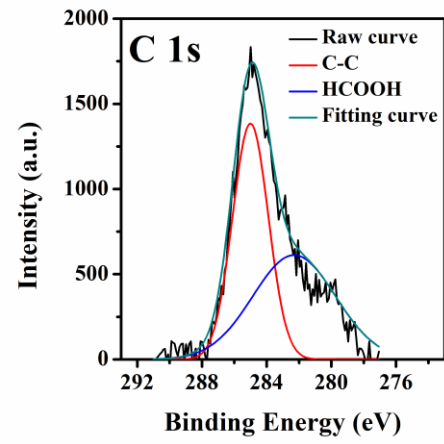
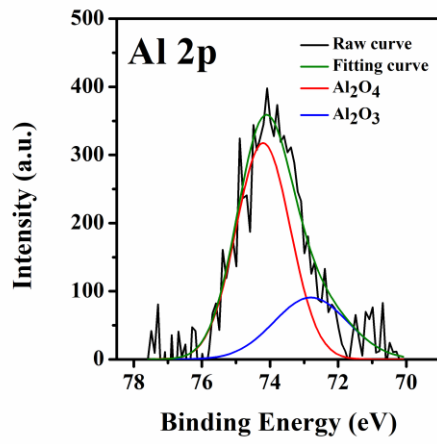
3. 3\_Ni/ZnO/Al<sub>2</sub>O<sub>3</sub> catalyst



4. 1\_Ni/ZnO/Al<sub>2</sub>O<sub>3</sub> catalyst



## 5. ZnO/Al<sub>2</sub>O<sub>3</sub> catalyst



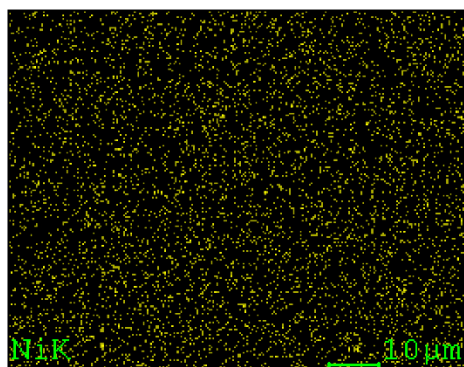
## APPENDIX F

### EDXS ELEMENTAL MAPPING

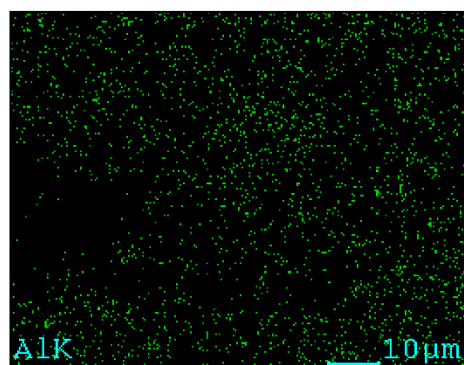
#### 1.0 Element Mapping Images

Element mapping of each sample are presented as follows:

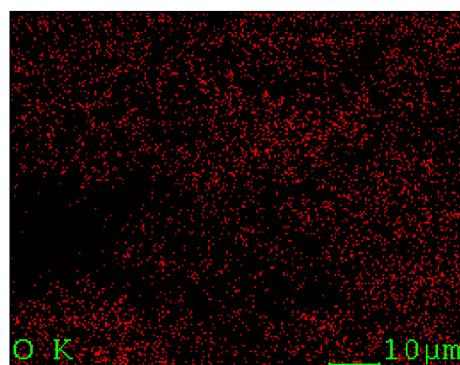
##### 1. Ni/Al<sub>2</sub>O<sub>3</sub> catalyst



(a)

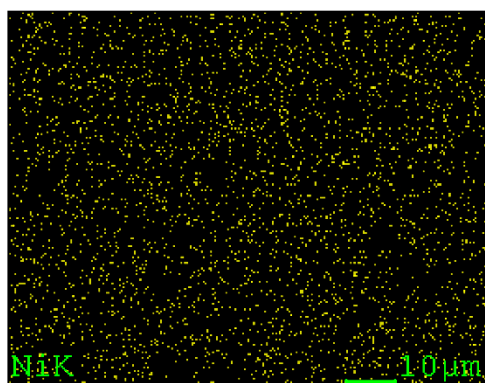


(b)

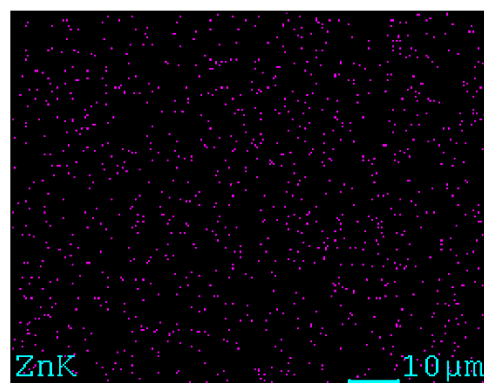


(c)

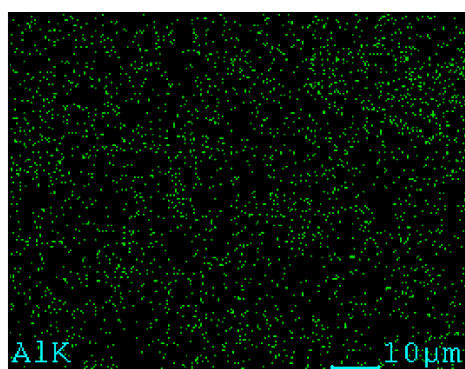
2. 2\_Ni/ZnO/Al<sub>2</sub>O<sub>3</sub> catalyst



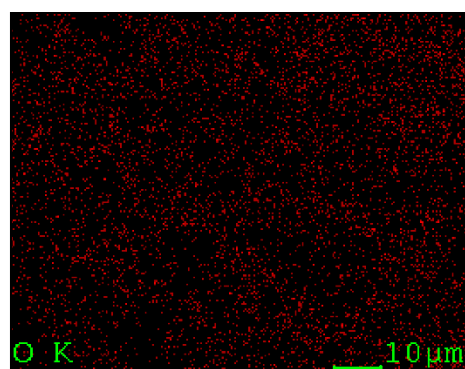
(a)



(b)

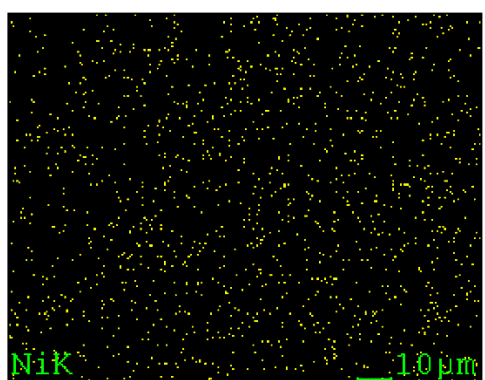


(c)

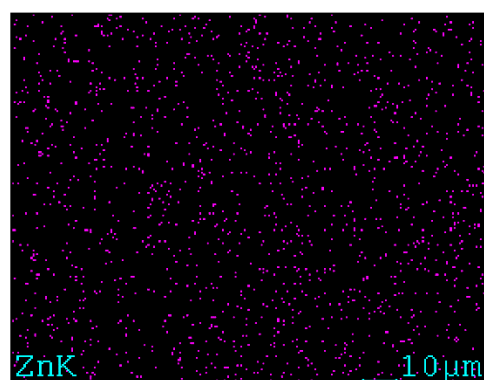


(d)

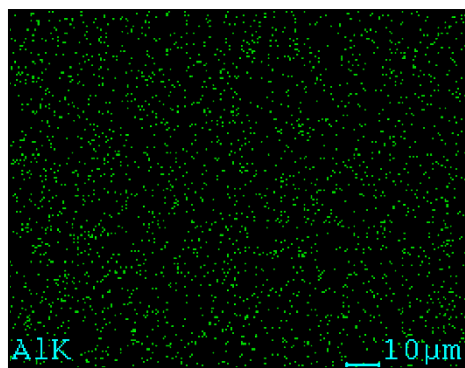
3. 1\_Ni/ZnO/Al<sub>2</sub>O<sub>3</sub> catalyst



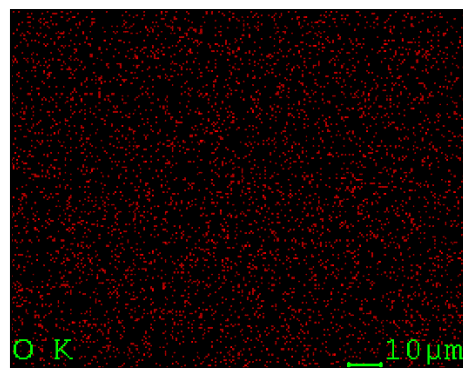
(a)



(b)

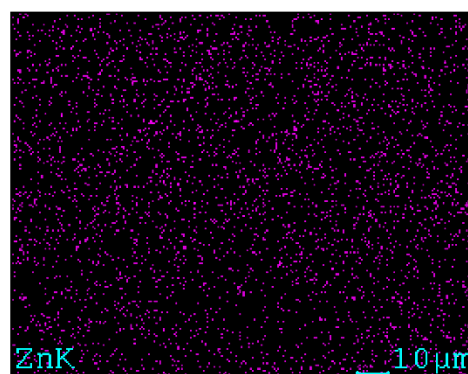


(c)

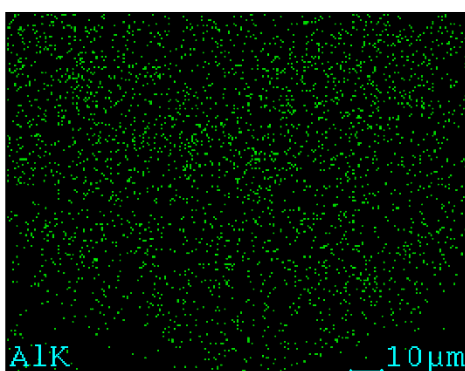


(d)

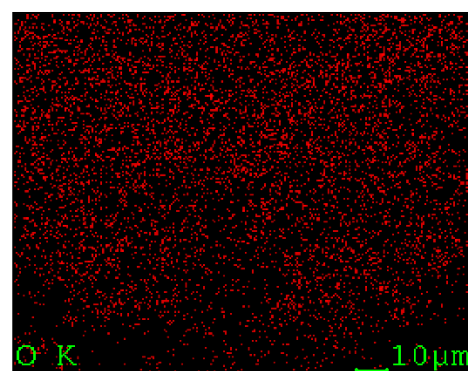
#### 4. ZnO/Al<sub>2</sub>O<sub>3</sub> catalyst



(a)



(b)



(c)

## APPENDIX G

### PULSE CHEMISORPTION ANALYSIS

#### 1.0 Calculation of Nickel Dispersion

Nickel dispersion on catalyst:

$$D_{Ni} = \frac{\text{Moles of metal on sample surface}}{\text{Moles of metal in sample}} \times 100\%$$

Moles of metal on sample surface = Amount of H<sub>2</sub> adsorbed × 2

$$\text{Moles of metal in sample} = \frac{M}{mw \times 100}$$

Where

$M$  is the weight percent of metal

$mw$  is the molecular weight or atomic mass of metal

Calculation of Ni dispersion for Ni/Al<sub>2</sub>O<sub>3</sub> catalyst are as follows:

$$\text{Volume of H}_2 \text{ adsorbed} = 6.24 \times 10^{-4} \frac{\text{mol H}_2}{\text{g catalyst}} \times \frac{1 \text{ g catalyst}}{61.5 \% \text{ Ni}}$$

$$\text{Volume of H}_2 \text{ adsorbed} = 6.24 \times 10^{-4} \frac{\text{mol H}_2}{\text{g catalyst}} \times \frac{100}{61.5}$$

$$\text{Volume of H}_2 \text{ adsorbed} = 1.02 \times 10^{-3} \frac{\text{mol H}_2}{\text{g metal}}$$

$$\text{Moles of metal on sample surface} = 1.02 \times 10^{-3} \frac{\text{mol H}_2}{\text{g metal}} \times 2$$

$$\text{Moles of metal on sample surface} = 2.04 \times 10^{-3} \frac{\text{mol H}_2}{\text{g metal}}$$

$$\text{Moles of metal in sample} = \frac{M}{mw \times 100}$$

$$\text{Moles of metal in sample} = \frac{61.5}{58.69 \frac{\text{g}}{\text{mol}} \times 100}$$

$$\text{Moles of metal in sample} = 1.05 \times 10^{-2} \frac{\text{mol Ni}}{\text{g metal}}$$

$$D_{Ni} = \frac{\text{Moles of metal on sample surface}}{\text{Moles of metal in sample}} \times 100 \%$$

$$D_{Ni} = \frac{2.04 \times 10^{-3}}{1.05 \times 10^{-2}} \times 100 \%$$

$$D_{Ni} = 19.38 \%$$

## 2.0 Calculation of Nickel Surface Area

Nickel surface area:

$$SA_{Ni} = a_m \left( \frac{N_a}{M} \right) D_{Ni}$$

$$a_m = \frac{1}{n_s}$$

Where

$a_m$  is the surface area occupied by an atom, in  $\text{nm}^2$

$n_s$  is the mean number of atoms for equal proportion of planes on the surface of crystalline plane

$N_a$  is the Avogadro's number

$M$  is the atomic mass

$D_{Ni}$  is the dispersion of nickel

Calculation of Ni surface area for Ni/Al<sub>2</sub>O<sub>3</sub> catalyst based on its Ni dispersion calculated above:

Assuming Ni has the proportion of low index plane FCC where (111):(100):(110) = 1:1:1,

$$n_s = 15.4 \frac{\text{atom}}{\text{nm}^2}$$

$$a_m = \frac{1}{n_s}$$

$$a_m = \frac{1}{15.4 \frac{\text{atom}}{\text{nm}^2}} = 0.0649 \frac{\text{nm}^2}{\text{atom}}$$

$$SA_{Ni} = a_m \left( \frac{N_a}{M} \right) D_{Ni}$$

$$SA_{Ni} = 0.0649 \frac{\text{nm}^2}{\text{atom}} \left( \frac{6.02 \times 10^{23} \frac{\text{atom}}{\text{mol}}}{58.69 \frac{\text{g}}{\text{mol}}} \right) (19.38 \%)$$

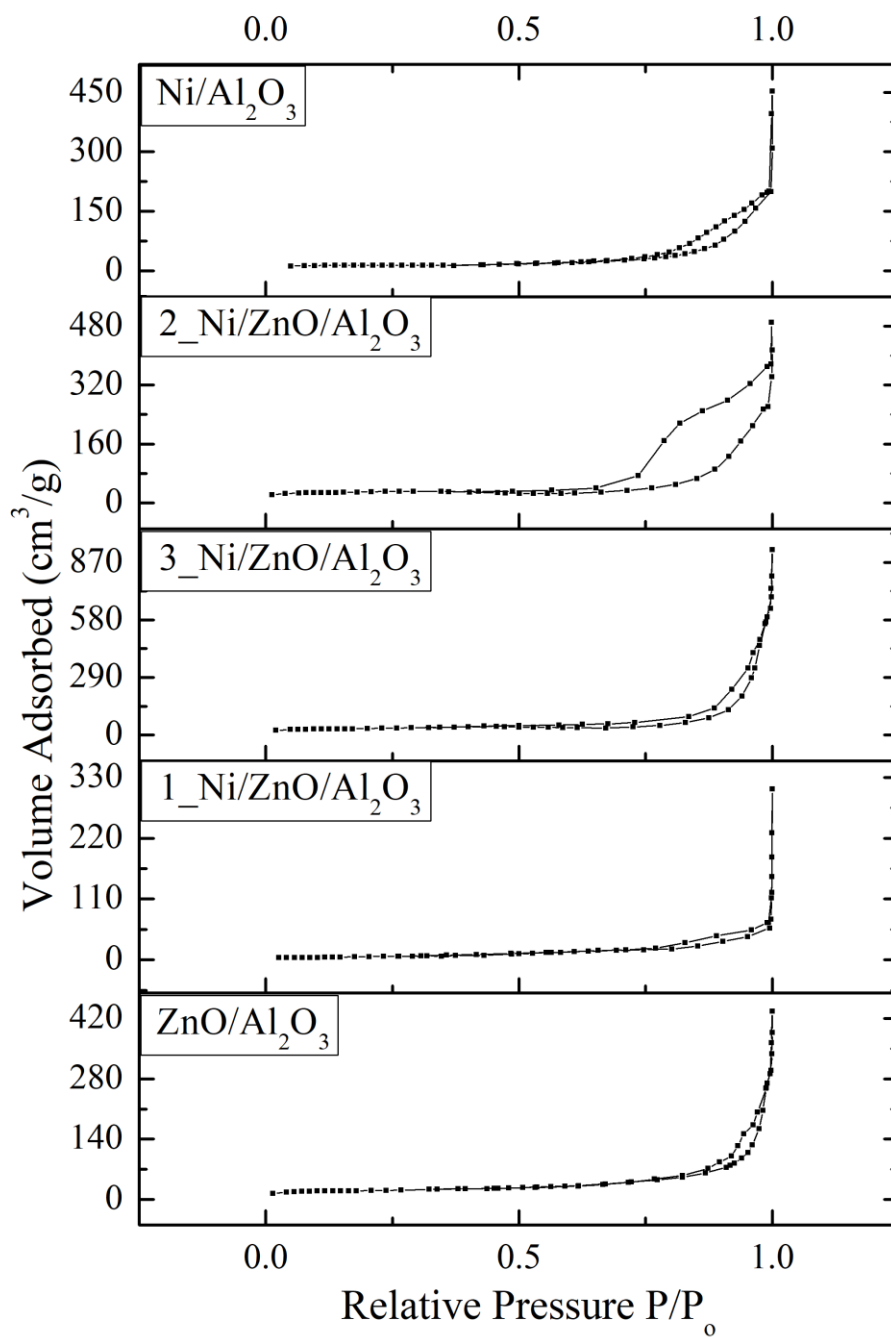
$$SA_{Ni} = 1.2905 \times 10^{20} \frac{\text{nm}^2}{\text{g}}$$

$$SA_{Ni} = 129.05 \frac{\text{m}^2}{\text{g}}$$

Similar calculation was repeated for other samples.

## APPENDIX H

### NITROGEN ADSORPTION-DESORPTION ISOTHERM



## LIST OF PUBLICATIONS

1. Wong, F.H., Tiong, T.J., Leong, L.K., Lin, K.-S. and Yap, Y.H., 2018. Effects of ZnO on characteristics and selectivity of co-precipitated Ni/ZnO/Al<sub>2</sub>O<sub>3</sub> catalysts for partial hydrogenation of sunflower oil. *Industrial & Engineering Chemical Research*, 57, pp.3163–3174.
2. Wong, F.H., Tiong, T.J., Leong, L.K., and Yap, Y.H., 2018. Role of ZnO in Ni/ZnO/Al<sub>2</sub>O<sub>3</sub> as catalytic materials for hydrogenation of oil. *AIP Conference Proceedings*, 2031, 02003.